

Научном већу Института за физику

Београд, 05. фебруар 2020.

**Предмет: Молба за покретање поступка за реизбор у звање научни сарадник**

Молим Научно веће Института за физику да у складу са Правилником о поступку и начину вредновања и квантитативном исказивању научно-истраживачких резултата истраживача покрене поступак за мој реизбор у звање научни сарадник.

У прилогу достављам:

1. Мишљење руководиоца лабораторије са предлогом чланова комисије за реизбор у звање
2. Стручну биографију
3. Преглед научне активности
4. Елементе за квалитативну оцену научног доприноса
5. Елементе за квантитативну оцену научног доприноса
6. Списак објављених научних радова и копије радова објављених након претходног избора у звање
7. Податке о цитираности
8. Фотокопију решења о претходном избору у звање
9. Додатне прилоге

Са поштовањем,

*Марина Лекић*

др Марина Лекић

ИНСТИТУТ ЗА ФИЗИКУ

ПРИМЉЕНО: 07. 02. 2020			
Рад. јед.	б р о ј	Арх. шифра	Прилог
0901	168/11		

Научном већу Института за физику

**Предмет: Мишљење руководиоца Лабораторије за реизбор др Марине Лекић у звање научни сарадник**

Др Марина Лекић је запослена у Лабораторији за биофотонику, у оквиру Центра за фотонику (Националног центра изузетних вредности) Института за физику у Београду. Ангажована је на проучавању ефеката у квантној оптици и кохерентној ласерској спектроскопији на пројектима финансираним од стране Министарства просвете, науке и технолошког развоја: III 45016 "Продукција и карактеризација нано-фотоничних функционалних структура у био-медицини и информатици" и ОИ 171038 "Холографски методи за генерисање специфичних таласних фронтана за ефикасну контролу квантних кохерентних ефеката у интеракцији атома и ласера".

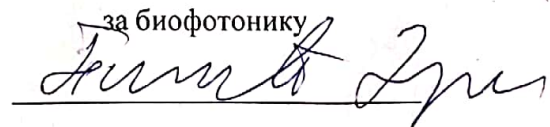
Обзиром да испуњава све предвиђене услове у складу са Правилником о поступку и начину вредновања и квантитативном исказивању научно-истраживачких резултата истраживача МПНТР, сагласан сам са покретањем поступка за реизбор др Марине Лекић у звање научни сарадник.

За састав комисије за реизбор др Марине Лекић у звање научни сарадник предлажем:

1. др Бранислав Јеленковић, научни саветник у пензији, Институт за физику у Београду
2. др Дејан Пантелић, научни саветник, Институт за физику у Београду, и
3. проф. др Братислав Обрадовић, редовни професор, Физички факултет у Београду.

Руководилац Лабораторије

за биофотонику



др Дејан Пантелић,

научни саветник

## 2. Биографски подаци

Марина Лекић је рођена у Јајцу 11. 09. 1978. године. Физички факултет – смер Општа физика завршила је на Универзитету у Београду 2003. године са просечном оценом 9,14. Од јула 2003. године кандидаткиња је запослена на Институту за физику у Београду као истраживач приправник. Последипломске студије на Физичком факултету Универзитета у Београду, смер Физика јонизованих гасова, плазме и квантна оптика, уписала је исте године. Докторску тезу под називом „Нелинеарна магнето оптичка ротација поларизације ласерског поља у пари рубидијума“ урадила је под руководством др Бранислава Јеленковића и одбранила је 22. 12. 2010. године на Физичком факултету. У звање научни сарадник изабрана је 13. 07. 2011. године. Од фебруара 2011. године кандидаткиња је годину дана боравила на постдокторском усавршавању у Француској, на Универзитету у Анжеу, где се бавила истраживањима из области нелинеарне оптике.

Кандидаткиња је била ангажована на неколико пројеката основних истраживања финансираних од стране МПНТР: "Прецизна ласерска спектроскопија: примене на оптичке замке, интерферометрију и оптичку метрологију“, “Квантна и оптичка интерферометрија”, “Производња и карактеризација нанофотонских функционалних структура и примена у биомедицини и информатици” и “Холографски методи за генерисање специфичних таласних фронтава за ефикасну контролу квантних кохерентних ефеката у интеракцији атома и ласера”. Поред поменутих пројеката Марина Лекић је учествовала и на међународним пројектима: европски пројекат FP6 “*Reinforcing the Center for quantum and optical metrology*” и SCOPES пројекат Швајцарске националне фондације за науку „*Modern optics and spectroscopy: from research to education*“, (2009-2012.). Тренутно је ангажована на билатералном пројекту са Белорусијом (2020-2021.).

Марина Лекић је један од оснивача и руководилац Лабораторије за оптоелектронику (2017-). Лабораторија је акредитована од стране Акредитационог тела Србије за еталонирање фиброоптичких мерних инструмената. Лабораторија тесно сарађује са привредним субјектима које послују у области телекомуникација, примењујући науку у привреди.

Кандидаткиња је члан научног комитета међународне радионице из фотонице. Организовала је неколико међународних и домаћих научних скупова. У периоду од 2007 – 2010. године била је члан комисије за републичка такмичења из физике ученика основних и средњих школа. Аутор је 16 радова објављених у међународним часописима као и бројних саопштења на домаћим и међународним скуповима. Укупан број цитата радова кандидаткиње је 114 (101 не рачунајући самоцитате), са Хиршовим индексом 6, према бази података *Web of Science*.

Од последњег избора у звање, породилско боловање и одсуство ради неге детета је користила три пута (3 године и 9 месеци).

### 3. Преглед научне активности

Научно-истраживачка активност кандидаткиње је у области квантне и нелинеарне оптике. Главни истраживачки правци обухватају проучавање: кохерентних и нелинеарних ефеката у квантној оптици, просторно-временских дисипативних мултидимензионих солитона и интеракција ултрабрзих ласерских снопова са маатријалима.

Приликом интеракције атома сложене структуре енергетских нивоа и ласерске светлости могу се испољити различити нелинеарни и кохерентни ефекти. Током рада на својој докторској дисертацији кандидаткиња је проучавала ефекте као што су: електромагнетски индукована транспаренција, електромагнетски индукована апсорпција и нелинеарна магнето-оптичка ротација (НМОР). Испитиван је утицај Раман-Ремзијевог ефекта на облик и ширину НМОР резонанци у вакуумској ћелији применом оригиналне конфигурације која омогућава просторно раздвајање снопова пумпе и пробе. У току израде дисертације, која је урађена у Лабораторији за фотонику у Институту за физику у Београду, реализована је експериментална поставка која је омогућила добијање веома узаних НМОР резонанци у вакуумској ћелији. Проучаван је утицај више параметара на ротацију поларизације пробног снопа као што су: различита растојања између снопова пумпе и пробе, различити углови између поларизација пумпајућег и пробног снопа, различити прелази у рубидијуму и различити интензитети пумпајућег и пробног снопа. Претходно поменути резултати су садржај радова:

- J. Krmpot, M. M. Mijailović, B. M. Panić, D. V. Lukić, A. G. Kovačević, D. V. Pantelić, and B. M. Jelenković, "Sub-Doppler absorption narrowing in atomic vapor at two intense laser fields," *Opt. Express* 13, Iss. 5, pp. 1448-1456, (2005)
- M. M. Mijailovic, J. Dimitrijevic, A. J. Krmpot, Z. D. Grujic, B. M. Panic, D. Arsenovic, D. V. Pantelic, and B. M. Jelenkovic "On non-vanishing amplitude of Hanle electromagnetically induced absorption in Rb" *Opt. Express* 15, Iss. 3, pp.1328-1339, (2007)
- Z. D. Grujić, M.M. Mijailović, B.M. Panić, M. Minić, A.G. Kovačević, M. Obradović, B.M. Jelenković and S. Cartaleva "Zeeman Coherences Narrowing due to Ramsey Effects Induced by Thermal Motion of Rubidium Atoms" *ACTA PHYSICA POLONICA A No. 5, Vol. 112* (2007)
- J. Dimitrijević, Z. Grujić, M. Mijailović, D. Arsenović, B. Panić and B.M. Jelenković "Effect of Laser Light Ellipticity on Hanle Electromagnetically Induced Absorption Amplitude and Line Width" *ACTA PHYSICA POLONICA A No. 5, Vol. 112* (2007)
- S. Cartaleva, T. Karaulanov, N. Petrov, D. Slavov, K. Vaseva, A. Yanev, M. Mijailović, Z. Grujić and B.M. Jelenković "All-Optical Magnetometer Based on Resonant Excitation of Rubidium Atoms by Frequency Modulated Diode Laser Light" *ACTA PHYSICA POLONICA A No. 5, Vol. 112* (2007)



- J. Dimitrijević, A. Krmpot, M. Mijailović, D. Arsenović, B. Panić, Z. Grujić, and B. M. Jelenković “Role of transverse magnetic fields in electromagnetically induced absorption for elliptically polarized light” *Phys. Rev. A* 77, 013814 (2008)
- J. Dimitrijevic, Z. Grujic, M. M. Mijailovic, D. Arsenovic, B. M. Panic, and B. M. Jelenkovic “Enhancement of electromagnetically induced absorption with elliptically polarized light - laser intensity dependent coherence effect“ *Opt. Express* 16, Iss. 2, pp.1343-1353, (2008)
- Z. D. Grujić, M. Mijailović, D. Arsenović, A. Kovačević, M. Nikolić, and B. M. Jelenković “Dark Raman resonances due to Ramsey interference in vacuum vapor cells” *Phys. Rev. A* 78, 063816 (2008)
- Zoran Grujić, Dušan Arsenović, Milan Radonjić, Marina Mijailović and Branislav Jelenković “Numerical simulation of Raman resonance due to the Ramsey interference induced by thermal motion of atoms” *Phys. Scr.* T135, 014026 (2009)
- M. Mijailović, Z. D. Grujić, M. Radonjić, D. Arsenović, and B. M. Jelenković ”Nonlinear magneto-optical rotation narrowing in vacuum gas cells due to interference between atomic dark states of two spatially separated laser beams” *Phys. Rev. A* 80, 053819, (2009)
- Z D Grujić, M M Lekić, M Radonjić, D Arsenović and B M Jelenković “Ramsey effects in coherent resonances at closed transition  $F_g = 2 \rightarrow F_e = 3$  of  $^{87}\text{Rb}$ ” *J. Phys. B: At. Mol. Opt. Phys.* 45, 245502, (2012)
- Ivan S. Radojičić, Milan Radonjić, Marina M. Lekić, Zoran D. Grujić, Dragan Lukić, and Branislav Jelenković “Raman–Ramsey electromagnetically induced transparency in the configuration of counterpropagating pump and probe in vacuum Rb cell ”, *J. Opt. Soc. Am. B* 32, 426-430 (2015)

Током постдокторског боравка на Универзитету у Анжеу, кандидаткиња се бавила проучавањем просторно-временских дисипативних мултидимензионих солитона као и вортекс солитона користећи аналитички варијациони метод и комбинујући га са одговарајућим нумеричким симулацијама и експериментима. Утврђени су услови постојања, пропагације и стабилности временских, просторних и просторно-временских вишедимензионих конзервативних и дисипативних солитона у атмосфери, полупроводницима са уском забрањеном зоном, наноконструкцијама и метаматеријалима са негативним индексом преламања.

- V. Skarka, N.B. Aleksic, M.M. Lekic, B. N. Aleksic, B.A. Malomed, D. Mihalache, H. Leblond, “ Formation of complex two-dimensional dissipative solitons via spontaneous symmetry breaking ”, *Phys. Rev. A*, vol. 90 (2), (2014)

Трећа област истраживања кандидаткиње је интеракција ласерског снопа и материјала приликом пропагације снопа кроз материјал. Бизмут-германијум оксид по структури припада материјалима типа силенита. Због својих особина (фотопроводност,

фоторефрактивност, пиезоелектрицитет), као и због подршке магнето-оптичких и електро-оптичких ефеката, погодан је за разне примене, као што су холографија, просторна модулација, оптичке меморије, фибер-оптички сензори, Покелсове ћелије, ... Пропагација ултрабрзих снопова кроз овај материјал, са модификацијом параметара, као и са променом особина снопа, експериментално је обрађивана и теоретски анализирана у радовима:

- G. Kovacevic, J. L. Ristic-Djurovic, M.M. Lekic, B. B. Hadzic, G.S.I. Abudagel, S.J. Petricevic, P. M. Mihailovic, B.Z. Matovic, D. M. Dramlic, Lj. M. Brajovic, N. Z. Romcevic, Influence of femtosecond pulsed laser irradiation on bismuth germanium oxide single crystal properties," Mater. Res. Bull., vol. 83, 284-289 ( 2016)
- GSI Abudagel, S.J. Petričević, P.M. Mihailović, A.G. Kovačević, J. Ristić-Djurović, M.M. Lekić, M.J. Romčević, S. Cirković, J.M. Trajić, N.Ž. Romčević, "Improvement of magneto-optical quality of high purity Bi<sub>12</sub>GeO<sub>20</sub> single crystal induced by femtosecond pulsed laser irradiation", Optoelectronics and Advanced Materials – Rapid Communications, vol. 11, br. 7-8, 477-481 (2017)
- V. Skarka, M. M. Lekić, A. G. Kovačević, B. Zarkov, N. Ž. Romčević "Solitons generated by self-organization in bismuth germanium oxide single crystals during the interaction with laser beam", Optical and quantum electronics, vol. 50 (1), (2018)

## **4. Елементи за квалитативну оцену научног доприноса**

### **4.1 Квалитет научних резултата**

#### **4.1.1 Научни ниво и значај резултата, утицај научних радова**

Др Марина Лекић је у свом досадашњем раду објавила 16 радова М20 категорије у међународним часописима са ISI листе и 26 саопштења, од којих 7 у категорији М21а, 2 у категорији М21, 2 у категорији М22, 5 у категорији М23, 10 у категорији М33 и 16 у категорији М34.

У периоду након стицања звања научни сарадник, др Марина Лекић је објавила 6 радова у међународним часописима са ISI листе и 8 саопштења на међународним конференцијама, од којих су 1 у категорији М21а, 2 у категорији М21, 1 у категорији М22, 2 у категорији М23, 8 у категорији М34.

#### **4.1.2. Позитивна цитираност научних радова кандидата**

Према бази података *Web of Science* радови кандидаткиње су цитирани **114** пута, док је број цитата без аутоцитата **101**. Према истој бази h-индекс кандидаткиње је **6**.

#### 4.1.3. Параметри квалитета часописа

Др Марина Лекић је објављивала радове у часописима категорија М21а, М21, М22 и М23, при чему су подвучени импакт-фактори часописа у којима су радови публиковани након избора у претходно звање:

- 4 рада у Physical Review A (два са ИФ 3.047, један са ИФ 3,042 и један са ИФ 2,908)
- 3 рада у Optics Express (два са ИФ 4.009 и један са ИФ 3,797)
- 1 рад у Materials Research Bulletin (ИФ 2.435)
- 1 рад у Journal of Physics. B: Atomic Molecular and Optical Physics (ИФ 2,031)
- 1 рад у Journal of the Optical Society of America. B: Optical Physics (ИФ 1,970)
- 1 рад у Optical and Quantum Electronics (ИФ 1,547)
- 1 рад у Physica Scripta (ИФ 1.088)
- 3 рада у Acta Physica Polonica A (ИФ 0.433)
- 1 рад у Journal of Optoelectronics and Advanced Materials (ИФ 0.470)

Укупан импакт-фактор радова др Марине Лекић износи 34.70, а фактор утицаја радова у периоду након избора у претходно звање је 11.495. Часописи у којима кандидаткиња објављује радове су цењени по свом угледу у њеним областима рада.

Додатни библиометријски показатељи према Упутству о начину писања извештаја о изборима у звања које је усвојио Матични научни одбор за физику приказани су у следећој табели:

	ИФ	М	СНИП
Укупно	11,495	37	4.794
Усредњено по чланку	1,916	6.167	0.799
Усредњено по аутору	1.746	5.485	0.626

#### 4.1.4. Степен самосталности и степен учешћа у реализацији радова

Кандидаткиња је међу прва два аутора на 7 радова и трећи аутор на 6 радова. При изради свих публикација, др Марина Лекић је учествовала у конкретној формулацији, дискусији и решавању проблема. У свим радовима, учествовала је у поставци експеримента и процесу мерења, у анализи добијених резултата и њиховом писању. Током израде докторске дисертације у Центру за фотонику, кандидаткиња је дала велики допринос у разумевању кохерентних ефеката у резонантној интеракцији ласерског зрачења са атомском паром рубидијума. Учествовала је у реализацији различитих квантно-оптичких ефеката у лабораторији, као што су електромагнетски индукована транспаренција и нелинеарна магнето-оптичка ротација. Остварила је научну сарадњу са групом проф. Стефке Карталеве из Института за електронику "Академик Емил Ђаков", Бугарске академије

наука. Кандидаткиња је била учесник SCOPEС пројекта у коме је сарађивала са професором Антоаном Вајсом из Швајцарске на писању и постављању студентских вежби из ласерске и атомске физике. У сарадњи са професором Владимиром Шкарком са Универзитета у Анжеу, кандидаткиња се бави проучавањем просторно-временских дисипативних солитона као и вортекс солитона. Учествује у планирању и постављању експеримента као и у обради резултата мерења и анализи експерименталних резултата. Др Марина Лекић је тренутно ангажована на билатералном пројекту са Белорусијом (2020-2021.), чија је тема нелинеарна пропaгација ласерског зрачења у наносуспензијама.

#### **4.2. Ангажованост у формирању научних кадрова**

- Др Марина Лекић је држала предавања о метрологији времена и атомским часовницима студентима треће и четврте године Физичког факултета (2016-2019.)
- Члан комисије за такмичења из физике ученика средњих и основних школа (2007-2010.)
- Учесник на пројекту „Подстицајна околина за активно учење природних наука (ПОКО)“ у периоду од 2011-2014. године
- Члан тима на манифестацији „Европска ноћ истраживача“ септембар 2019. године.
- Учесник у изради и промоцији изложбе „Милева Марић и Алберт Ајнштајн кроз простор и време“.

#### **4.3. Нормирање броја коауторских радова, патената и техничких решења**

У складу са Правилником о вредновању научно истраживачког рада узета је пуна вредност М бодова за све радове до 7 аутора, а за радове са више од 7 аутора по формули  $K/(1+0.2(n-7))$ , где је К пун број М поена према категорији часописа, а n број коаутора ( $n > 7$ ). Сви радови кандидаткиње спадају у природноматематичке и експерименталне. Од избора у претходно звање кандидаткиња има 6 публикованих радова, од којих је на 2 рада више од 7 аутора.

#### **4.4. Руководијење пројектима, потпројектима и пројектним задацима**

У оквиру националног пројекта “Продукција и карактеризација нанофотонских функционалних структура и примена у биомедицини и информатици”, др Марина Лекић је руководила пројектним задатком “Генерисање различитих мода ласерског снопа и њихова примена у квантној оптици”.

Др Марина Лекић је имала водећу улогу у оснивању Лабораторије за оптоелектронику, чији је руководилац од новембра 2017. године. Лабораторија за оптоелектронику је акредитована од стране Акредитационог тела Србије за еталонирање фибер-оптичких

мерних инструмената: оптичких рефлектометара у временском домену и фибер-оптичких мерила снаге. Током 2019. године лабораторија је успешно учествовала на међународно признатом тесту провере оспособљености. Валидована је метода за еталонирање фибер-оптичких мерила снаге по апсолутној снази, на таласној дужини од 1310 nm. Билатерално поређење је извршено са националном лабораторијом Чешког метролошког института у складу са адекватним стандардима. Лабораторија за оптоелектронику је једина лабораторија у земљи и региону која пружа услуге еталонирања фибер-оптичких мерних инструмената и на тај начин сарађује са привредним субјектима у Републици Србији.

#### **4.5. Активност у научним и научно-стручним друштвима**

- Гост уредник у часопису *Optical and Quantum Electronics*, „Focus on Optics and Bio-photonics, Photonica 2017“ (2017-2018.)
- Члан Одељења Друштва физичара Србије за научна истраживања и високо образовање у Одсеку за Оптику и фотонику
- Члан програмског одбора међународне радионице 13th Photonics Workshop
- Члан организационог одбора бројних међународних и националних научних скупова:
  - Генерални секретар међународног скупа *Photonica2017 – VI International School and Conference on Photonics, 28 August - 1 September 2017, Belgrade, Serbia*
  - Председник организационог одбора *11th Photonics Workshop, March 11 – 15, 2018, Kopaonik, Serbia*
  - Председник организационог одбора *13th Photonics Workshop, March 08 – 12, 2020, Kopaonik, Serbia*
  - Члан организационог одбора *PHOTONICA09 - II International School and Conference on Photonics, 24-28 August, 2009, Belgrade, Serbia*
  - Члан организационог одбора *15th Central European Workshop on Quantum Optics CEWQO 2008, 30 May - 03 June 2008, Belgrade, Serbia*
- Члан Комисије за такмичења из физике ученика средњих и основних школа (2007-2010.)
- Члан је Оптичког друштва Србије од 2013. године.

#### **4.6. Утицајност научних резултата**

Утицајност научних радова др Лекић је детаљно приказана у одељку 4.1. овог документа. (У прилогу је списак радова и цитата)

#### **4.7. Конкретан допринос кандидата у реализацији радова у земљи и иностранству**



Кандидаткиња је значајно допринела сваком раду на коме је учествовала. У истраживањима у квантној оптици, тачније у кохерентној спектроскопији паре рубидијума, кандидаткиња је још као докторанд поставила експеримент и покренула истраживања на тему утицаја Раман-Ремзијевог ефекта на облик и ширину резонанци нелинеарне магнето-оптичке ротације у вакуумској ћелији применом оригиналне конфигурације која омогућава просторно раздвајање снопова пумпе и пробе. Кандидаткиња је поставила експеримент, вршила мерења, обрађивала резултате и у највећем броју случајева писала радове и вршила кореспонденцију са часописима. На основу својих искустава прикупљених током постдокторског боравка у иностранству (Лабораторија за фотонику, Универзитет у Анжеу) др Лекић је поставила експеримент за истраживање само-организованих дводимензионалних дисипативних солитона коришћењем фемтосекундних ласера. Резултати и анализа мерења на овом експерименту објављени су у раду у међународном часопису и на међународним конференцијама.

## 5. Елементи за квантитативну оцену научног доприноса кандидата

Остварени резултати у периоду након претходног избора у звање:

Категорија	М бодова по раду	Број радова	Укупно М бодова	Нормирани број М бодова
M21a	10	1	10	10
M21	8	2	16	12,45
M22	5	1	5	5
M23	3	2	6	4,88
M28b	2,5	1	2,5	2,5
M34	0,5	8	4,0	4,0
M36	1,5	1	1,5	1,5
M66	1,0	1	1,0	1,0

Поређење са минималним квантитативним условима за реизбор у звање научни сарадник

Минимални број М бодова		Остварено М бодова без нормирања	Остварено, нормирани број М бодова
Укупно	16	46	41,33
M10+M20+M31+M32+M33+M41+M42	10	39,5	34,83
M11+M12+M21+M22+M23	6	37	32,33

## **6. Списак радова др Марине Лекић (Мијаиловић)**

### **Рад у међународном часопису изузетних вредности (M21a)**

*Радови објављени након претходног избора у звање:*

1. V. Skarka, N.B. Aleksic, M.M. Lekic, B. N. Aleksic, B.A. Malomed, D. Mihalache, H. Leblond, "Formation of complex two-dimensional dissipative solitons via spontaneous symmetry breaking", Phys. Rev. A, vol. 90 (2), (2014)

*Радови објављени пре претходног избора у звање:*

1. A. J. Krmpot, M. M. Mijailović, B. M. Panić, D. V. Lukić, A. G. Kovačević, D. V. Pantelić, and B. M. Jelenković, "Sub-Doppler absorption narrowing in atomic vapor at two intense laser fields", Opt. Express 13, Iss. 5, pp. 1448-1456, (2005)

2. M. M. Mijailovic, J. Dimitrijevic, A. J. Krmpot, Z. D. Grujic, B. M. Panic, D. Arsenovic, D. V. Pantelic, and B. M. Jelenkovic, "On non-vanishing amplitude of Hanle electromagnetically induced absorption in Rb", Opt. Express 15, Iss. 3, pp.1328-1339, (2007)

3. J. Dimitrijević, A. Krmpot, M. Mijailović, D. Arsenović, B. Panić, Z. Grujić, and B. M. Jelenković, "Role of transverse magnetic fields in electromagnetically induced absorption for elliptically polarized light" Phys. Rev. A 77, 013814 (2008)

4. J. Dimitrijevic, Z. Grujic, M. M. Mijailovic, D. Arsenovic, B. M. Panic, and B. M. Jelenkovic "Enhancement of electromagnetically induced absorption with elliptically polarized light - laser intensity dependent coherence effect", Opt. Express 16, Iss. 2, pp.1343-1353, (2008)

5. Z. D. Grujić, M. Mijailović, D. Arsenović, A. Kovačević, M. Nikolić, and B. M. Jelenković "Dark Raman resonances due to Ramsey interference in vacuum vapor cells" Phys. Rev. A 78, 063816 (2008)

6. M. Mijailović, Z. D. Grujić, M. Radonjić, D. Arsenović, and B. M. Jelenković "Nonlinear magneto-optical rotation narrowing in vacuum gas cells due to interference between atomic dark states of two spatially separated laser beams", Phys. Rev. A 80, 053819, (2009)

### **Радови у врхунским међународним часописима (M21)**

*Радови објављени након претходног избора у звање:*

1. Z D Grujić, M M Lekić, M Radonjić, D Arsenović and B M Jelenković "Ramsey effects in coherent resonances at closed transition  $F_g = 2 \rightarrow F_e = 3$  of  $87\text{Rb}$ " J. Phys. B: At. Mol. Opt. Phys. 45, 245502, (2012)

2. A. G. Kovacevic, J. L. Ristic-Djurovic, M.M. Lekic, B. B. Hadzic, G.S.I. Abudagel, S.J. Petricevic, P. M. Mihailovic, B.Z. Matovic, D. M. Dramlic, Lj. M. Brajovic, N. Z. Romcevic,

Influence of femtosecond pulsed laser irradiation on bismuth germanium oxide single crystal properties,” Mater. Res. Bull., vol. 83, 284-289 ( 2016)

### **Радови у истакнутим међународним часописима (M22)**

*Радови објављени након претходног избора у звање:*

1. Ivan S. Radojčić, Milan Radonjić, Marina M. Lekić, Zoran D. Grujić, Dragan Lukić, and Branislav Jelenković “Raman–Ramsey electromagnetically induced transparency in the configuration of counterpropagating pump and probe in vacuum Rb cell ”, J. Opt. Soc. Am. B 32, 426-430 (2015)

*Радови објављени пре претходног избора у звање:*

1. Zoran Grujić, Dušan Arsenović, Milan Radonjić, Marina Mijailović and Branislav Jelenković “Numerical simulation of Raman resonance due to the Ramsey interference induced by thermal motion of atoms” Phys. Scr. T135, 014026 (2009)

### **Радови у међународним часописима (M23)**

*Радови објављени након претходног избора у звање:*

1. GSI Abudagel, S.J. Petričević, P.M. Mihailović, A.G. Kovačević, J. Ristić-Djurović, M.M. Lekić, M.J. Romčević, S. Cirković, J.M. Trajić, N.Ž. Romčević, "Improvement of magneto-optical quality of high purity Bi<sub>12</sub>GeO<sub>20</sub> single crystal induced by femtosecond pulsed laser irradiation", Optoelectronics and Advanced Materials – Rapid Communications, vol. 11, br. 7-8, 477-481 (2017)

1. V. Skarka, M. M. Lekić, A. G. Kovačević, B. Zarkov, N. Ž. Romčević "Solitons generated by self-organization in bismuth germanium oxide single crystals during the interaction with laser beam", Optical and quantum electronics, vol. 50 (1), (2018)

*Радови објављени пре претходног избора у звање:*

1. Z. D. Grujić, M.M. Mijailović, B.M. Panić, M. Minić, A.G. Kovačević, M. Obradović, B.M. Jelenković and S. Cartaleva  
“Zeeman Coherences Narrowing due to Ramsey Effects Induced by Thermal Motion of Rubidium Atoms“, ACTA PHYSICA POLONICA A No. 5, Vol. 112 (2007)

2. J. Dimitrijević, Z. Grujić, M. Mijailović, D. Arsenović, B. Panić and B.M. Jelenković  
“Effect of Laser Light Ellipticity on Hanle Electromagnetically Induced Absorption Amplitude and Line Width“, ACTA PHYSICA POLONICA A No. 5, Vol. 112 (2007)

3. S. Cartaleva, T. Karaulanov, N. Petrov, D. Slavov, K. Vaseva, A. Yanev, M. Mijailović, Z. Grujić and B.M. Jelenković, “All-Optical Magnetometer Based on Resonant Excitation of Rubidium Atoms by Frequency Modulated Diode Laser Light“, ACTA PHYSICA POLONICA A No. 5, Vol. 112 (2007)

## Саопштења са међународних скупова штампана у целини (М33)

*Радови објављени пре претходног избора у звање:*

1. M. M. Lekić, A. Krmpot, B. M. Panić, B. M. Jelenković and D. Pantelić, “Study of the Coherent Population Trapping with the Hanle Effect Configuration” Proceedings of 22nd Summer School and International Symposium on the Physics of Ionized Gases SPIG 2004 Pg 35-38 (2004)
2. A. Krmpot, M. Lekić, B. Panić, D. Pantelić and B. M. Jelenković, “Electromagnetically Induced Transparency and Absorption in a Three Level  $\Lambda$  and V Systems”, Proceedings of 22nd Summer School and International Symposium on the Physics of Ionized Gases SPIG 2004 Pg 39-42 (2004)
3. A. J. Krmpot, M. M. Lekić, B. M. Panić, D. Lukić, A. Kovačević, D. Pantelić, B. M. Jelenković, “SUB-DOPPLER NARROWING OF ABSORPTION IN V-TYPE AND  $\Lambda$ -TYPE ATOM AT INTENSE LASER FIELDS”, 13th International School on Quantum Electronics: Laser physics and applications, Proc. SPIE Vol. 5830, 186 (2005)
4. Z. D. Grujić, M. M. Mijailović, A. J. Krmpot, A. G. Kovačević, D. V. Pantelić, and B. M. Jelenković, “Enhanced polarization in bright states via atomic coherence”, Proceedings of 23rd Summer School and International Symposium on the Physics of Ionized Gases SPIG 2006 Pg 33-36 (2006)
5. M. M. Mijailović, Z. D. Grujić, N. Petrov, A. J. Krmpot, B. M. Panić, D. Arsenović, D. V. Pantelić, and B. M. Jelenković, “Electromagnetically Induced Transparency in Hanle Configuration: The Case of Closed Atomic System”, Proceedings of 23rd Summer School and International Symposium on the Physics of Ionized Gases SPIG 2006, Pg 51-54 (2006)
6. Marina M. Mijailović, Jelena Dimitrijević, Zoran Grujić, Bratimir M. Panić, Dušan Arsenović, Dejan Pantelić, and Branislav M. Jelenković, “Absorption of elliptically polarized light in closed transitions of Rb vapor” , 14th International School on Quantum Electronics: Laser Physics and Applications Proc. SPIE, Vol. 6604, 66040D (2007)
7. Z. D. Grujić, M. M. Mijailović, A. J. Krmpot, B. M. Panić, D. V. Pantelić, and B. M. Jelenković, “Non-linear magneto-optical polarization rotation in dark and bright coherent states” 14th International School on Quantum Electronics: Laser Physics and Applications, Proc. SPIE, Vol. 6604, 66040E (2007)
8. T. Karaulanov, A. Yanev, S. Cartaleva, D. Slavov, N. Petrov, M. M. Mijailović, Z. D. Grujić, and A. J. Krmpot, “Coherent population trapping resonances on the D1 line of rubidium”, 14th International School on Quantum Electronics: Laser Physics and Applications, Proc. SPIE, Vol. 6604, 66040C (2007)
9. B. M. Jelenković, D. Arsenović, Z. Grujić, M. Radonjić, and M. Mijailović, “Open system CPT with spatially separated pump and probe beams” 15th International School on Quantum Electronics: Laser Physics and Applications, Proc. SPIE, Vol. 7027, 70270D (2008); DOI:10.1117/12.822450

10. Zoran D. Grujić, Marina M. Mijailović, Dimitar G. Slavov, Dušan Arsenović, Branislav M. Jelenković, “Nonlinear magneto-optical rotation narrowing due to Ramsey effect induced by thermal motion of atoms”, 15th International School on Quantum Electronics: Laser Physics and Applications, Proc. SPIE, Vol. 7027, 70270L (2008); DOI:10.1117/12.822460

### **Саопштења са међународних скупова штампана у изводу (M34)**

*Радови објављени након претходног избора у звање:*

1. I. S. Radojičić, Z. D. Grujić, M. M. Lekić, D. V. Lukić and B. M. Jelenković, “Narrowing of EIT resonance in the configuration of counter-propagation laser beams”, PHOTONICA 2011 International School and Conference on Photonics 29 August – 02 September 2011 Belgrade, Serbia
2. M. Radonjić, Z. Grujić, M. Lekić, S. Nikolić, A. Krmpot, N. Lučić, B. Zlatković, I. Radojičić, D. Arsenović and B. M. Jelenković, “Influence of Ramsey interference in space and time domains on electromagnetically induced coherent resonances”, PHOTONICA 2013, IV International School and Conference on Photonics, 26<sup>th</sup> - 30<sup>th</sup> August, 2013 Belgrade, Serbia
3. I. S. Radojičić, M. M. Radonjić, Z. D. Grujić, M. M. Lekić, D. V. Lukić, and B. M. Jelenković, “Ramsey effect on linewidth of coherent resonances in vacuum Rb cell”, PHOTONICA 2013, IV International School and Conference on Photonics, 26<sup>th</sup> - 30<sup>th</sup> August, 2013 Belgrade, Serbia
4. I. Radojičić, M. Radonjić, Z. Grujić, M. Lekić, D. Lukić and B. M. Jelenković ”Robust narrowing of dark resonances in Rb vapor with coaxial counter-propagating laser beams”, 18th International School on Quantum Electronics “Laser physics and applications” 29 September – 3 October 2014, Sozopol, Bulgaria
5. V. Skarka, M. Lekić, A. Kovačević, B. Zarkov, and N. Z. Romčević, “Solitons generated by self-organization in bismuth germanium oxide single crystals during the interaction with laser beam”, PHOTONICA 2017 The Sixth International School and Conference on Photonics, 28 August – 1 September 2017 Belgrade, Serbia
6. A. G. Kovačević, S. Petrović, M. Lekić, Branislav M. Jelenković, ” Inducing LIPSS by multi-pass and cross-directional scanning of femtosecond beam over surface of thin metal films”, Book of Abstracts UltrafastLight-2018 (2018), 108 (International Conference on Ultrafast Optical Science, Moscow, 2018-10- 01—05)
7. M. Lekić, I. Milosević, S. Rokotoarimalala and V. Skarka, ”Self-organization of soliton-tweezers in suspensions of nanocomposites and graphens”, PHOTONICA 2019 The Seventh International School and Conference on Photonics, 26 August – 30 August 2019 Belgrade, Serbia
8. A. G. Kovačević, S. M. Petrović, B. Salatić, M. Lekić, B. Vasić, R. Gajić, D. Pantelić and B. M. Jelenković, ” Inducing LIPSS on multilayer thin metal films by femtosecond laser beam of different orientations”, PHOTONICA 2019 The Seventh International School and Conference on Photonics, 26 August – 30 August 2019 Belgrade, Serbia



*Радови објављени пре претходног избора у звање:*

1. Krmpot, M. Lekić, B. Panić, D. Lukić, D. Pantelić, B. M. Jelenković, "COHERENT POPULATION TRAPPING IN DIFFERENT  $\square$  SYSTEMS - WITH NEAR DEGENERATE AND WELL SEPARATED TWO LOWER LEVELS", Proceedings of The eighth European Conference on Atomic and Molecular Physics (ECAMP VIII), July 6-10, 2004, Rennes, France, Volume 28F, Part II, Pg 4-67
2. Z. D. Grujić, M. M. Mijailović, A. J. Krmpot, B. M. Panić, D. V. Pantelić, and B.M Jelenković, "Dark resonances in the D2 line of 87Rb in the vapor cell with co- and counter-propagating waves", Proceedings of 37th European Group for Atomic Systems (EGAS), 3-6 August, Dublin, Ireland, 2005, Pg 153
3. M. M. Mijailović, Z. D. Grujić, A. J. Krmpot, B. M. Panić, D. M. Arsenović D. V. Pantelić, and B.M Jelenković, "Switching from electromagnetically induced absorption to transmission in CPT-Hanle experiment in 85Rb", Proceedings of 37th European Group for Atomic Systems (EGAS), 3-6 August, Dublin, Ireland, 2005, Pg 154
4. Z. D. Grujić, M. M. Mijailović, A. J. Krmpot, B. M. Panić, D. V. Pantelić, and B.M Jelenković, "Enhanced non-linear Faraday effect in bright coherent state" Proceedings of 38th European Group for Atomic Systems (EGAS), 7-10 June, Ischia, Italy, 2006, Pg 221
5. M. M. Mijailović, Z. D. Grujić, A. J. Krmpot, B. M. Panić, D. Arsenović, D. V. Pantelić, and B.M Jelenković, "Enhanced non-linear Faraday effect in bright coherent state" Proceedings of 38th European Group for Atomic Systems (EGAS), 7-10 June, Ischia, Italy, 2006, Pg 222
6. J. Dimitrijević, A. J. Krmpot, M. M. Mijailović, Z. D. Grujić, D. Arsenović, and B.M Jelenković, "ELECTROMAGNETICALLY INDUCED TRANSPARENCIES IN CIRCULARLY POLARIZED LIGHT IN CROSSED MAGNETIC FIELD", Proceedings of the 9th European Conference on Atomic and Molecular Physics (ECAMP IX), May 6-11, 2007, Heraklion, Greece, Europhysics conference abstracts, Pg Mo4-9
7. A. J. Krmpot, J. Dimitrijević, M. M. Mijailović, Z. D. Grujić, D. Arsenović, and B.M Jelenković, "INTENSITY DEPENDENT LINE-WIDTHS OF HANLE ELECTROMAGNETICALLY INDUCED ABSORPTION TO TRANSVERSE MAGNETIC FIELDS", Proceedings of The 9th European Conference on Atomic and Molecular Physics (ECAMP IX), May 6-11, 2007, Heraklion, Greece, Europhysics conference abstracts, Pg Mo4-23
8. Z. Grujić, M. Mijailović, D. Arsenović M. Radonjić and B. M. Jelenković, "DARK RESONANCE NARROWING IN UNCOATED RUBIDIUM VACUUM VAPOR CELL", Proceedings of 40th European Group for Atomic Systems (EGAS), 2-5 July, Graz, Austria, 2008, Pg 172



## POTVRDA

Ovom izjavom potvrđujemo da je MARINA LEKIĆ – naučni saradnik zaposlena u Institutu za fiziku u Beogradu, u periodu 2016-2019 godine, držala predavanja iz Metrologije vremena (dva časa po semestru), a u okviru nastavnih predmeta Metrologija i Metrologija sa standardizacijom na Fizičkom fakultetu Univerziteta u Beogradu.

Beograd

06.02.2020. god.

Predmetni nastavnik

Prof.dr. Bećko Kasalica

A handwritten signature in cursive script, written in black ink, positioned above a horizontal line. The signature appears to read 'Bećko Kasalica'.

Dekan Fizičkog fakulteta

Univerziteta u Beogradu

Prof.dr. Ivan Belča

A handwritten signature in cursive script, written in black ink, positioned above a horizontal line. The signature appears to read 'Ivan Belča'.



**48. РЕПУБЛИЧКО ТАКМИЧЕЊЕ ИЗ ФИЗИКЕ  
УЧЕНИКА СРЕДЊИХ ШКОЛА ШКОЛСКЕ 2009/2010. ГОДИНЕ**

17.4.2010. Гимназија “Вељко Петровић”, СОМБОР

ПРЕГЛЕДАЧИ ЗАДАТАКА  
(прелиминарна листа састављена на дан 14.04.2010)

I разред, 92 ученика

1. мр Зоран Мијић (аутор), Институт за физику, Београд-Земун
2. **Марина Мијаиловић, Институт за физику, Београд-Земун**
3. мр Срђан Марјановић, Институт за физику, Београд-Земун
4. др Имре Гут, Департман за физику, ПМФ, Нови Сад
5. Мирко Киселички, Гимназија Суботица
6. Сања Матијашевић, Министарство просвете, Крушевац

II разред, 82 ученика

1. Маја Рабасовић (аутор), Институт за физику, Београд-Земун
2. др Драган Маркушев (рецензент), Институт за физику, Београд-Земун
3. Драгана Павловић, Институт за физику, Београд-Земун
4. мр Сања Тошић, Институт за физику, Београд-Земун
5. Наташа Каделбург, Математичка гимназија, Београд
6. Саша Стојановић, Гимназија Лесковац

III разред, 72 ученика

1. др Андријана Жекић (аутор)
2. др Срђан Ракић, Департман за физику, ПМФ, Нови Сад
3. мр Александра Нина, Институт за физику, Београд-Земун
4. мр Маја Стојановић, Департман за физику, ПМФ, Нови Сад
5. Катарина Ђорђевић, 1. Краг. Гимназија, Крагујевац

IV разред, 66 ученика

1. мр Александар Крмпот (аутор), Институт за физику, Београд-Земун
2. др Ђорђе Спасојевић (рецензент), Физички факултет, Београд
3. Стеван Јанков, Департман за физику, ПМФ, Нови Сад
4. др Драгана Марић, Институт за физику, Београд-Земун
5. др Невена Пуач, Институт за физику, Београд-Земун
6. Предраг Стојаковић, Гимназија Ваљево



**47. РЕПУБЛИЧКО ТАКМИЧЕЊЕ ИЗ ФИЗИКЕ  
УЧЕНИКА СРЕДЊИХ ШКОЛА ШКОЛСКЕ 2008/2009. ГОДИНЕ**

04.4.2009. VIII београдска гимназија, БЕОГРАД

**ПРЕГЛЕДАЧИ ЗАДАТАКА**

**I разред**

1. мр. Зоран Мијић (аутор), Институт за физику, Београд-Земун
2. мр Александра Нина, Институт за физику, Београд-Земун
3. **Марина Мијаиловић, Институт за физику, Београд-Земун**
4. др. Невена Пуач, Институт за физику, Београд-Земун
5. Стеван Јанков, Департман за физику, ПМФ, Нови Сад
6. Никола Шкоро, Институт за физику, Београд-Земун

**II разред**

1. Маја Рабасовић (аутор), Институт за физику, Београд-Земун
2. др Драган Маркушев (рецензент), Институт за физику, Београд-Земун
3. Драгана Павловић, Институт за физику, Београд-Земун
4. мр Ненад Сакан, Институт за физику, Београд-Земун
5. др Марија Радмиловић-Рађеновић, Институт за физику, Београд-Земун
6. мр Сања Тошић, Институт за физику, Београд-Земун

**III разред**

1. доц. др Андријана Жекић (аутор), Физички факултет, Београд
2. Проф. др Иван Манчев, Одсек за физику, ПМФ, Ниш
3. Сања Матијашевић, Министрство просвете, Крушевац
4. др Маја Стојановић, Департман за физику, ПМФ, Нови Сад
5. др Душан Поповић, Физички факултет, Београд
6. Проф. др Имре Гут, Департман за физику, ПМФ, Нови Сад

**IV разред**

1. мр Александар Крмпот (аутор), Институт за физику, Београд-Земун
2. доц. др Ђорђе Спасојевић (рецензент), Физички факултет, Београд
3. Зоран Грујић, Институт за физику, Београд-Земун
4. доц. др Срђан Ракић, Департман за физику, ПМФ, Нови Сад
5. Др Драгана Марић, Институт за физику, Београд-Земун

Председник Комисије за такмичења Друштва физичара Србије  
Проф. др Мићо Митровић, Физички факултет, Београд



*Комисија за преглед задатака на Републичком такмичењу из физике ученика основних школа одржаном 31.03.2007.године у Трстенику*

*Председник комисије за основну школу*

*Проф. др Надежда Новаковић*

*Председник комисије за такмичења*

*Проф. Мићо Митровић*

*Потпредседник Друштва Физичара Србије*

*Проф. др Илија Савић*

**Шести разред:**

- 1. Проф. др Надежда Новаковић*
- 2. Проф. др Мирослав Николић*
- 3. Марина Мијаиловић***
- 4. Стана Мишић Ковачевић*
- 5. Сања Матијашевић*



**Седми разред:**

- 1. Проф. др Иван Манчев*
- 2. Др Драган Маркушев*
- 3. Доц. др Горан Попарић*
- 4. Мр Зоран Мијић*
- 5. Зоран Грујић*

**Осми разред:**

- 1. Доц. др Срђан Ракић*
- 2. Доц. др Љубиша Нешић*
- 3. Александар Крмпот*
- 4. Стеван Јанков*



## 45.Републичко такмичење из физике

### Комисија за преглед задатака

Председник комисије

Проф. др Мићо Митровић, Физички факултет, Београд

I разред

1. Проф. др Александар Срећковић, Физички Факултет, Београд
2. мр Зоран Мијић, Институт за физику, Београд
3. др Велибор Новаковић, Институт за физику, Београд
4. Предраг Стојаковић, Гимназија, Ваљево
5. Мирјана Нешић, Институт за физику, Београд
6. **Марина Мијаиловић, Институт за физику, Београд**
7. Милутин Вучковић, Гимназија, Смедерево
8. Катарина Ђорђевић, Прва Крагујевачка гимназија
9. Мирко Киселички, Гимназија, Суботица
10. Далибор Делибашић, Гимназија, Аранђеловац

II разред

1. Зоран Грујић, Институт за физику, Београд
2. Александра Нина, Институт за физику, Београд
3. Стеван Јанков, ПМФ, Нови Сад
4. Љиљана Сворцан, Пета Београдска гимназија
5. Наташа Каделбург, Математичка гимназија, Београд

III разред

1. доц. др Андријана Жекић, Физички Факултет, Београд
2. др Душан Поповић, Физички Факултет, Београд
3. Проф. др Иван Манчев, ПМФ, Ниш
4. Сања Матијашевић, Министарство просвете, Крушевац
5. мр Владимир Срећковић, Институт за физику, Београд

IV разред

1. Александар Крмпот, Институт за физику, Београд
2. др Драгана Марић, Институт за физику, Београд
3. доц. Др Срђан Ракић, ПМФ, Нови Сад
4. Никола Шкоро, Институт за физику, Београд
5. мр Невна Пуач, Институт за физику, Београд



Projekt	3D Udžbenik	Publikacije	Prikazi u medijima	Promotivne aktivnosti	Smart phone science	Linkovi	Kontakt
---------	-------------	-------------	--------------------	-----------------------	---------------------	---------	---------

## ***TIM SARADNIKA***

na projektima

"Podsticajna okolina za aktivno učenje prirodnih nauka"

„Naučna vizuelizacija u školskom prostoru i na pametnom telefonu“

### ***Tim saradnika u 2015.***

Mirjana Popović-Božić, Institut za fiziku, Univerzitet u Beogradu, vodja tima

Ilija Savić, Fizički fakultet, Univerzitet u Beogradu

Nenad Vukmirović, Institut za fiziku, Univerzitet u Beogradu

Darko Vasiljević, Institut za fiziku, Univerzitet u Beogradu

Zoran Mijić, Institut za fiziku, Univerzitet u Beogradu

Milena Davidović, Građevinski fakultet, Univerzitet u Beogradu

Jovica Milisavljević, Matematička gimnazija, Beograd

Biljana Stojičić, Zemunski gimnazija, Beograd

Goran Stojićević, Centar za stručno usavršavanje, Šabac

Milenija Joksimović, Hemijsko-prehrambena tehnološka škola, Beograd

Ljiljana Ivančević, Osnovna škola „Djordje Krstić“, Beograd

Marijana Jović Lučić, Osnovna škola „Djordje Krstić“, Beograd

Tatjana Marković Topalović, Medicinska škola dr Andra Jovanović, Šabac

Jovana Mišić, Osnovna škola Ujedinjenih nacija, Beograd

Jelena Živanović, Zemunski gimnazija, Beograd

Sanja Bulat, Osnovna škola „Branislav Nušić“, Beograd

Milica Cvetković, Institut za fiziku, Univerzitet u Beogradu

### ***Tim saradnika u 2014.***

Mirjana Popović-Božić, Marina Lekić, Zoran Mijić - Institut za fiziku, Beograd-Zemun

Goran Stojićević, direktor; Tatjana Marković-Topalović (Medicinska škola u Šapcu), Centar za stručno usavršavanje, Šabac

Dragoljub Cucić, direktor - Centar za talente Mihajlo Pupin, Pančevo

Ljiljana Ivančević, Jelena Volarov, Tatjana Ilić-Marković, Ivan Starčević Osnovna škola Đorđe Krstić

Jovica Milosavljević, Dragica Ivković, Slobodan Spremo - Matematička gimnazija, Beograd

Biljana Stojičić, - Zemunski gimnazija

Grujović Danijela, Aleksandra Milošević - Šesta beogradska gimnazija

Ilija Savić, Društvo fizičara Srbije

Josip Sliško, Facultad de Ciencias Fisico Matematicas, Benemerita Universidad Autonoma de Puebla, Mexico

Milena Davidović, Građevinski fakultet, Beograd

Dušanka Obadović, Pedagoški fakultet, Sombor

Boban Zarkov, Direkciji za mere i dragocene metale

Gordana Božić-Ivanović, Viša strukovna tekstilna škola za dizajn i menadžment, Beograd

Društvo fizičara Srbije (skoro svi saradnici su članovi DFS)

### ***Tim saradnika u 2013.***

Mirjana Popović-Božić, Marina Lekić, Zoran Mijić - Institut za fiziku, Beograd-Zemun

Goran Stojićević, direktor; Tatjana Marković-Topalović (Medicinska škola u Šapcu), Centar za stručno usavršavanje, Šabac

Dragoljub Cucić, direktor - Centar za talente Mihajlo Pupin, Pančevo

Ljiljana Ivančević, Jelena Volarov, Tatjana Ilić-Marković, Ivan Starčević Osnovna škola Đorđe Krstić

Jovica Milosavljević, Dragica Ivković, Slobodan Spremo - Matematička gimnazija, Beograd

Biljana Stojičić, - Zemunski gimnazija

Grujović Danijela, Aleksandra Milošević - Šesta beogradska gimnazija

Ilija Savić, Društvo fizičara Srbije

Josip Sliško, Facultad de Ciencias Fisico Matematicas, Benemerita Universidad Autonoma de Puebla, Mexico

Milena Davidović, Građevinski fakultet, Beograd

Dušanka Obadović, Pedagoški fakultet, Sombor

Boban Zarkov, Direkciji za mere i dragocene metale

Gordana Božić-Ivanović, Viša strukovna tekstilna škola za dizajn i menadžment, Beograd

Društvo fizičara Srbije (skoro svi saradnici su članovi DFS)

### ***Tim saradnika u 2012.***

Ažuriranje u toku

### ***Tim saradnika u 2011.***

Jelena Volarov, OŠ "Đorđe Krstić", Beograd

Boban Zarkov, Direkcija za mere i dragocene metale, Beograd

Ljiljana Ivančević, OŠ "Đorđe Krstić", Beograd

Marina Lekić, Institutu za fiziku, Beograd

Zoran Mijić, Institut za fiziku, Beograd

Bratimir Panić, Institut za fiziku, Beograd

Mr Goran Stojićević, CSU Šabac - Centar za stručno usavršavanje

Nataša Čaluković, Matematička gimnazija, Beograd

Tim za školsko razvojno planiranje OŠ "Đorđe Krstić"

### ***Tim saradnika u 2010.***

Prof. Dr. Mirjana Popović Božić (koordinator, Institut za fiziku i Fizički fakultet, Beograd)

Dr. Milena Davidović, Građevinski fakultet, Beograd

Dr. Ljiljana Kostić, Prirodnomatemički fakultet, Niš

Vigor Majić, Istraživačka stanica, Petnica

Dragana Milićević, Gimnazija Kruševac

Vesna Milićević, d.i.a.

Dragoljub Milutinović, arhitekta, TES, Šabac

Prof. Dr. Dušanka Obadović, Departman za fiziku, PMF, Novi Sad

Dr. Dejan Pantelić, Institut za fiziku, Beograd

Aleksandar Petrović, Geografski fakultet, Beograd

Dr. Marko Popović, Institut za fiziku, Beograd

Dr. Đorđe Spasojević, Fizički fakultet, Beograd

Prof. Dr. Ilija Savić, Društvo fizičara Srbije

Mr. Nataša Stanić, Narodna observatorija i planetarijum, Beograd

Branislav Stanković, Narodni muzej, Šabac

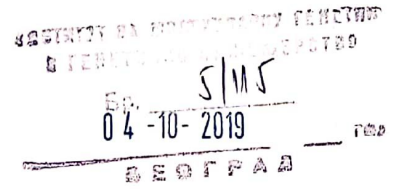
Mr. Tatjana Marković Topalović, Medicinska škola, Šabac

Mr. Dragoljub Cucić, Centar za talente "Mihajlo Pupin", Pančevo



INSTITUT ZA MOLEKULARNU GENETIKU  
I GENETIČKO INŽENJERSTVO  
Univerzitet u Beogradu

Vojvode Stepe 444a | P. Fah 23 | 11010 Beograd | Republika Srbija  
Tel. (011) 397 57 44 | Faks (011) 397 58 08 | t.r. 160-350089-28 | PIB 101736673



POTVRDA

Marina Lekić, zaposlena u Institutu za fiziku Univerziteta u Beogradu, učestvovala je na manifestaciji Evropska noć istraživača održanoj 27. i 28. septembra 2019. godine u okviru projekta "Science in Motion for Friday Night Commotion 2018-19" (SCIMFONICOM2018-19, EU projekat H2020-MSCA-NIGHT-818747), u organizaciji Instituta za molekularnu genetiku i genetičko inženjerstvo i Fakulteta za fizičku hemiju Univerziteta u Beogradu.

*Zubayr*

Dr Aleksandra Divac Rankov  
Rukovodilac SCIMFONICOM2018-19  
Institut za molekularnu genetiku i genetičko inženjerstvo  
Vojvode Stepe 444a, 11010 Beograd, Srbija  
tel: 011/3976658  
e-mail: aleksandrdivac@imgge.bg.ac.rs



## ПОТВРДА

О ангажовању др Марине Лекић на вођењу задатка на пројекту Министарства просвете, науке и технолошког развоја:

*Продукција и карактеризација нанофотонских функционалних структура и примена у биомедицини и информатици – ИИИ 45016*

Марина Лекић је руководила задатком *Генерисање различитих мода ласерског снопа и њихова примена у квантној оптици.*

Задатак је за циљ имао примену холографских узорака за реализовање недифрактујућег снопа са вортекс профилем. Такав профил снопа је омогућио оригинални начин примене Ремзијеве методе одвојених побуда рубидијумових атома. Метода, позната у примени атомских снопова за атомске еталоне фреквенције и времена, омогућила је да се добију знатно уже ЕИТ (електромагнетна индукована транспаренција) резонанце.

Руководилац пројекта 45016



Бранислав Јеленковић

Научни саветник Института за физику Београд

UNIVERZITET U BEOGRADU  
INSTITUT ZA FIZIKU  
0801/Br. 1595/1  
26-09-2016 год.



На основу члана 27. Статута Института за физику 0801 бр. 285/4 од 30. маја 2011. године (измене и допуне на седницама 17.06.2013.год. и 23.12.2014.год.), директор Института за физику доноси

### О Д Л У К У

У Институту за физику се формира Лабораторија за оптоелектронику као саставни део Центра изузетних вредности за фотонику.

У лабораторији има 4 извршиоца послова и радних задатака и то:

- Руководилац Лабораторије
- Руководилац квалитета Лабораторије
- Технички руководиоца Лабораторије
- Стручни сарадник Лабораторије

Број извршилаца послова и радних задатака усклађује се сагласно плану и програму рада Института за физику и Лабораторије за оптоелектронику као и Правилника о систематизацији радних места Института за физику.

Ова одлука је допуна раније одлуке од 04.06.2015. године.

У Београду, 26. септембар 2016. године



ДИРЕКТОР ИНСТИТУТА ЗА ФИЗИКУ

др Александар Богојевић



На основу члана 27. Статута Института за физику 0801 бр. 285/4 од 30. маја 2011. године (измене и допуне на седницама 17.06.2013.год. и 23.12.2013.год.) и Пословника о квалитету Лабораторије за оптоелектронику а у складу са стандардом SRPS ISO IEC 17025:2006, директор Института за физику издаје

### ОВЛАШЋЕЊА ЗА РАД

- 1) Др Марина Лекић, овлашћује се да ради на месту руководиоца Лабораторије за оптоелектронику на пословима који су за ту функцију дефинисани Пословником о квалитету Лабораторије за оптоелектронику.
- 2) Проф. др Дејан Пантелић, овлашћује се да ради на месту руководиоца квалитета Лабораторије за оптоелектронику на пословима који су за ту функцију дефинисани Пословником о квалитету Лабораторије за оптоелектронику. Исти се овлашћује и за заменика руководиоца Лабораторије за оптоелектронику.
- 3) Душан Грујић, овлашћује се да ради на месту техничког руководиоца Лабораторије за оптоелектронику на пословима који су за ту функцију дефинисани Пословником о квалитету Лабораторије за оптоелектронику.
- 4) Иван Радојичић, овлашћује се да ради на месту стручног сарадника Лабораторије за оптоелектронику на пословима који су за ту функцију дефинисани Пословником о квалитету Лабораторије за оптоелектронику.

У Београду,

01. 11. 2017. године



Директор Института за физику

Др Александар Богојевић



**Акредитационо тело Србије**

Accreditation Body of Serbia

**01533**



**Београд**

Belgrade

**додељује**  
awards

# **СЕРТИФИКАТ О АКРЕДИТАЦИЈИ**

Accreditation Certificate

**којим се потврђује да тело за оцењивање усаглашености**  
confirming that Conformity Assessment Body

**Институт за физику, Центар за фотонику  
Лабораторија за оптоелектронику  
Београд-Земун**

**акредитациони број**

accreditation number

**02-067**

**задовољава захтеве стандарда**

fulfils the requirements of  
**SRPS ISO/IEC 17025:2017**  
(*ISO/IEC 17025:2017*)

**те је компетентно за обављање послова еталонирања**  
and is competent to perform calibration activities

**који су специфицирани у важећем издању Обима акредитације**  
as specified in the valid Scope of Accreditation

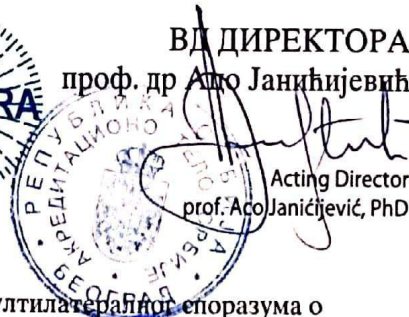
Важеће издање Обима акредитације доступно је на интернет адреси: [www.ats.rs](http://www.ats.rs)  
Valid Scope of Accreditation can be found at: [www.ats.rs](http://www.ats.rs)

Акредитација додељена  
Date of issue

**02.12.2019.**

Акредитација важи до  
Date of expiry

**19.01.2021.**



**ВД ДИРЕКТОРА**

**проф. др Ацо Јанићјевић**

Acting Director

prof. Aco Janićević, PhD

Акредитационо тело Србије је потписник Мултилатералних споразума о признавању еквивалентности система акредитације Европске организације за акредитацију (EA MLA) и ILAC MRA споразума у овој области. / ATS is a signatory of the EA MLA and ILAC MRA in this field.

**Institute of Physics Belgrade,  
Laboratory for optoelectronics  
Marina Lekić  
Pregrevica 118  
11080 Zemun, Belgrade  
Serbia**

Our reference number: CMI-4547/2019/0318      Contact person: Mgr. Jiří Herec, Ph.D.      Datum: 11.09.2019      Brno

**Final evaluation of the bilateral interlaboratory comparison**

Your laboratory has participated in the following bilateral interlaboratory comparison:

**BILC      196-18      OPTICAL POWER METER**

After evaluation of the measurement results stated in your Calibration Certificate according to EN ISO/IEC 17043 document we can confirm that the differences of your measurement results from the reference values are in conformance with your declared uncertainties and your laboratory herewith fulfilled the conditions stated for this BILC program and

**has proved its technical competence.**

This conclusion can be appealed in writing within 15 days of receipt of this Decision.

Enclosed we are sending the final report and Certificate on successful participation in this BILC program.

Thank you for your cooperation during the BILC process.

Yours sincerely

 **Český metrologický institut**  
Okružní 31  
638 00 BRNO  
-20-

**Ing. František Staněk, Ph.D.**  
Director for Legal Metrology

**Annexes:**      BILC final report      1 x  
                    Certificate on successful participation in the BILC program      1 x  
**Copy:**      ÚLM/MPZ





**CZECH METROLOGY INSTITUTE**

Český metrologický institut, Referát MPZ



# CERTIFICATE

## ON PARTICIPATION IN THE BILATERAL INTERLABORATORY COMPARISON

No. 0318-OV-A196-18

Subject of the BILC:

### OPTICAL POWER METER

BILC identification: **51-196-18**

Participant:

**Institute of Physics Belgrade,  
Laboratory for optoelectronics**

**Pregrevica 118, 11080 Zemun, Belgrade, Serbia**

#### Final statement

On the basis of the Report No. 0318-ZV-A196-18 on evaluation of the measurement results the above mentioned participant

**c o m p l i e s w i t h**

the requirements of this interlaboratory comparison based on EN ISO/IEC 17043.

Date of issue: **11.09.2019**



**Mgr. Jiří Herec, Ph.D.**

Deputy Head of the ILC Department

**Ing. František Staněk, PhD.**

Director for Legal Metrology

[Skip to main content](#)



## Optical and Quantum Electronics

ISSN: 0306-8919 (Print) 1572-817X (Online)

This journal was previously published under other titles ([view Journal History](#))

- [Volumes](#)
- [Topical Collections](#)

### **2015 Conference on “Numerical Simulation of Optoelectronic Devices”**

Guest Editors: Julien Javaloyes, Weida Hu, Slawek Sujecki and Yuh-Renn Wu

35 Articles

### **2017 - Optical Wave and Waveguide Theory and Numerical Modelling**

Bastiaan Pieter de Hon, Sander Johannes Floris, Manfred Hammer, Dirk Schulz, Anne-Laure Fehrembach

9 Articles

### **2017 Numerical Simulation of Optoelectronic Devices**

Matthias Auf der Maur, Weida Hu, Slawomir Sujecki, Yuh-Renn Wu, Niels Gregersen, Paolo Bardella

32 Articles

### **2018 - Optical Wave and Waveguide Theory and Numerical Modelling**

Stefan Helfert, Manfred Hammer, Dirk Schulz

14 Articles

### **Advanced Materials for photonics and electronics**

Guest Editors: Bouchta Sahraoui, Yahia Boughaleb, Kariem Arof and Anna Zawadzka

28 Articles

### **Advanced Photonics Meets Machine Learning**

Guest Editors: Goran Gligoric, Jelena Radovanovic and Aleksandra Maluckov

6 Articles

### **Advances in the Science of Light**

Guest Editors: Jelena Radovanovic, Milutin Stepic, Mikhail Sumetsky, Mauro Pereira and Dragan Indjin

46 Articles

### **Focus on Optics and Bio-photonics, Photonica 2017**

Guest Editors: Jelena Radovanovic, Aleksandar Krmpot, Marina Lekic, Trevor Benson, Mauro Pereira and Marian Marciniak

40 Articles

### **Fundamentals of Laser Assisted Micro- & Nanotechnologies**

Guest Editors: Eugene Avrutin, Vadim Veiko, Tigran Vartanyan and Andrey Belikov

# Одељење Друштва физичара Србије за научна истраживања и високо образовање

Председник Одељења: **Татјана Вуковић**, ФФ, [tanja37@rcub.bg.ac.rs](mailto:tanja37@rcub.bg.ac.rs)  
Потпредседник Одељења: Братислав Обрадовић, ФФ, [obrat@ff.bg.ac.rs](mailto:obrat@ff.bg.ac.rs);  
Секретар Одељења:

## Одсеци Одељења НИВО ДФС

### 1. Одсек за квантну и математичку физику (8)

Председник:	<b>Милан Дамњановић</b>	ФФ	<a href="mailto:yqoq@afrodita.rcub.bg.ac.rs">yqoq@afrodita.rcub.bg.ac.rs</a> ;
	Љубица Давидовић	ИФ	<a href="mailto:ljubica.davidovic@ipb.ac.rs">ljubica.davidovic@ipb.ac.rs</a> ;
	Игор Франовић	ИФ	<a href="mailto:igor.franovic@ipb.ac.rs">igor.franovic@ipb.ac.rs</a> ;
	Далибор Чевизовић	Винча	<a href="mailto:cevzd@vinca.rs">cevzd@vinca.rs</a> ;
	Татјана Вуковић	ФФ	<a href="mailto:tanja37@rcub.bg.ac.rs">tanja37@rcub.bg.ac.rs</a> ;
	Милан Пантић	ПМФ Нови Сад	<a href="mailto:mpantic@df.uns.ac.rs">mpantic@df.uns.ac.rs</a> ;
	Мирољуб Дугић	ПМФ Крагујевац	<a href="mailto:dugic@kg.ac.rs">dugic@kg.ac.rs</a> ;
	Ненад Милојевић	ПМФ Ниш	<a href="mailto:nenad81@pmf.ni.ac.rs">nenad81@pmf.ni.ac.rs</a> ;

### 2. Одсек за физику језгра, елементарних честица и основних интеракција (9)

Председник:	<b>Петар Аџић</b>	ФФ	<a href="mailto:adzic@ff.bg.ac.rs">adzic@ff.bg.ac.rs</a> ;
	Ненад Врањеш	ИФ	<a href="mailto:nenad.vranjes@ipb.ac.rs">nenad.vranjes@ipb.ac.rs</a> ;
	Марко Војиновић	ИФ	<a href="mailto:mako.vojinovic@ipb.ac.rs">marko.vojinovic@ipb.ac.rs</a> ;
	Иванка Божовић-Јелисавчић	Винча	<a href="mailto:ibozovic@vinca.rs">ibozovic@vinca.rs</a> ;
	Маја Бурић	ФФ	<a href="mailto:majab@ipb.ac.rs">majab@ipb.ac.rs</a> ;
	Јована Николов	ПМФ Нови Сад	<a href="mailto:jovana.nikolov@df.uns.ac.rs">jovana.nikolov@df.uns.ac.rs</a> ;
	Светислав Савовић	ПМФ Крагујевац	<a href="mailto:savovic@kg.ac.rs">savovic@kg.ac.rs</a> ;
	Драгољуб Димитријевић	ПМФ Ниш	<a href="mailto:ddrag@pmf.ni.ac.rs">ddrag@pmf.ni.ac.rs</a> ;
	Ковиљка Станковић	ЕТФ	<a href="mailto:kstankovic@etf.bg.ac.rs">kstankovic@etf.bg.ac.rs</a> ;

### 3. Одсек за астрономију и астрофизику (9)

Председник:	<b>Лука Поповић</b>	АО	<a href="mailto:lpopovic@aob.bg.ac.rs">lpopovic@aob.bg.ac.rs</a> ;
	Владимир Срећковић	ИФ	<a href="mailto:vladimir.sreckovic@ipb.ac.rs">vladimir.sreckovic@ipb.ac.rs</a> ;
	Весна Борка Јовановић	Винча	<a href="mailto:vborka@vinca.rs">vborka@vinca.rs</a> ;
	Тијана Продановић	ПМФ Нови Сад	<a href="mailto:prodanvc@df.uns.ac.rs">prodanvc@df.uns.ac.rs</a> ;
	Јована Петровић	ПМФ Нови Сад	<a href="mailto:jovana.petrovic@df.uns.ac.rs">jovana.petrovic@df.uns.ac.rs</a> ;
	Саша Симић	ПМФ Крагујевац	<a href="mailto:ssimic@kg.ac.rs">ssimic@kg.ac.rs</a> ;
	Драган Гајић	ПМФ Ниш	<a href="mailto:dgaja@junis.ni.ac.rs">dgaja@junis.ni.ac.rs</a> ;
	Мирослав Мићић	АО	<a href="mailto:micic@aob.rs">micic@aob.rs</a> ;
	Зорица Цветковић	АО	<a href="mailto:zcvetkovic@aob.bg.ac.rs">zcvetkovic@aob.bg.ac.rs</a> ;

#### 4. Одсек за физику кондензоване материје и статистичку физику (10)

Председник:

	Марија Митровић Данкулов	ИФ	<a href="mailto:marija.mitrovic@ipb.ac.rs">marija.mitrovic@ipb.ac.rs</a> ;
	Ивана Васић	ИФ	<a href="mailto:ivana.vasic@scl.rs">ivana.vasic@scl.rs</a> ; <a href="mailto:ivana.vidanovic@ipb.ac.rs">ivana.vidanovic@ipb.ac.rs</a> ;
	Наташа Бибић	Винча	<a href="mailto:ntasabi@vinca.rs">ntasabi@vinca.rs</a> ;
	Ивица Брадарић	Винча	<a href="mailto:bradaric@vinca.rs">bradaric@vinca.rs</a> ;
	Ђорђе Спасојевић	ФФ	<a href="mailto:djordjes@ff.bg.ac.rs">djordjes@ff.bg.ac.rs</a> ;
	Милан Кнежевић	ФФ,	<a href="mailto:knez@ff.bg.ac.rs">knez@ff.bg.ac.rs</a> ;
	Милица Павков Хрвојевић	ПМФ Нови Сад	<a href="mailto:milica@df.uns.ac.rs">milica@df.uns.ac.rs</a> ;
	Федор Скубан	ПМФ Нови Сад	<a href="mailto:skubi@uns.ac.rs">skubi@uns.ac.rs</a> ;
	Драган Тодоровић	ПМФ Крагујевац	<a href="mailto:tosa@kg.ac.rs">tosa@kg.ac.rs</a> ;
	Јована Гојановић	ЕТФ	<a href="mailto:jovana@etf.bg.ac.rs">jovana@etf.bg.ac.rs</a> ;

#### 5. Одсек за атомску и молекулску физику (8)

Председник:	Иван Манчев,	ПМФ Ниш	<a href="mailto:mancev@pmf.ni.ac.rs">mancev@pmf.ni.ac.rs</a> ;
	Јелана Маљковић,	ИФ	<a href="mailto:jelena.maljkovic@ipb.ac.rs">jelena.maljkovic@ipb.ac.rs</a> ;
	Сања Тошић,	ИФ	<a href="mailto:sanja.tosic@ipb.ac.rs">sanja.tosic@ipb.ac.rs</a> ;
	Душко Борка,	Винча	<a href="mailto:dusborka@vinca.rs">dusborka@vinca.rs</a> ;
	Сава Галијаш,	ФФ	<a href="mailto:galijas@ff.bg.ac.rs">galijas@ff.bg.ac.rs</a> ;
	Наташа Недељковић	ФФ	<a href="mailto:hekata@ff.bg.ac.rs">hekata@ff.bg.ac.rs</a> ;
	Игор Савић	ПМФ Нови Сад	<a href="mailto:savke@uns.ac.rs">savke@uns.ac.rs</a> ;
	Владимир Ристић	ПМФ Крагујевац	<a href="mailto:ristic@kg.ac.rs">ristic@kg.ac.rs</a> ;

#### 6. Оптика и фотоника (7)

Председник:	Љупчо Хацијевић	Винча	<a href="mailto:ljupcoh@vinca.rs">ljupcoh@vinca.rs</a> ;
	Марина Лекић	ИФ	<a href="mailto:marina.lekic@ipb.ac.rs">marina.lekic@ipb.ac.rs</a> ;
	Александар Крмпот	ИФ	<a href="mailto:aleksandar.krmpot@ipb.ac.rs">aleksandar.krmpot@ipb.ac.rs</a> ;
	Јована Петровић	Винча	<a href="mailto:jovanap@vinca.rs">jovanap@vinca.rs</a> ;
	Ана Симовић	ПМФ Крагујевац	<a href="mailto:asimovic@kg.ac.rs">asimovic@kg.ac.rs</a> ;
	Петар Матавуљ	ЕТФ	<a href="mailto:matavulj@etf.bg.ac.rs">matavulj@etf.bg.ac.rs</a> ;
	Бранко Дрљача	ПМФ К. Митровица	<a href="mailto:brdrljaca@gmail.com">brdrljaca@gmail.com</a> ;

ABSTRACTS OF TUTORIAL, KEYNOTE, INVITED LECTURES,  
PROGRESS REPORTS AND CONTRIBUTED PAPERS

of

The Sixth International School and Conference on Photonics  
**PHOTONICA2017**

28 August – 1 September 2017  
Belgrade Serbia

*Editors*

Marina Lekić and Aleksandar Krmpot

*Technical assistance*

Marko Nikolić and Danica Pavlović

*Publisher*

Institute of Physics Belgrade  
Pregrevica 118  
11080 Belgrade, Serbia

*Printed by*

Serbian Academy of Sciences and Arts

*Number of copies*

300

ISBN 978-86-82441-46-5



## Committees

### Scientific Committee

Aleksandar Krmpot, Serbia  
Antun Balaž, Serbia  
Arlene D. Wilson-Gordon, Israel  
Bojan Resan, Switzerland  
Boris Malomed, Israel  
Branislav Jelenković, Serbia  
Dejan Gvozdić, Serbia  
Detlef Kip, Germany  
Dragan Indjin, United Kingdom  
Edik Rafailov, United Kingdom  
Feng Chen, China  
Francesco Cataliotti, Italy  
Giannis Zacharakis, Greece  
Goran Isić, Serbia  
Goran Mašanović, United Kingdom  
Isabelle Philippa Staude, Germany  
Jelena Radovanović, Serbia  
Jerker Widengren, Sweden  
Jovana Petrović, Serbia  
Laurent Sanchez, France  
Ljupčo Hadžievski, Serbia  
Marco Santagiustina, Italy  
Milan Mashanović, United States of America  
Milan Trtica, Serbia  
Miloš Živanov, Serbia  
Milutin Stepić, Serbia  
Milivoj Belić, Qatar  
Nikola Stojanović, Germany  
Pavle Andus, Serbia  
Peđa Mihailović, Serbia  
Radoš Gajić, Serbia  
Schaaf Peter, Germany  
Sergei Turitsyn, United Kingdom  
Suzana Petrović, Serbia  
Ticijana Ban, Croatia  
Vladana Vukojević, Sweden  
Zoran Jakšić, Serbia  
Željko Šljivančanin, Serbia

## Organizing Committee

Aleksandar Krmpot, (Chair)  
Marina Lekić (Secretary)  
Stanko Nikolić (webmaster)  
Marko Nikolić,  
Vladimir Veljić  
Danica Pavlović

## Technical Organizer





Kopaonik, March 08 – 12, 2020

## Organizing committee

- Marina Lekić (chair)**, Institute of Physics Belgrade, University of Belgrade  
**Marja Čurčić (secretary)**, Institute of Physics Belgrade, University of Belgrade  
**Zoran Grujić (webmaster)**, Institute of Physics Belgrade, University of Belgrade  
**Aleksander Kovačević**, Institute of Physics Belgrade, University of Belgrade  
**Dragan Lukić**, Institute of Physics Belgrade, University of Belgrade  
**Branislav Jelenković**, Institute of Physics Belgrade, University of Belgrade  
**Igor Popov**, Institute for Multidisciplinary Research, University of Belgrade

### Login Form

Remember Me

[Log in](#)

[Create an account](#)  
[Forgot your username?](#)  
[Forgot your password?](#)

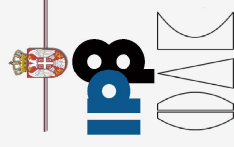
### Useful links

- [Previous workshops](#)
- [Optical Society of Serbia](#)
- [Grand Hotel & Spa](#)

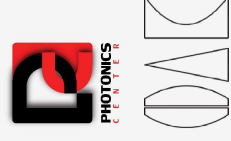
### Important dates

- Registration open:**  
October 10, 2019
- Early registration up to:**  
December 31, 2019
- First announcement:**  
October 10, 2019
- Abstract submit deadline:**  
February 09, 2020
- Notification of abstract acceptance:**  
February 15, 2020
- Conference begin:**  
March 08, 2020
- Conference end:**  
March 12, 2020

### Sponsors



### Organisers



## Scientific Committee

- Wolfgang Fritzsche**, Leibniz Institute of Photonic Technology, Germany  
**Lars Klimaschewski**, Innsbruck Medical University, Austria  
**Srdan Antić**, Institute for Systems Genomics, Stem Cell Institute, University of Connecticut  
**Theo Scholtes**, Leibniz Institute of Photonic Technology, Germany  
**Hrvoje Skenderović**, Institute of Physics, Zagreb, Croatia  
**Gülnur Aygün**, Izmir Institute of Technology, Turkey  
**Ljupčo Hadžijevski**, Vinča Institute of Nuclear Sciences  
**Pavle Andus**, Faculty of Biology, University of Belgrade  
**Branislav Jelenković**, Institute of Physics Belgrade  
**Marina Lekić**, Institute of Physics Belgrade  
**Aleksander Kovačević**, Institute of Physics Belgrade  
**Zoran Grujić**, Institute of Physics Belgrade

# PHOTONICS WORKSHOP

11<sup>th</sup> Workshop: Kopaonik, March 11 – 15, 2018

HOME
WORKSHOP
PARTICIPANT
ABSTRACT
ORGANIZATION
REGISTRATION
SPEAKERS
CONTACT



Previous Workshops

IPB

INN "Vinča"

FP

ETF

ICTM

Photonica09

Photonica 2011

ORGANIZATION >>

Send link to a friend

## Committees

Members of the Program and Organization Committees.

### Program Committee:

Branislav Jelenković (chair)  
Ljupčo Hadžievski  
Zoran Jakšić  
Dejan Pantelić  
Darko Vasiljević  
Aleksander Kovačević

### Organization Committee:

Marina Lekić (chair)  
Darko Vasiljević  
Aleksander Kovačević  
Dragan Lukić  
Branislav Jelenković

IMPO

Registrat  
(final): M  
Abstract  
(final): F€

Worksho

SPON



ORGA



PHOT  
C E N

MPN

Facebook

Institute of Physics, University of Belgrade ♦ Pregrevica 118 ♦ 11080 Belgrade, Serbia ♦ phone +381 (11) 3713-000 ♦ fax +381 (11) 3162-190 ♦ PIB 100105980 ♦ MB 07018029

© Institute of Physics, University of Belgrade. All rights reserved.





# CEWQO 2008

## 15<sup>th</sup> Central European Workshop on Quantum Optics 2008

Belgrade, Serbia, 30 May - 03 June 2008

→ HOME PAGE

→ 16th CEWQO 2009

→ 17th CEWQO 2010

→ Announcements

→ Registration

↓ Committees

→ Topics

→ Invited speakers

→ VISAS

→ Programme

→ Travel

→ Venue

→ Proceedings

→ Accommodation

→ Sponsors

→ FAQ

Contact

## Committees

### Advisory board

Vladimir Buzek (Bratislava, Slovak Republic)  
 Slobodan Cvejanović (Rijeka, Croatia)  
 Victor Dodonov (Brazilia, Brazil)  
 Martial Ducloy (Paris, France)  
 Zdenek Hradil (Olomouc, Czech Republic)  
 Jozsef Janszky (Budapest, Hungary)  
 Nikola Konjević (Belgrade, Serbia)  
 Ulf Leonhardt (St Andrews, UK)  
 Margarita Man'ko (Moscow, Russia)  
 Antonino Messina (Palermo, Italy)  
 Paulina Marian (Bucharest, Romania)  
 Saverio Pascazio (Bari, Italy)  
 Anton Ramsak (Ljubljana, Slovenia)  
 Helmut Rauch (Vienna, Austria)  
 Ryszard Tanas (Poznan, Poland)  
 Nikolay V. Vitanov (Sofia, Bulgaria)  
 Werner Vogel (Rostock, Germany)  
 Leposava Vušković (Norfolk, USA)

### Organizing committee

Mirjana Božić (chairperson)  
 Dušan Arsenović (secretary)  
 Zoran Grujić (webmaster)  
 Nikola Burić  
 Milena Davidović  
 Miroljub Dugić  
 Radoš Gajić  
 Nikola Konjević  
 Marina Mijailović  
 Milan Tadić

Total 1 article(s).

### Program

**Book of abstracts:**

(DOC) (PDF)

**CEWQO 08  
Program with  
the talks titles**

**Prizes**

**CEWQO 08  
Program with  
presentations**

### Conference Photos:

*30 May - Serbian  
Academy of Sciences  
and Arts, Opening;  
Lectures, Welcome  
cocktail  
31 May - Rectorate,  
Lectures, Poster session  
1 Jun - Rectorate,  
Lectures; Excursion  
2 Jun - Rectorate,  
Lectures; Poster  
session; Conference  
dinner  
3 Jun - Rectorate,  
Lectures; Closing; Visit  
to Institute of Physics*

*Photos by Aurelian Isar*

### Proceedings:

The proceedings of the 15th Central European Workshop on Quantum optics will be published as a Topical Issue of Physica Scripta.



### Co-organiser

Serbian Academy of Sciences  
and Arts  
http://www.sanu.ac.yu



Direction des Ressources Humaines  
Service du personnel BIATOSS  
Gestion du personnel contractuel

MINISTÈRE DE L'ÉDUCATION  
NATIONALE  
MINISTÈRE DE L'ENSEIGNEMENT  
SUPÉRIEUR ET DE LA RECHERCHE  
**UNIVERSITÉ D'ANGERS**  
40, rue de Rennes  
BP 73532  
49035 ANGERS CEDEX 01

## PROCES-VERBAL D'INSTALLATION

de Mademoiselle LEKIC Marina  
dans les fonctions d'agent contractuel

Nous soussigné, Daniel MARTINA, Président de l'Université d'ANGERS,  
Vu le contrat en date du 26 janvier 2011, par lequel **Mademoiselle LEKIC Marina** est  
recruté(e) à temps complet en qualité d'agent contractuel à l'Université d'Angers à  
compter du 9 février 2011 et jusqu'au 31 janvier 2012.

**Mademoiselle LEKIC Marina** s'étant présenté(e) devant nous, l'avons, installé(e) dans  
ses fonctions au 09 février 2011.

Angers, le 09 février 2011

Signature de l'intéressé(e)

*Lu et Approuvé*  
*Marina Lekic*



Pour le Président de l'Université d'Angers  
et par délégation  
le Directeur général des services

*H-M Pavaoine*

**H-M PPAVOINE**

Précédée de la mention « Lu et Approuvé »

# Ramsey effects in coherent resonances at closed transition $F_g = 2 \rightarrow F_e = 3$ of $^{87}\text{Rb}$

Z D Grujić, M M Lekić, M Radonjić, D Arsenović and B M Jelenković

Institute of Physics, University of Belgrade, Pregrevica 118, 11080 Belgrade, Serbia

E-mail: [milan.radonjic@ipb.ac.rs](mailto:milan.radonjic@ipb.ac.rs)

Received 22 August 2012, in final form 8 October 2012

Published 30 November 2012

Online at [stacks.iop.org/JPhysB/45/245502](http://stacks.iop.org/JPhysB/45/245502)

## Abstract

Experimental and theoretical investigations show the strong effect of the pump beam, spatially separated from the probe beam, on the probe's electromagnetically induced absorption (EIA) and nonlinear magneto-optical rotation (NMOR). Linearly polarized pump and probe laser beams are locked to the  $F_g = 2 \rightarrow F_e = 3$  transition of the  $^{87}\text{Rb}$   $D_2$  line and pass a vacuum Rb gas cell coaxially. We show that the observed narrowing of EIA and NMOR resonances is due to the Ramsey effect. Linewidths of the resonances decrease when the size of the dark region between pump and probe lasers increases. Variation of the angle between pump and probe linear polarizations strongly influences the phases of atomic coherences generated by the pump beam and consequently the line-shapes of the probe EIA and NMOR resonances. Complete change of the resonance sign is possible if the phases of the ground state coherences,  $\Delta m_g = 2$ , are altered by  $\pi$ . The central EIA fringe becomes less pronounced if the probe intensity increases, due to the larger probe contribution to atomic evolution. Ramsey-like interference is a manifestation of the evolution of ground state Zeeman coherences, required for EIA, in the dark region in the presence of a small magnetic field.

(Some figures may appear in colour only in the online journal)

## 1. Introduction

In the work of Akulshin *et al* [1], a new kind of resonance was observed, one in which atomic coherence produces an increase of laser absorption. This coherent phenomena is termed electromagnetically induced absorption or EIA. Conditions for observing EIA have been recently identified: a narrow absorption resonance can be obtained when the laser frequency is scanned across a degenerate two-level transition such that  $F_g \rightarrow F_e = F_g + 1$ , where  $F_g$  and  $F_e$  are total angular momentum quantum numbers of hyperfine levels of ground and excited states, respectively. It is worth mentioning that Kazantsev *et al* [2] theoretically predicted that optical pumping in the case of such transitions leads to an enhanced absorption of the medium. It is now well known that EIA is a multilevel effect, meaning that the degeneracy of the ground level is necessary. In comparison to electromagnetically induced transparency (EIT) [3] EIA has an opposite sign of resonance. Unlike EIT, which is due to coherent population trapping (CPT) and ground level dark states [4], EIA has not been associated with a particular coherent superposition of atomic ground states. While both EIT and CPT were intensely investigated over the past decade,

this is not the case for EIA. A better knowledge of the phenomena is necessary, including a better understanding of excitation and emission processes that lead to the development of EIA.

The first observations of EIA were performed by perpendicularly polarized pump and probe lasers, interacting with a cycling degenerate two-level transition in which  $F_e = F_g + 1$  and  $F_g > 0$  [1, 5]. In later experiments, EIA was also found in non-cycling degenerate two-level systems [6, 7]. Both two-photon resonances in a bichromatic light field (pump-probe spectroscopy) and magneto-optical resonances in the Hanle configuration have been explored. The influence of various parameters like laser intensity, light ellipticity and magnetic fields on EIA amplitudes and linewidths was studied in [8–11].

Assuming the simplest system presenting EIA, a four-level  $N$ -atomic system of a near degenerate two-level atom, Taichenachev *et al* [13] obtained an analytic expression for the probe light absorption. A direct link between the efficiency of spontaneous coherence transfer and the appearance of EIA indicates that the Zeeman coherence, after being developed in the excited level, is transferred to the ground level



by spontaneous emission. Analytic expressions of different perturbation orders for Zeeman and optical coherences and populations have shown such ordering of events in the development of EIA [14].

EIA media have some similarities but also differences from EIT media. Since these two coherent phenomena have different origins, their temporal behaviour is different, as given in [15]. Slower development of EIA and its consequent narrowing after turning on the excitation pulse was notable in comparison with EIT. EIA media have a steep anomalous dispersion that is related to subluminal light propagation, as demonstrated in [16]. As a consequence, in EIA media light pulses can also be stored and retrieved like in EIT media, but only the storage of a smaller part of the initial pulse is possible [17]. In some open atomic systems, minor changes of the pump laser Rabi frequency can transform EIT to EIA (and vice versa) [18]. A modest change of the buffer gas cell's temperature can alter the sign of the transmission resonance from positive (EIT) to negative (EIA) [12].

Ramsey's method of separated fields is often used in atomic and molecular beam experiments [19]. Ramsey fringes that are induced by the two spatially or temporally separated excitation fields lead to a considerable narrowing of the corresponding resonances. In this work, we test if the Ramsey effects of separated pump and probe laser beams can be effective for narrowing EIA as they are for EIT. Repeated interaction of coherently prepared alkali-metal atoms with a pair of laser fields in Raman resonance leads to a strong Ramsey narrowing of EIT in cells with buffer gas [20, 21], and in vacuum gas cells if a specific pump–probe laser beam geometry is used [22, 23]. The Ramsey effects on EIA were recently explored in gas cells with anti-relaxation coating experimentally [24] and, using a four-level  $N$ -atomic system, theoretically [25]. We look for the Ramsey effects introduced by separated excitation fields in an EIA medium in a vacuum gas cell without anti-relaxation coating by measuring and calculating the probe's transmission and nonlinear magneto-optical rotation (NMOR) when the laser fields couple the  $F_g = 2 \rightarrow F_e = 3$  transition of the  $^{87}\text{Rb}$   $D_2$  line. In  $V$  atomic schemes supporting EIA, polarization rotation has the opposite sign to that in EIT atomic systems, e.g.  $\Lambda$  or  $M$  systems. There have been numerous studies of NMOR in EIT media in buffer-gas-free vapour cells and without anti-relaxation coating [26–29]. A change of the NMOR sign in the case of the closed transition  $F_g = 4 \rightarrow F_e = 5$  of the Cs  $D_2$  line was first reported in [27].

In our work, we use a pump laser beam to coherently prepare the atoms and a spatially separated probe laser beam to check the pump-induced atomic coherence. We studied the Ramsey effects on narrowing EIA and NMOR, theoretically and experimentally, using a similar pump–probe geometry as in [22]. Both pump and probe laser beams are linearly polarized and resonant to the closed transition,  $F_g = 2 \rightarrow F_e = 3$  in  $^{87}\text{Rb}$ . EIA measurements were carried out by monitoring the probe beam's transmission. NMOR of the linear probe polarization, for a given pump polarization, is obtained using a balanced polarimeter. The measurements were performed as a function of the external axial magnetic field for different angles between the electric vectors of the pump and probe

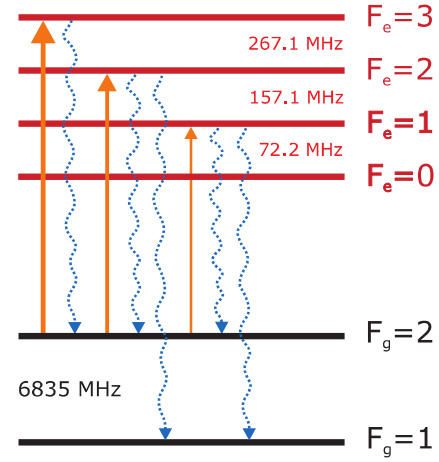


**Figure 1.** Energy level diagram for  $D_2$  line transitions considered in the theoretical model. Solid arrows pointing up represent the transitions induced by the laser, while dotted wavy arrows pointing down correspond to possible spontaneous emission channels from excited levels. Frequency differences between adjacent hyperfine levels are shown.

beams. Obtained EIA and NMOR line-shapes are compared with the results of the theoretical model. The model solves time-dependent optical Bloch equations for the density matrix elements for all sublevels of the  $F_g = 2 \rightarrow F_e = 3$  transition. The atomic state evolution is calculated when an atom passes the pump, the dark region and the probe beam. The probe's total transmission was calculated after averaging over all atom velocity components parallel and perpendicular to the laser beam and over all possible atomic trajectories. The probe beam's transmission and polarization rotation are obtained from the calculated change of the probe's electric field due to the Rb vapour polarization.

## 2. Theory

We used a density-matrix formalism to model the dynamics of the interaction between Rb atoms and spatially separated pump and probe laser beams. Figure 1 shows a Rb  $D_2$  line atomic level diagram, the hyperfine levels either coupled by the laser light, or populated via spontaneous emission.

The external magnetic field  $\mathbf{B}$ , along the propagation direction of the laser beam, splits the adjacent Zeeman sublevels by the amount  $\mu_B g_F B$ , where  $\mu_B$  is the Bohr magneton and  $g_F$  is the gyromagnetic factor of the level. The temporal evolution of the atomic density matrix is obtained from time-dependent optical Bloch equations for a moving atom

$$\frac{d\hat{\rho}}{dt} = -\frac{i}{\hbar}[H_{\text{atom}}(\mathbf{B}) + H_{\text{int}}(t), \hat{\rho}] + \left(\frac{d\hat{\rho}}{dt}\right)_{\text{SE}}, \quad (1)$$

where

$$H_{\text{atom}}(\mathbf{B}) = \sum_j \hbar\omega_j(\mathbf{B})|g_j\rangle\langle g_j| + \sum_k \hbar\omega_k(\mathbf{B})|e_k\rangle\langle e_k|, \quad (2)$$

is the atomic Hamiltonian corresponding to ground (excited) states  $|g_j\rangle$  ( $|e_k\rangle$ ) with Zeeman-shifted energies  $\hbar\omega_j(\mathbf{B})$  ( $\hbar\omega_k(\mathbf{B})$ ). The laser–atom interaction is given by

$$H_{\text{int}}(t) = -\sum_{j,k} \mathbf{E}(t) \cdot \mathbf{d}_{jk}(|g_j\rangle\langle e_k| + |e_k\rangle\langle g_j|), \quad (3)$$

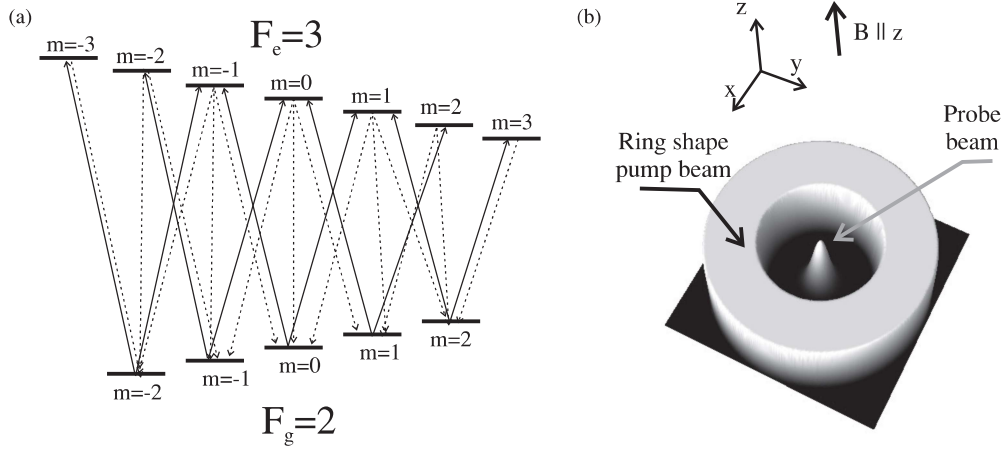


**Figure 2.** (a) The energy level diagram for magnetic sublevels of the  $F_g = 2 \rightarrow F_e = 3$  transition and (b) pump and probe laser beam radial profiles used in the theoretical model. In (a) solid lines represent transitions induced by the linearly polarized laser fields, while dotted lines correspond to possible spontaneous emission channels from excited levels.

where  $\mathbf{E}(t)$  is the time-dependent electric field of the laser seen by the atom and  $\mathbf{d}_{jk}$  is the atomic electric dipole moment for the transition between states  $|g_j\rangle$  and  $|e_k\rangle$ . Spontaneous emission is treated using the Lindblad-form term

$$\left(\frac{d\hat{\rho}}{dt}\right)_{SE} = \sum_m 2\Gamma_m \hat{\rho} \Gamma_m^\dagger - \Gamma_m^\dagger \Gamma_m \hat{\rho} - \hat{\rho} \Gamma_m^\dagger \Gamma_m, \quad (4)$$

where  $\Gamma_m$  are operators related to dipole transitions from the excited to ground state manifold. Although the laser is frequency locked to the  $F_g = 2 \rightarrow F_e = 3$  transition, due to Doppler broadening, the excited hyperfine levels  $F_e = 2$  and  $F_e = 1$  are also laser-coupled and therefore have to be included in the calculations. Equations for density matrix elements related to the  $F_g = 1$  ground level are excluded since that level is not coupled by the laser. For additional details about the resulting equations please refer to [30].

Both the pump and probe are linearly polarized, have the same frequency  $\omega_0$  and propagate along the  $z$  axis. As schematically given in figure 2, the probe laser beam is at the centre of the coaxial hollow pump beam. The initial probe beam radial profile is a Gaussian

$$I_{\text{probe}}(r) = 2\bar{I}_{\text{probe}} \exp(-2r^2/r_0^2), \quad (5)$$

where  $r_0$  is the  $1/e^2$  radius of the probe beam and  $\bar{I}_{\text{probe}}$  is the probe beam's intensity (total probe power divided by  $r_0^2\pi$ ). The pump beam's intensity profile along the radial distance  $r$  is modelled as

$$I_{\text{pump}}(r) = \bar{I}_{\text{pump}} a(\text{erf}(p(r-r_1)) - \text{erf}(p(r-r_2))), \quad (6)$$

where  $\bar{I}_{\text{pump}}$  is the pump beam's intensity,  $a$  is the normalization constant,  $p$  affects the steepness of the profile near the beam's edge determined by the parameters  $r_1$  and  $r_2$ .

It is assumed that every collision with the cell wall resets the state of an atom. Therefore, the atoms entering the pump beam from the direction of the wall have equally populated Zeeman sublevels of both hyperfine levels of the ground state. The density of the rubidium vapour at room temperature is low enough, so that Rb–Rb collisions are negligible. Therefore, an atom moves through the laser beams with constant velocity

$\mathbf{v} = \mathbf{v}_{\parallel} + \mathbf{v}_{\perp}$ , where  $\mathbf{v}_{\parallel}$  and  $\mathbf{v}_{\perp}$  are velocity components parallel and perpendicular to the direction of laser propagation, respectively. When calculating the density matrix at a given value of  $z$ , we neglect longitudinal changes of the beam profiles compared to the transverse ones so that only the transverse direction of the trajectory matters. From the reference frame of the moving atom, the electric field varies and the rate of variation depends only on  $\mathbf{v}_{\perp}$ . Assume that the transverse projection of the atomic trajectory at some  $z$  is given by  $\mathbf{r}_{\perp}(t) = \mathbf{r}_{0\perp} + \mathbf{v}_{\perp}t$ , where  $\mathbf{r}_{0\perp}$  is the transverse component of the atom position vector at  $t = 0$ . The temporal variation of the laser intensity seen by the atom is given by

$$I(t, z) \equiv I(\mathbf{r}_{\perp}(t), z) = I(\mathbf{r}_{0\perp} + \mathbf{v}_{\perp}t, z), \quad (7)$$

corresponding to the transverse laser intensity variation along the trajectory of the atom in the laboratory frame. Additionally, due to cylindrical symmetry of the beam profiles, the transverse dependence becomes a purely radial dependence.

The observed experimental resonances are the probabilistic average of contributions due to many individual, mutually non-interacting Rb atoms. The atoms traverse the laser beams at different paths with different velocities. The Maxwell–Boltzmann velocity distribution, diversity of atomic trajectories and custom cylindrical symmetric radial beam profiles are treated similarly as in [30]. Atomic trajectories having different distances from the centre of the probe beam are chosen so that the probe beam's cross-section is uniformly covered. For a suitable set of atomic velocities, the atomic density matrix  $\hat{\rho}(B; \mathbf{v}; \mathbf{r})$  along a given trajectory is calculated assuming constant magnetic field  $B$  during the atomic transit through the laser beams. Numerical integration of the optical Bloch equations is carried out from the moment when the atom enters the pump beam's region until it exits the probe beam. To obtain the atomic ensemble density matrix  $\hat{\rho}(B; r, z)$  across the beam's cross-section at some  $z$  and for a set of radial distances  $r$ , the calculated density matrices are averaged over the Maxwell–Boltzmann velocity distribution and integrated over trajectories containing points at given radial distance  $r$ .



The velocity-averaged density matrix will possess cylindrical symmetry arising from the cylindrical symmetry of the laser beam profiles and the atomic velocity distribution. Thus, the angular integral appearing in the averaging over velocity  $\mathbf{v}(\theta) = (\theta, v_{\perp}, v_{\parallel})$  can be replaced by an angular integral over space

$$\hat{\rho}(B; r, z) = \int_0^{2\pi} \frac{d\theta}{2\pi} \int_0^{\infty} dv_{\perp} W_{\perp}(v_{\perp}) \int_{-\infty}^{\infty} dv_{\parallel} W_{\parallel}(v_{\parallel}) \times \hat{\rho}(B; 0, v_{\perp}, v_{\parallel}; r \cos \theta, r \sin \theta, z), \quad (8)$$

with the Maxwell–Boltzmann velocity distribution given by

$$W_{\perp}(v_{\perp}) = \frac{2v_{\perp}}{u^2} e^{-(v_{\perp}/u)^2}, \quad W_{\parallel}(v_{\parallel}) = \frac{1}{u\sqrt{\pi}} e^{-(v_{\parallel}/u)^2}, \quad (9)$$

where  $u = (2k_B T/m_{\text{Rb}})^{1/2}$  is the most probable velocity.

In order to make a comparison with the experiment, we calculate the transmission and the angle of the polarization rotation of the linearly polarized probe laser’s light as a function of the magnetic field. The effects of the probe beam’s propagation and variation in its intensity along the Rb cell are treated using

$$\frac{\partial \mathbf{E}(B; r, z)}{\partial z} = \frac{i\omega_0}{2\epsilon_0 c} \mathbf{P}(B; r, z), \quad (10)$$

where  $\epsilon_0$  is the vacuum dielectric constant and  $c$  the speed of light in vacuum. The accompanying initial condition is given by (5) and by the angle of the probe’s incident linear polarization. The Rb vapour ensemble density matrix  $\hat{\rho}(B; r, z)$  at some values of  $z$  is computed using the electric field  $\mathbf{E}(B; r, z)$ . The polarization of the Rb vapour is obtained from the ensemble density matrix

$$\mathbf{P}(B; r, z) = n(T) \text{Tr}(\hat{\rho}(B; r, z) \hat{\mathbf{d}}), \quad (11)$$

where the  $^{87}\text{Rb}$  concentration  $n(T)$  at absolute temperature  $T$  is taken from [31]. Due to the trace operation including the dipole operator  $\hat{\mathbf{d}}$ , the polarization  $\mathbf{P}$  depends only on the optical coherences between the ground and excited Zeeman sublevels. Using the computed Rb polarization, we are able to calculate the change of the probe’s electric field due to propagation through the Rb vapour from (10). Following that procedure, we calculate the transmitted electric field  $\mathbf{E}(B; r, z = L)$ , where  $L$  is the cell length, used in the calculation of the transmission and the angle of the polarization rotation of the probe laser beam. During the calculation of the probe beam’s propagation, we also treated the pump beam’s propagation effects in an analogous manner.

The angle of the polarization’s rotation is calculated in a similar manner as measured from signals of the two detectors  $S_1$  and  $S_2$  behind the polarizing beam-splitter rotated at  $45^\circ$  with respect to the incident probe’s polarization. The polarization’s rotation angle is given by

$$\varphi = \frac{1}{2} \arcsin \frac{S_1 - S_2}{S_1 + S_2}. \quad (12)$$

Values of  $S_1$  and  $S_2$  were obtained from

$$S_{1,2} = \int_{S_p} |\mathbf{u}_{1,2} \cdot \mathbf{E}(B; r, z = L)|^2 d^2 \mathbf{r}, \quad (13)$$

where  $\mathbf{u}_{1,2} = (\sqrt{2}/2)(\mathbf{e}_x \pm \mathbf{e}_y)$  are unity vectors corresponding to the polarizing beam splitter’s,  $s$  and  $p$ , polarization axes and  $S_p$  is the probe beam’s cross-section.

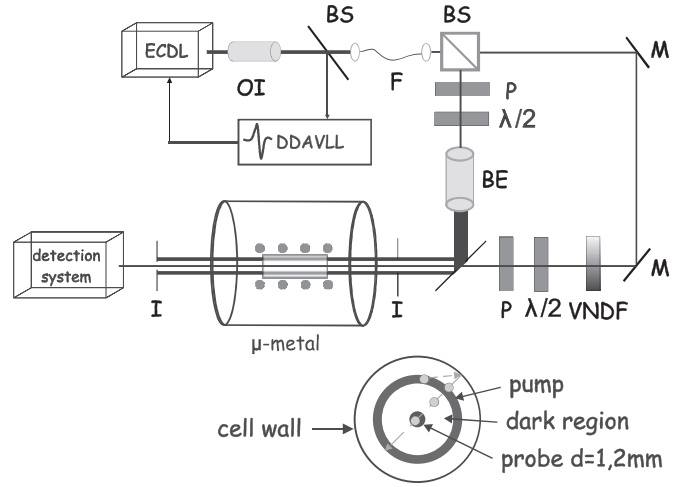


**Figure 3.** Experimental setup: ECDL-external cavity diode laser, OI-optical isolator, DDAVLL-Doppler free dichroic atomic laser lock, BS-beam splitter, F-optical fibre, M-mirrors, I-iris, P-polarizer, VNDf-variable neutral density filter, BE-beam expander,  $\lambda/2$ -retardation plate. Inset: transverse cross-section of the Rb cell with typical atomic trajectory.

### 3. Experimental setup

Figure 3 shows the experimental setup. An external cavity diode laser with a linewidth of about 1 MHz was used in the experiment. The laser frequency was locked to the  $D_2$  transition  $F_g = 2 \rightarrow F_e = 3$ , in  $^{87}\text{Rb}$ , using the Doppler-free dichroic atomic vapour laser lock (DDAVLL) technique [33]. The Gaussian laser beam is split into two beams, the pump beam and the probe beam. The diameter of the pump beam is enlarged and sent through a 12 mm diameter iris. The linear polarizations of the pump and probe beams, and the angle between their polarizations, are adjusted by a linear polarizer and  $\lambda/2$  retardation plate. The important element for generating a laser beam like a hollow cylinder, as shown in figure 3(b), is a mirror with a hole [34]. The diameter of the hole thus determines the inner diameter of the hollow pump beam. We used two mirrors with central holes of 5 and 7 mm in diameter, respectively. The probe beam, 1.2 mm in diameter, comes from behind the mirror and passes through the hole’s centre. The vacuum Rb gas cell is 85 mm long and its diameter is 25 mm. The cell is at room temperature. A scanning magnetic field along the laser beam’s propagation is generated by the solenoid around the gas cell. Magnetic shielding from stray laboratory fields is achieved by three layers of  $\mu$ -metal cylinders around the Rb cell. Behind the cell, the probe beam first passes through a pair of irises (in order to minimize the contribution of the pump beam) and then passes through the polarizing beam splitter with the fast axis oriented at  $45^\circ$  with respect to the direction of the initial polarization of the probe beam. Two beams emerging from the polarizing beam splitter were detected with two photodiodes. The sum  $S_1 + S_2$  and the difference  $S_1 - S_2$  of these two signals were recorded by a digital oscilloscope, while  $B$  was scanned around its zero value. The sum signal gives Hanle EIA, while the difference

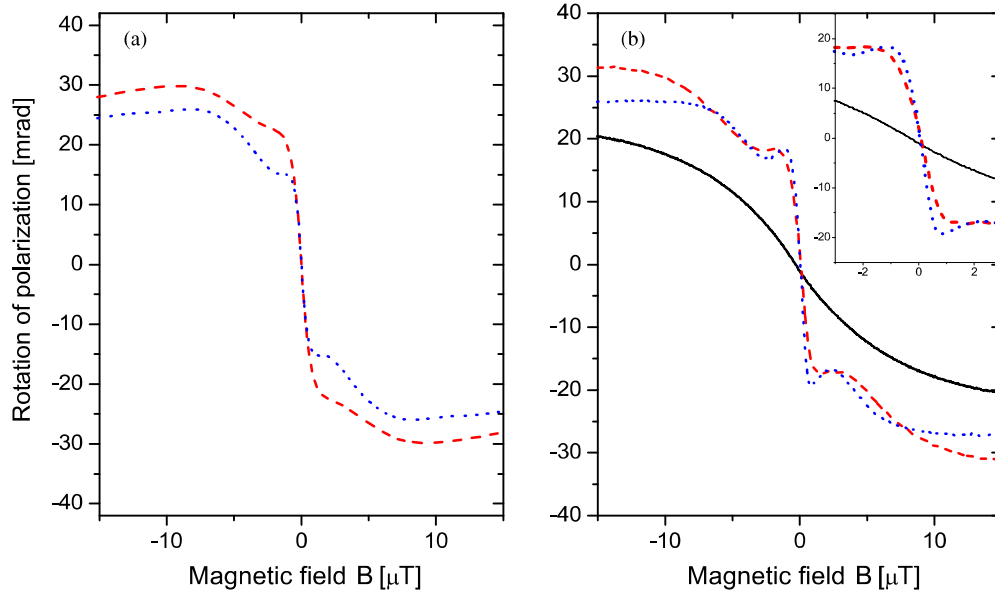


**Figure 4.** Calculated (a) and measured (b) probe NMOR for the  $F_g = 2 \rightarrow F_e = 3$  transition in  $^{87}\text{Rb}$  as a function of the axial magnetic field  $B$ . Dashed and dotted lines are for two inner pump beam diameters of 5 and 7 mm (corresponding to the ‘dark region’ size of 2 and 3 mm), respectively. Both pump and probe beams have the same linear polarization. The probe laser power is  $10 \mu\text{W}$ , while the pump laser power is 1.2 mW. Solid line in (b) is NMOR for single wide laser beam having power of  $10 \mu\text{W}$  and diameter of 7 mm. Inset in (b) shows the recorded resonances near  $B = 0$ .

signal gives NMOR. In this configuration, the rotation angle of the probe’s polarization is given by

$$\phi = \frac{1}{2} \arcsin \frac{S_1 - S_2}{S_1 + S_2}. \quad (14)$$

#### 4. Discussion

In this section, we present results concerning the probe laser’s transmission and polarization rotation when the probe laser interacts with Rb atoms prepared into coherent superposition of Zeeman sublevels of the  $F_g = 2$  ground hyperfine level by the spatially separated pump beam. We intend to demonstrate that the Ramsey effects play a role here as they do for dark resonances [22] by measuring and calculating the line-shapes of EIA and NMOR resonances for different sizes of the dark region, and for different atomic states generated by the pump beam. Both probe and pump beams are linearly polarized and resonant to the  $F_g = 2 \rightarrow F_e = 3$  transition in  $^{87}\text{Rb}$ . The pump beam fills almost the entire 25 mm diameter Rb cell except for the hole at its centre, which is either 5 or 7 mm in diameter. The probe beam of 1.2 mm in diameter is collinear with the pump beam and passes along the axis of the hollow pump beam. This configuration allows, like in the Rb cells with anti-relaxation coating or buffer gas, repeated interaction of atoms and laser fields. It provides higher influx of atomic states prepared by the pump beam that reach the probe beam passing through the central hole, in comparison with co-propagating parallel but spatially separated Gaussian laser beams in [21]. In addition, the use of two separate laser beams gives the ability to independently control the properties of the beams, like polarization and power. Our experimental geometry is similar to the geometry used in [32], where the sub-Doppler feature was observed in the transmission of the hollow probe,

through the very thin ( $10 \mu\text{m}$ ) cell, while the pump beam is placed in the centre of the probe.

We first present theoretical and experimental line-shapes of the probe’s NMOR, calculated and measured from the signals at the two detectors of the balanced polarimeter as a function of the external magnetic field  $B$ . The direction of the magnetic field is along the laser beam’s propagation. In the experiment, the magnetic field varies slowly (50 Hz) so that the period of a magnetic sweep is much longer than typical atom transit time across the cell. This validates the assumption made in the theoretical model that  $B$  is constant while the atom passes through three regions of the Rb cell: the pump laser beam, the dark region and the probe laser beam. In all figures, spatially displaced pump and probe beams have the same frequency. Figures 4(a) and (b) present the calculated and measured angle of rotation of the linear probe polarization as a function of the axial magnetic field. The linear polarizations of the pump and probe beams are parallel. When the pump laser is turned on, the probe’s NMOR resonance has a central dispersive shape and a pair of much weaker sidebands around the centre. Results are given for the two inner diameters of the pump beam, 5 and 7 mm. The resonance width decreases with the distance between the pump and the probe laser beam, which is a characteristic of the Ramsey effect. For dark regions of sizes 2 and 3 mm, the NMOR width is 2.4 and  $1.6 \mu\text{T}$ , respectively. The results given in figures 4(a) and (b) show good agreement between theoretical predictions and experimental measurements. The solid curve in figure 4(b) corresponds to NMOR resonance of a single wide laser beam of 7 mm in diameter and  $10 \mu\text{W}$  of power. It is notably wider and has smaller amplitude than the probe resonances obtained in pump–probe configuration, although the probe beam’s diameter is much smaller, 1.2 mm. The amplitudes of NMOR and EIA are larger than for an open

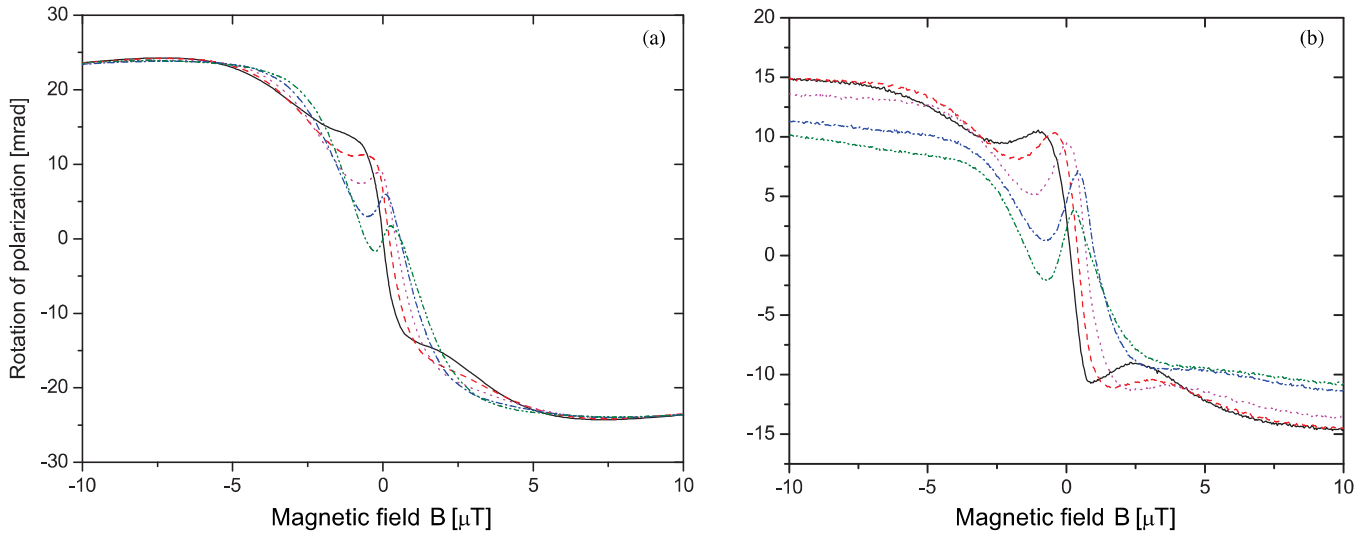


**Figure 5.** Theoretical (a) and experimental (b) results for the angle of rotation of the probe polarization for different angles between linear polarization of the pump and probe beams ( $0^\circ$  black,  $22.5^\circ$  red,  $45^\circ$  green,  $67.5^\circ$  blue and  $90^\circ$  magenta). The pump and probe beams couple the  $F_g = 2 \rightarrow F_e = 3$  transition in  $^{87}\text{Rb}$ . The probe and pump laser powers are  $20 \mu\text{W}$  and  $1.2 \text{ mW}$ , respectively. The pump beam’s inner diameter is  $7 \text{ mm}$ .

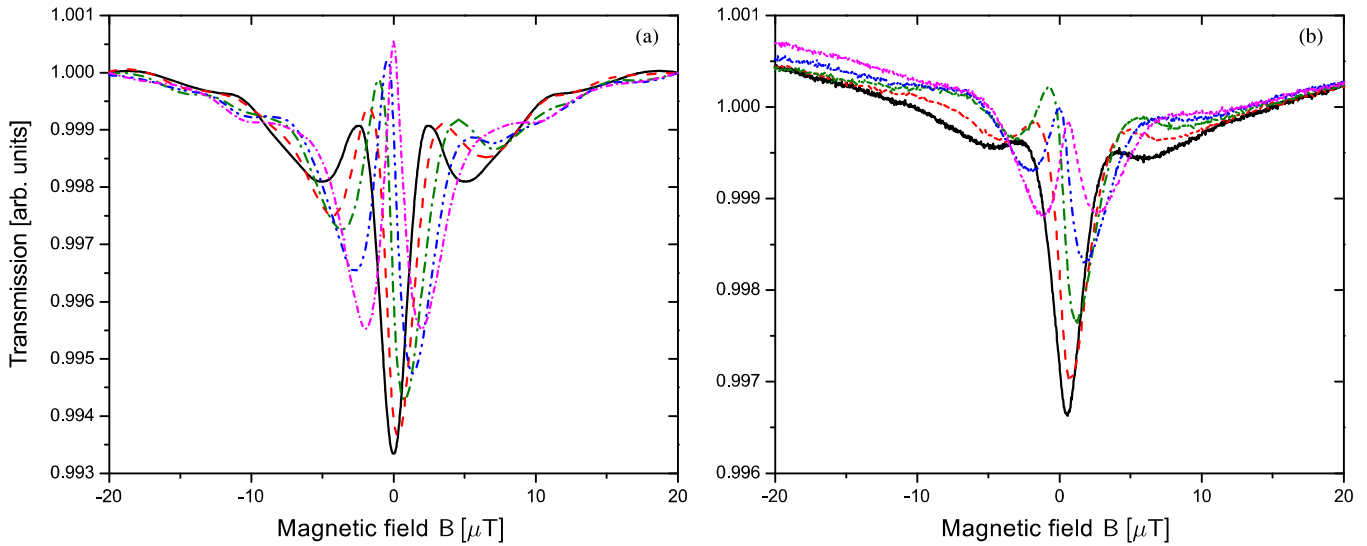


**Figure 6.** Theoretical (a) and experimental (b) results of the probe’s absorption spectra for the  $F_g = 2 \rightarrow F_e = 3$  transition in  $^{87}\text{Rb}$ , for linearly polarized pump and probe beams and different probe beam polarization angles with respect to the pump beam’s polarization ( $0^\circ$  black,  $22.5^\circ$  red,  $45^\circ$  green,  $67.5^\circ$  blue and  $90^\circ$  magenta). The probe and pump powers are  $20 \mu\text{W}$  and  $1.2 \text{ mW}$ , respectively. The pump beam’s inner diameter is  $7 \text{ mm}$ .

EIT transition [23] because the closed transition limits losses of population to the hyperfine level of the uncoupled ground state.

The initial phases of atomic ground state coherences created in the pump beam can be controlled by varying the relative angle between pump and probe beam polarizations. Rotating the polarization of the pump beam by the angle  $\varphi$ , the phase between the circular components of the pump beam is changed by  $2\varphi$ . This leads to the change of the phase of the atomic ground state coherences entering the probe beam by  $2\varphi$ , for a constant magnetic field. In figure 5, we present the results for the probe beam’s polarization rotation for several angles between the electric vectors of linearly polarized pump and probe beams. When we set the angle between the two

electric field vectors to  $\varphi = \pi/2$ , we obtain the opposite sign for the probe beam’s polarization rotation ( $2\varphi = \pi$ ). For the angle  $\varphi$  between  $0$  and  $\pi/2$ , the dispersion-like curves for the probe NMOR beam are centred at an external magnetic field different from zero. The magnetic field corresponding to the centre of the NMOR resonance increases with the angle between the polarizations of two beams because different phases of the coherence require a different magnetic field for the constructive interference to occur. The comparison between results in figures 5(a) and (b) shows that calculated and measured line-shapes have very similar behaviour.

Figure 6 presents the Ramsey interference effects on the shape of EIA resonances. It shows the probe beam’s transmission for several angles between the electric vectors

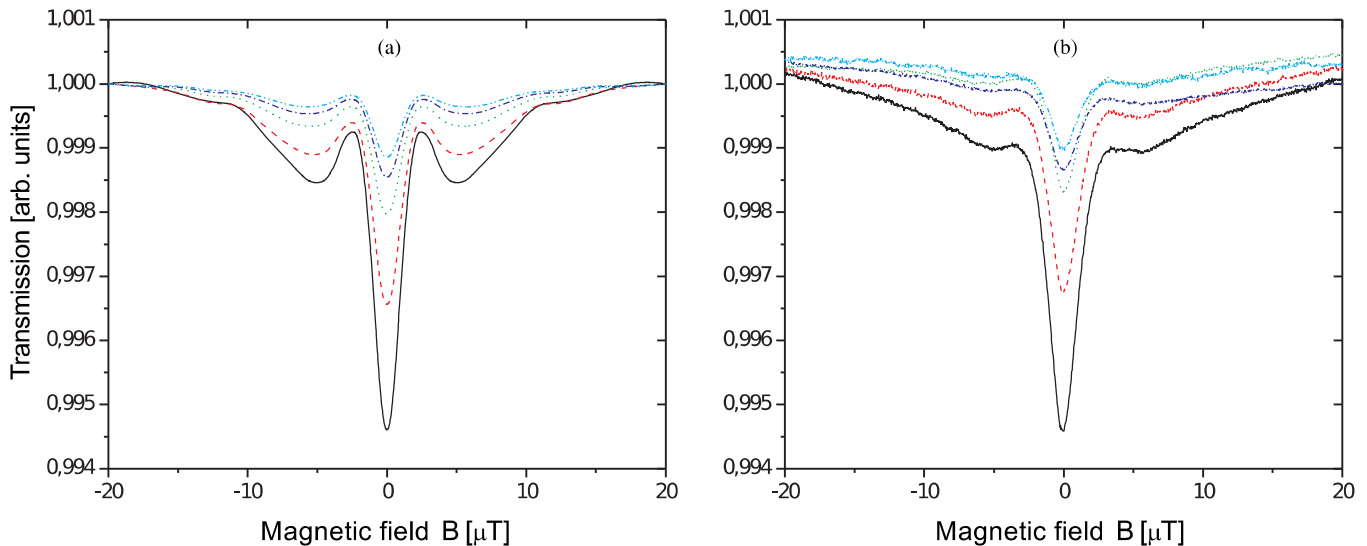


**Figure 7.** Theoretical (a) and experimental (b) results of the probe's absorption spectra for the  $F_g = 2 \rightarrow F_e = 3$  transition in  $^{87}\text{Rb}$ , for linearly polarized pump and probe beams and different powers of the probe beam (10  $\mu\text{W}$  solid, 20  $\mu\text{W}$  dashed, 40  $\mu\text{W}$  dotted, 60  $\mu\text{W}$  dash-dot, 80  $\mu\text{W}$  dash-dot-dot lines). The pump laser power is 1.2 mW. The inner pump beam's diameter is 7 mm.

of linearly polarized pump and probe beams. Interference between the coherently prepared atoms and the probe field will give a probe transmission dip (for  $2\varphi = 0$ ) or transmission gain (for  $2\varphi = \pi$ ) around the same magnetic field values. These two cases are presented by solid and dash-dot-dot lines, respectively. For other values of  $\varphi$ , the transmission has a dispersion-like shape. As the angle between two polarizations increases, the main transmission dip shifts towards higher values of  $B$ , since a larger magnetic field is necessary for the occurrence of constructive interference. The comparison between the results in figures 6(a) and (b) shows that calculated line-shapes are very similar to the measured line-shapes. Similar dispersion-like line-shapes for an arbitrary angle between the linear polarizations of two laser fields have been theoretically predicted for EIA in a bichromatic laser field [35]. The behaviour observed from figures 5 and 6 supports the fact that the atomic ground state coherences essentially determine the development of EIA and NMOR in the considered atomic system.

The effects of the probe laser's power on the probe's transmission are given in figure 7. Both theory and experiment show that the increase of the probe beam's power lowers the amplitudes of the narrow central transmission dip. Higher probe beam power increases the probe beam's contribution to EIA resonance and at the same time lowers the effects of the pump beam induced atomic coherence. As long as the effect of atomic coherence entering the probe beam dominates over the probe's contribution, the resonance width of the central dip remains the same.

## 5. Conclusion

Experimental and theoretical evidences imply that probe EIA and NMOR in a vacuum Rb gas cell at room temperature are strongly affected by interference effects between the probe beam and atomic states prepared by the spatially separated

pump beam in the presence of a small magnetic field. By increasing the size of dark region between the pump and probe, the resonances become narrower. By changing the initial phase of the atomic coherence in the pump beam, fully constructive interference with the probe beam can change into fully destructive interference yielding the change of the sign of the resonances. Moreover, the Ramsey effects seem to be even more pronounced on the EIA linewidth and amplitude than for EIT (developed on atomic transition  $F_g \rightarrow F_e = F_g - 1$ ), as found by comparing the results for both phenomena using the same geometry of the laser beams [22, 23]. Among many differences between EIT and EIA, these results show that the response of ground state Zeeman coherences in an atomic system showing EIA to Ramsey-type excitation is very similar to the previously observed response of Zeeman coherences in atomic systems showing EIT [22, 23].

## Acknowledgments

This work was supported by the Ministry of Education and Science of Serbia, under grant nos III45016 and OI171038 and also by SCOPES JRP IZ73Z0\_127942.

## References

- [1] Akulshin A M, Barreiro S and Lezama A 1998 *Phys. Rev. A* **57** 2996
- [2] Kazantsev A, Smirnov V, Tumaikin A and Yagofarov I 1984 *Opt. Spectrosc. (USSR)* **57** 116  
Kazantsev A, Smirnov V, Tumaikin A and Yagofarov I 1984 *Opt. Spektrosk.* **57** 189
- [3] Harris S E 1997 *Phys. Today* **50** 36
- [4] Arimondo E and Orriols G 1976 *Lett. Nuovo Cimento Soc. Ital. Fis.* **17** 333
- [5] Lezama A, Barreiro S and Akulshin A M 1999 *Phys. Rev. A* **59** 4732
- [6] Dancheva Y, Alzetta G, Cartaleva S, Taslakov M and Andreeva C 2000 *Opt. Commun.* **178** 103

- [7] Kim S K, Moon H S, Kim K and Kim J B 2003 *Phys. Rev. A* **68** 063813
- [8] Brazhnikov D V, Tumaikin A M, Yudin V I and Taichenachev A V 2005 *J. Opt. Soc. Am. B* **22** 57
- [9] Dimitrijević J, Arsenović D and Jelenković B M 2007 *Phys. Rev. A* **76** 013836
- [10] Dimitrijević J, Krmpot A, Mijailović M, Arsenović D, Panić B, Grujić Z and Jelenković B M 2008 *Phys. Rev. A* **77** 013814
- [11] Dimitrijević J, Grujić Z, Mijailović M, Arsenović D, Panić B and Jelenković B M 2008 *Opt. Express* **16** 1343
- [12] Failache H, Valente P, Ban G, Lorent V and Lezama A 2003 *Phys. Rev. A* **67** 043810
- [13] Taichenachev A V, Tumaikin A M and Yudin V I 1999 *Phys. Rev. A* **61** 011802
- [14] Dimitrijević J, Arsenović D and Jelenković B M 2011 *New J. Phys.* **13** 033010
- [15] Valente P, Failache H and Lezama A 2003 *Phys. Rev. A* **67** 013806
- [16] Akulshin A M, Barreiro S, Sidorov A I, Hammafard P and Opat G I 2003 *Phys. Rev. A* **67** 011801
- [17] Akulshin A M, Sidorov A I and Hannaford P 2006 *Phys. Rev. A* **73** 033806
- [18] Goren C, Wilson-Gordon A D, Rosenbluh M and Friedmann H 2003 *Phys. Rev. A* **67** 033807
- [19] Ramsey N 1956 *Molecular Beams* (London: Oxford University Press)
- [20] Xiao Y, Novikova I, Phillips D F and Walsworth R L 2006 *Phys. Rev. Lett.* **96** 043601
- [21] Zibrov A S and Matsko A B 2001 *Phys. Rev. A* **65** 013814
- [22] Grujić Z D, Mijailović M, Arsenović D, Kovacević A, Nikolić M and Jelenković B M 2008 *Phys. Rev. A* **78** 063816
- [23] Mijailović M M, Grujić Z D, Radonjić M, Arsenović D and Jelenković B M 2009 *Phys. Rev. A* **80** 053819
- [24] Kim H-J and Moon H S 2011 *Opt. Express* **19** 168
- [25] Kim H-J and Moon H S 2012 *Opt. Express* **20** 9485
- [26] Barkov L M, Melik-Pashayev D and Zolotarev M 1989 *Opt. Commun.* **70** 467–72
- [27] Kanorsky S I, Weis A, Wurster J and Hänsch T W 1993 *Phys. Rev. A* **47** 1220
- [28] Budker D, Kimball D F, Rochester S M and Yashchuk V V 2000 *Phys. Rev. Lett.* **85** 2088
- [29] Budker D, Gawlik W, Kimball D F, Rochester S M, Yashchuk V V and Weis A 2002 *Rev. Mod. Phys.* **74** 1153
- [30] Radonjić M, Arsenović D, Grujić Z and Jelenković B M 2009 *Phys. Rev. A* **79** 023805
- [31] Nesmeyanov A N 1963 *Vapour Pressure of the Chemical Elements* (Amsterdam: Elsevier)
- [32] Briaudeau S, Saltiel S, Leite J R R, Oria M, Weis A, Bloch D and Ducloy M 2000 *J. Phys. IV France* **10** Pr8–145
- [33] Corwin K L, Lu Z T, Hand C F, Epstein R J and Wieman C E 1998 *Appl. Opt.* **37** 3295
- [34] Chang Chun Bo Xin Photoelectric Co. Ltd. (Chang Chun, Ji Lin, China), [www.bxoptic.com/](http://www.bxoptic.com/)
- [35] Zhukov A A, Zibrov S A, Romanov G V, Dudin Y O, Vassiliev V V, Velichansky V L and Yakovlev V P 2009 *Phys. Rev. A* **80** 033830



**Formation of complex two-dimensional dissipative solitons via spontaneous symmetry breaking**V. Skarka,<sup>1,2,3,\*</sup> N. B. Aleksić,<sup>2,3</sup> M. Lekić,<sup>2</sup> B. N. Aleksić,<sup>2,3</sup> B. A. Malomed,<sup>4</sup> D. Mihalache,<sup>5</sup> and H. Leblond<sup>1</sup><sup>1</sup>*Laboratoire de Photonique d'Angers, EA 4464, Université d'Angers, 2 Boulevard Lavoisier, 49045 Angers Cedex 01, France*<sup>2</sup>*Institute of Physics, University of Belgrade, 11000 Belgrade, Serbia*<sup>3</sup>*Texas A&M University at Qatar, PO Box 23874, Doha, Qatar*<sup>4</sup>*Department of Physical Electronics, Faculty of Engineering, Tel Aviv University, Tel Aviv 69978, Israel*<sup>5</sup>*Horia Hulubei National Institute for Physics and Nuclear Engineering, 407 Atomistilor, Magurele-Bucharest, 077125, Romania*

(Received 12 May 2013; published 25 August 2014)

We propose a complex Ginzburg-Landau equation (CGLE) with localized linear gain as a two-dimensional model for pattern formation proceeding via spontaneous breaking of the axial symmetry. Starting from steady-state solutions produced by an extended variational approximation, simulations of the CGLE generate a vast class of robust solitary structures. These are varieties of asymmetric rotating vortices carrying the topological charge (TC), and four- to ten-pointed revolving stars, whose angular momentum is decoupled from the TC. The four- and five-pointed stars feature a cyclic change of their structure in the course of the rotation.

DOI: [10.1103/PhysRevA.90.023845](https://doi.org/10.1103/PhysRevA.90.023845)

PACS number(s): 42.65.Tg, 42.65.Sf, 47.20.Ky

**I. INTRODUCTION**

The generation of self-organized dissipative structures in nonlinear systems is driven by external energy and/or matter supplies [1]. Various species of self-trapped localized structures are represented by dissipative solitons acting as *attractors* [2,3]. The self-organization is based on the balance of antagonistic effects, with gain compensating losses, and nonlinearity-induced self-contraction arresting the linear diffraction and/or dispersion. The ensuing formation of vast varieties of patterns is apparently spontaneous, and in many cases its origins are not yet understood well, in spite of the great deal of work done on this subject. Generically, the pattern formation proceeds via spontaneous breaking of an underlying continuous symmetry, followed by the emergence of novel forms which feature reduced symmetries [4]. Since the pioneering work of Turing [5], many works have been dealing with models for spontaneous pattern formation in diverse settings; see, e.g., Refs. [6,7].

Complex Ginzburg-Landau equations (CGLEs) constitute a class of ubiquitous models to describe the generation of dissipative-soliton structures in plenty of systems ranging from nanophotonics, plasmonics, nonlinear optics, fluids, and plasmas through superconductivity, superfluidity, quantum field theory, and biological systems [2,3,8–11]. The great deal of work done in this field has demonstrated cogently that CGLEs are appropriate models for studying the spontaneous pattern formation *per se*.

In this work, we demonstrate that the above-mentioned crucially important aspect of the pattern formation, viz., the spontaneous breaking of the continuous symmetry, leading to the emergence of localized structures featuring reduced symmetries, may be adequately modeled by a suitably chosen two-dimensional (2D) CGLE with the competing cubic-quintic (CQ) nonlinear terms. We resort to the synergy of the variational approximation (VA) and parallelized numerical simulations to demonstrate spontaneous formation of previously unexplored solitonic structures, which have diverse

counterparts in nature. Using the CGLE with a spatially modulated linear loss, which features a minimum at the center, we have previously demonstrated that vortices may spontaneously evolve into stably rotating ellipsoidal or crescent vortical structures [12]. The CGLE model developed in the present work offers a vast potential for modeling transitions between different types of spontaneously established patterns, through the generation a broad class of localized states, such as periodically metamorphosing and rotating four- to ten-pointed stars, which resemble complex natural objects, but were not produced by previously studied models.

As mentioned above, the dissipative-soliton pattern formation is the result of the concurrent balance between losses and gain, and between diffraction and cubic self-focusing, which must be supplemented by the quintic self-defocusing, to prevent the collapse in the 2D geometry. The creation of (2+1)D optical solitons (two transverse coordinates  $x$  and  $y$ , with  $+1$  standing for the propagation distance  $z$ , which plays the role of the evolutionary variable) in a CQ medium has been recently directly demonstrated in an experiment [13]. Dissipative solitons have been found in many varieties of CGLEs [2,3,8,14–16]. In particular, (2+1)D solitons with embedded vorticity  $m$ , featuring zero intensity at the center, carry the angular momentum,  $M = mP$ , where  $P$  is their total power (norm); see Eq. (3) below [17]. As a result of the spontaneous pattern change, the intrinsic angular momentum can transmute into explicit rotation of solitonic patterns, as shown in the movie in the Supplemental Material [18] (examples of this are known, e.g., in the form of *azimuthons* [19] and vortex gap solitons [20]).

**II. MODEL FOR SELF-ORGANIZED PATTERN FORMATION**

The present model is based on the (2+1)D CGLE with the CQ nonlinearity that governs the evolution of wave amplitude  $E(x, y, z)$  in the nonlinear medium:

$$iE_z + (1/2)(E_{xx} + E_{yy}) + (1 - i\varepsilon)|E|^2E - (v - i\mu)|E|^4E = ig(r)E, \quad (1)$$

\*vladimir.skarka@univ-angers.fr

where positive coefficients  $\varepsilon$ ,  $\mu$ , and  $\nu$ , account, respectively, for the cubic gain, quintic loss, and quintic saturation of the cubic self-focusing. A crucially important ingredient of the model is represented by an “iceberg of the gain,”  $g(r) = \gamma - \Gamma r^2$  (with radial variable  $r = \sqrt{x^2 + y^2}$ , gain amplitude  $\gamma > 0$ , and gain curvature  $\Gamma > 0$ ) protruding above the surface of the “loss sea,” contrary to the above-mentioned model with the “submerged iceberg,” where the main control parameter  $\gamma$  is negative [12]. A straightforward physical implementation of Eq. (1) is provided by optically pumped laser cavities (especially end-pump solid-state ones). The pumped beam is focused in order to increase the gain, hence the gain is localized [21]. The transverse localization of the laser beam known as “gain guiding” is used in titanium-sapphire, solid-state, Raman, free-electron, and x-ray lasers [22]. The pump beam is typically Gaussian with intensity  $I(r) = I_0 \exp(-r^2/R^2)$ , where  $R$  is its waist. The gain curvature  $\Gamma \propto 1/R^2$  depends mainly on  $R$ , so that the localized gain is determined by the Taylor expansion of intensity  $I(r)$ , which makes the model generic [21–23]. The laser cavity can be adjusted by selecting parameters of the saturable absorber [2,8,9,12,21–23]. Thus, the pattern-formation scenarios reported below can be directly realized in the lasers, as well as in other self-organized systems.

Barring rare exceptions [24], the CGLEs, due to their complexity, do not admit exact solutions. Nevertheless, an analytical approximation for dissipative solitons has been developed using the VA adapted to dissipative systems [11,12], see also Ref. [25]. The VA makes use of the following Gaussian trial function representing the electric field of an axisymmetric Gaussian laser beam with vorticity (topological charge, TC)  $m = 1$ :

$$E = A(r/R) \exp[-r^2/(2R^2) + iCr^2 + i\theta + i\Psi], \quad (2)$$

where amplitude  $A$ , radius  $R$ , wave-front curvature  $C$ , and phase  $\Psi$  have to be optimized.  $\theta$  is the angular coordinate. The total power and angular momentum of the vortex are, respectively,

$$P = \int_0^\infty r dr \int_0^{2\pi} d\theta |E(r,\theta)|^2 = \pi A^2 R^2, \quad (3)$$

$$M = i \int_0^\infty r dr \int_0^{2\pi} d\theta \frac{\partial E^*}{\partial \theta} E.$$

Skipping straightforward details, the following system of evolution equations is produced by the VA (although formally similar to the one derived in Ref. [12], it produces essentially different results, as shown below):

$$dA/dz = \gamma A - \Gamma R^2 A + 5\varepsilon A^3/16 - 8\mu A^5/81 - 2AC, \quad (4)$$

$$dR/dz = 2CR - \Gamma R^3 - \varepsilon A^2 R/16 + 2\mu A^4 R/81, \quad (5)$$

$$dC/dz = -2C^2 + 1/(2R^4) - A^2/(16R^2) + 2\nu A^4/(81R^2), \quad (6)$$

$$d\Psi/dz = -2/R^2 + 3A^2/8 - 10\nu A^4/81, \quad (7)$$

with Eq. (7) decoupled from (4)–(6). Fixed points (FPs) of these equations correspond to steady-state solutions with a small wave-front curvature. Setting  $dR/dz = 0$  in Eq. (5) leads to  $C = \Gamma R^2/2 + \varepsilon A^2/32 - \mu A^4/81$ . In Eq. (6) with  $dC/dz = 0$ , small  $C^2$  may be neglected

giving  $R^2 = 8(A^2 - 32\nu A^4/81)^{-1}$ . The remaining relation for the FP, following from Eqs. (4) with  $dA/dz = 0$ , is  $\gamma + \varepsilon A^2/4 - 2\mu A^4/27 = 2\Gamma R^2$ , which gives rise to two physically relevant steady-state solutions for amplitude  $A$  (solutions for which both  $A$  and  $R$  are real and positive). According to general principles of the analysis of dissipative systems [24,11], the solution with larger  $A$  may be stable, while the one with smaller  $A$  is always unstable. The former solution satisfies condition  $C < 0$ , which is necessary for the simultaneous stable balance of the diffraction and CQ nonlinearity, and of the gain and loss, thus rendering the dissipative solitons stable stationary modes [14,26].

The linear stability analysis of the FPs against small perturbations of amplitude, radius, and wave-front curvature within the framework of Eqs. (4)–(6) was performed via the computation of eigenvalues produced by the respective equation  $\lambda^3 + \alpha_1 \lambda^2 + \alpha_2 \lambda - \alpha_3 = 0$ ,

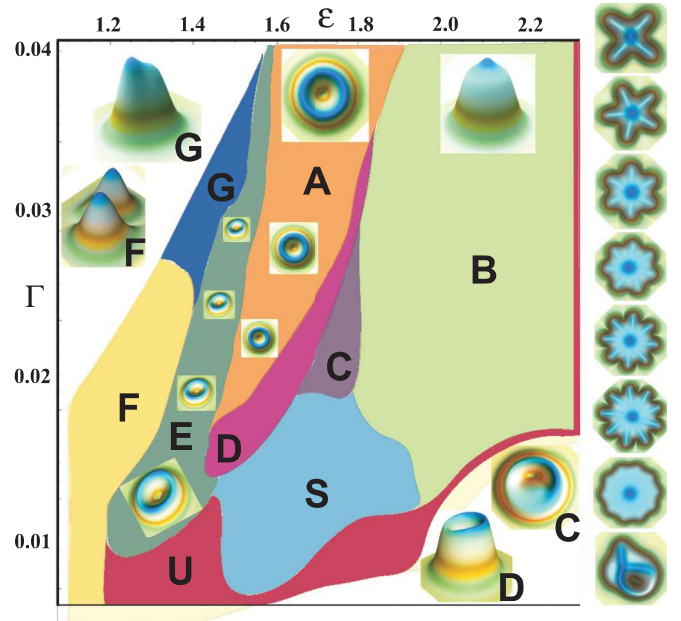


FIG. 1. (Color online) Stability domains produced by the VA-generated fixed points, which are used as the input for direct simulations of Eq. (1), in the plane of the nonlinear-gain strength,  $\varepsilon$ , and the linear-gain curvature,  $\Gamma$  (dimensionless units). Stable axisymmetric vortices are established in region A. In region B, the spontaneous symmetry breaking expels the vortical phase dislocation, resulting in the transition to a bell-shaped axisymmetric mode without the central crater. In intermediate area C, the vortex mutates into a rotating crescent-shaped soliton that fills only half of the original crater, thus breaking the inner circular symmetry. In region D, the vortex crater gets slanted but remains centrosymmetric. In area E, the modulational instability spontaneously breaks the axial symmetry, converting the circular vortex into a rotating elliptic one. In area F, the ring splits into two bell-shaped fragments. For larger  $\Gamma$  in region G, they merge into a stable double-hump shape. In the region of star-shaped patterns, S, small variations of  $\Gamma$  and  $\varepsilon$  result in the self-trapping of revolving four-, five-, six-, seven-, eight-, nine-, and ten-pointed stars with zero TC (examples are shown on the right). The strongly asymmetric steadily rotating “cobra” pattern, shown at the bottom of the right column, appears in interstices between different regions. Structure fails to form only in region U.

stable FPs being identified by the Routh-Hurwitz conditions [11]:  $\alpha_1 \equiv 2\Gamma R^2 - 5\varepsilon A^2/8 + 32\mu A^4/81 > 0$ ,  $\alpha_2 \equiv 8\nu A^4 R^{-2}/81 - \Gamma A^2 R^2(3\varepsilon/2 - 80\mu A^2/81) > 0$ ,  $\alpha_3 \equiv (A^2 - 16R^{-2})\Gamma - (\varepsilon - 16\mu A^2/9)A^2 R^{-4} > 0$ , and  $\alpha_1\alpha_2 - \alpha_3 > 0$ . They cover the entire area charted in Fig. 1 in the plane of the nonlinear-gain and linear-gain curvature parameters,  $\varepsilon$  and  $\Gamma$ , which are most essential for the control of the patterns and transitions between them. For effective saturable absorbers in laser cavities, such as those created by means of a Kerr lens, nonlinear polarization rotation, or an appropriate dopant, these parameters can be easily adjusted in the experiment [21–23]. For instance, different concentrations of the rhodamine dye in ethanol, used as a dopant, can be used in order to recover different values of the nonlinear-gain parameter,  $\varepsilon$  in Fig. 1. The linear-gain curvature parameters  $\Gamma$  can be adjusted to fit values in Fig. 1 by changing the pump-beam intensity. Other coefficients are fixed here as  $\nu = 0.4$ ,  $\mu = 1.4$ , and  $\gamma = 0.08$ , which adequately represent the generic situation (varying these parameters does not entail essential changes). Steady-state solutions do not exist in the white corners of Fig. 1.

Next, Gaussian electric field (2) with parameters of the stable FP adopted by the VA was used as the input for parallelized [27] simulations of Eq. (1). As a result, a variety of stable patterns have been generated, some of them similar to the one assumed by Eq. (2), and some completely different, as summarized in Fig. 1.

### III. SELF-GENERATED DISSIPATIVE VORTEX SOLITONS

In area A of Fig. 1, stable axisymmetric vortex solitons (shown by insets) quickly self-trap by  $z = 10$ . In fact, only in this area does the model give rise to the simple vortex solitons assumed by Eq. (2), while in other domains unique patterns appear. First, in “filamentation” region F, the modulation instability breaks the vortices into two fragments (see the inset also labeled F), as the total power  $P$  given by Eq. (3) is not strong enough to keep the vortex structure stable. In contrast, in area G, the power and strength of the pinning to the localized gain (provided by the pump laser) are much larger, leading to coalescence of the fragments into a revolving double-hump soliton above an “effective threshold” for the pattern formation (see movie [18]); cf. Ref. [17]. An example of this stable pattern is shown in inset G.

In region E adjacent to F, with larger cubic-gain coefficient  $\varepsilon$ , the modulational instability is not strong enough to destroy the vortex, but it breaks the axial symmetry and deforms it into a stable elliptic rotating vortex. Adjacent to A, but on the opposite side (region D), the vortex remains centrosymmetric, but with a slanted shape (see inset D in Fig. 1). At still larger  $\varepsilon$ , in region C, the circular symmetry of the vortex is broken by its transformation into a crescent mode, featuring a half-filled vortical ring.

The common feature of these modes is that they start the self-organization as axisymmetric vortices, and the spontaneous symmetry breaking sets in after a period of a quasistable evolution, which may last for up to thousands of propagation units (unless a symmetry-breaking perturbation is added initially). The robustness of the finally established symmetry-reduced modes has been confirmed by the propagation over

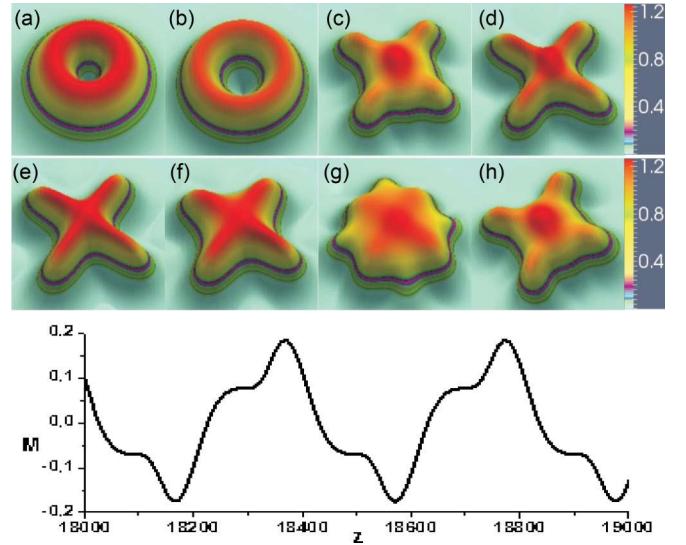


FIG. 2. (Color online) The spontaneous formation of four-pointed patterns. The input ring structure (a) evolves into a vortex soliton at  $z \approx 40$  (b), whose spontaneous symmetry breaking in (c) produces a Celtic-cross structure (at  $z \approx 1400$ ) that subsequently transmutes into other varieties of cross patterns from  $z \approx 1440$  until  $z \approx 1560$  (d)–(g). (h) After a half period ( $T_M \approx 400$ ), a rotated Celtic-cross reappears at  $z \approx 1600$ . Graph M shows oscillations of the angular momentum between  $M = -0.18$  and  $M = +0.18$  (dimensionless units).

$z > 20000$ . On the other hand, small gain curvature  $\Gamma$  cannot prevent quick destruction of vortices in the bottom region U (“unstable”) of Fig. 1.

At larger values of  $\Gamma$  and  $\varepsilon$  (in region B), the original mode undergoes a faster transient evolution, lasting for several hundreds of units, in the form of oscillating breathers, before losing the intrinsic vorticity. Thus, a spontaneous change of the shape occurs, expelling the phase dislocation [see also Fig. 4(a)] and filling the corresponding “crater,” while the former vortex transmutes into a stable fundamental (2+1)D soliton (with  $m = 0$ ), as seen in inset B (a detailed dynamical picture is provided in the movie in the Supplemental Material [18]).

The most remarkable manifestation of the spontaneous formation of complex patterns induced by the symmetry breaking above the effective threshold is the transmutation of vortices into various stars (see the right-hand-side column in Fig. 1), caused by small changes of  $\Gamma$  and  $\varepsilon$  in region S. How the circular symmetry is broken can be seen in detail in movies S1–S6 [18] that display the dynamics of the spontaneous emergence of four-, five-, six-, eight-, and ten-pointed stars, as well as of double-hump localized structures. For instance, at  $\varepsilon = 1.7$  and  $\Gamma = 0.018$ , close to the junction of domains C and D, the input vortex [Fig. 2(a)] at first self-traps into a vortex soliton [Fig. 2(b)]. Then, the vortex loses its inner circular symmetry at  $z \approx 140$ , transforming into a crescent, while the phase dislocation continues to drift, until it escapes at  $z \approx 730$  [18]. Therefore, the outer circular symmetry is gone too. At  $z > 900$ , persistent oscillations commence, corresponding to a robust breather with period  $T_A \approx 5$  and a superimposed beat period,  $T_B \approx 40$ . During another, much longer, beat period,  $T_M \approx 400$ , the angular momentum oscillates between



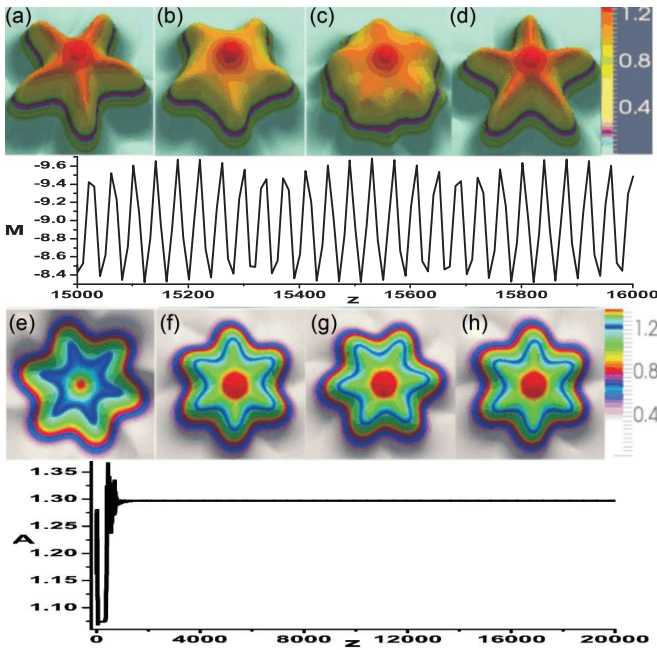


FIG. 3. (Color online) The evolution of the revolving five- and six-pointed stars. The five-pointed star at  $z = 1000$  (a) gets fatter from  $z \approx 1010$  until  $z \approx 1020$  (b) and (c), before rotating by  $30^\circ$  at  $z \approx 1040$  (d). The period of the cyclic evolution is  $T_C \approx 40$ . Angular momentum  $M$  oscillates between  $M = -8.3$  and  $M = -9.7$ , with period  $T_M \approx 360$  (dimensionless units). (e) The transient six-pointed star self-traps into the permanent shape. (f)–(h) The rotation of the star in the course of  $T/6 \approx 36$  from  $z \approx 1080$  until  $z \approx 1116$  (only one sixth of the period is displayed, as the symmetry of the star makes the subsequent evolution tantamount to that shown here). Variations of amplitude  $A$  in the course of the soliton self-formation are displayed in the bottom plot (dimensionless units).

$M = -0.18$  and  $M = +0.18$  (see graph  $M$  in Fig. 2). In the course of beatings, a “Celtic-cross” shape transmutes into a sequence of crosslike ones [see Figs. 2(c)–2(g)], and eventually returns to a rotated “Celtic cross” [Fig. 2(h)] [18]. The robustness of the cyclic shape transmutions in this regime was tested up to  $z = 70\,000$ . Reducing the gain curvature to  $\Gamma = 0.014$ , at the same  $\varepsilon = 1.7$ , increases the number of arms in the pattern, converting it into a five-pointed star, as shown in Figs. 3(a)–3(d) [18]. The scenario of breaking the axial symmetry to the reduced (fivefold) form is the same as in the previous case. However, the angular momentum now oscillates between  $M = -8.3$  and  $M = -9.7$ , with period  $T_M \approx 360$  as in diagram  $M$  in Fig. 3. This star rotates and simultaneously changes its shape, with period  $T_C \approx 40$ , between four particular five-pointed configurations.

Gradually decreasing the gain curvature ( $\Gamma$ ), and increasing the nonlinear gain ( $\varepsilon$ ), a sequence of six-, seven-, eight-, nine-, and ten-pointed stars is generated. After a transient period, each of them rotates at a constant angular velocity, keeping a permanent shape, unlike the cyclic “metamorphosis” featured by the four- and fivefold solitons. An example of a revolving six-pointed star (which resembles snowflakes [28]) is displayed in Figs. 3(e)–3(h), for  $\Gamma = 0.013$  and  $\varepsilon = 1.75$  (see movie in Supplemental Material [18]). The evolution of amplitude  $A$  in the course of the soliton self-organization

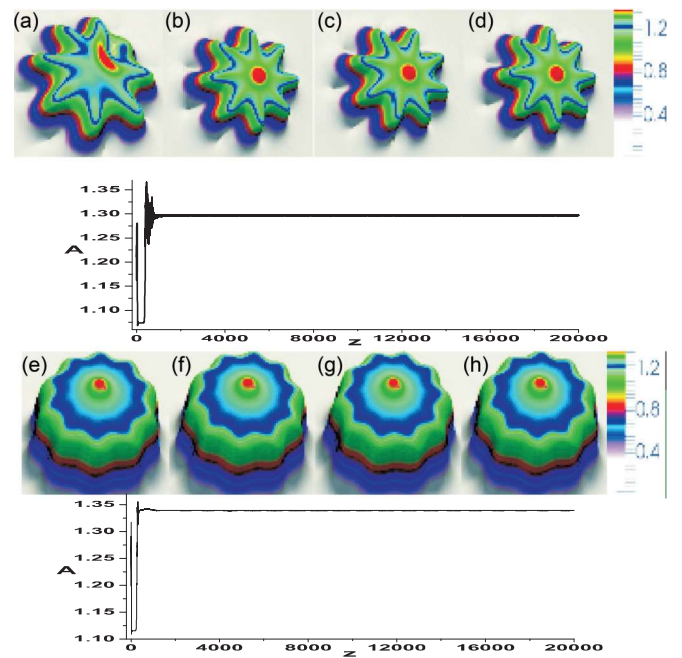


FIG. 4. (Color online) The evolution of the revolving eight- and ten-pointed stars. To establish the reduced symmetry, the phase dislocation is expelled from the vortical structure (a), and an “octopus” soliton emerges at  $z \approx 960$  (b), which rotates, in the course of  $T/8 \approx 24$ , through (c) at  $z \approx 972$  into an identical configuration at  $z \approx 984$  (d). Its spontaneous self-organization is illustrated by the bottom plot displaying the evolution of the amplitude,  $A(z)$ . (e)–(h) The rotation of a ten-pointed star (“decapod”), from (e) at  $z \approx 1200$  to (h) at  $z \approx 1248$  in the course of  $T/10 \approx 48$ . Its self-generation is illustrated by the bottom plot for  $A(z)$ .

is presented in the same figure. In this case, the angular momentum, defined as per Eq. (3), is  $M = -24$ . Further, a typical eightfold “octopus” is presented in Figs. 4(a)–4(d), for the same  $\varepsilon$  but a smaller gain curvature,  $\Gamma = 0.007$ , featuring a smaller radius of the pattern’s core [18]. The self-formation of the eight-pointed soliton star is shown in diagram A. Finally, the spontaneous self-organization of a ten-pointed star for  $\varepsilon = 1.95$  and  $\Gamma = 0.01$  is shown in Figs. 4(e)–4(h), and additionally illustrated by the plot for amplitude  $A$  versus propagation distance  $z$ , which is displayed beneath panels 4(e)–4(h) [18]. All the stars are stable objects with a nonzero angular momentum but zero TC.

Structures with more than ten rays turn out to be transients evolving towards axially symmetric bell-shaped solitons in area B of Fig. 1. Lastly, at borderlines between B, S, and U areas there occur strongly asymmetric steadily rotating structures in the form of “cobras” (shown in the right bottom corner of Fig. 1).

It is precisely the spatially inhomogeneous linear gain ( $\gamma > 0$ ) protruding above the loss sea, which drives, above an effective threshold, in synergy with the nonlinear gain, the spontaneous transition from vortices with topological charge  $m = 1$  to the various species of fundamental solitons with  $m = 0$ , including the above-mentioned class of the star-shaped solitons. Such a spontaneous transition is not possible with the gain submerged into the sea of loss, which was the distinctive

feature of the model considered in Ref. [12]. Therefore, the two models are substantially different, although they include similar terms. As a result, in the model with  $\gamma < 0$ , i.e., without the explicit linear gain, the stability chart in the same parameter plane is totally different [12].

It is relevant to stress the difference of the variety of patterns produced by the spontaneous breaking of the axial symmetry in systems of the CGLE type from their conservative counterparts, based on nonlinear Schrödinger equations (NLSEs). In the latter case, the angular momentum is always related to the TC, while the CGLE allows decoupling of the momentum from the TC, and (2+1)D NLSEs do not give rise to star-shaped patterns [29].

#### IV. CONCLUSIONS

In conclusion, we have established that the evolution of the 2D complex Ginzburg-Landau equation with the cubic-quintic nonlinearity and localized linear gain gives rise to spontaneous formation of many species of patterns, including asymmetric vortices, modes which feature cyclic metamorphosis, and revolving stars without intrinsic TC (topological charge). Starting from the input provided by the variational approximation, systematic simulations have generated the localized structures whose stability areas are charted in Fig. 1 (only in a small part of the parameter space, the input decays without initiating the pattern formation). The instability-induced spontaneous reduction of the continuous rotational symmetry to a discrete subsymmetry is the generic route to the pattern formation in the present setting. In particular, the modulational instability breaks the vortex into two fragments, which fuse into a

double-hump pattern above an effective threshold for the pattern formation, depending of the pump-beam intensity. More sophisticated species of the robust localized modes include four- and fivefold ones, which evolve through cycles of periodically changing forms. On the other hand, six-, seven-, eight-, nine-, and ten-pointed stars steadily revolve, keeping the constant shape and constant angular momentum, with zero TC, unlike vortices, whose angular momentum is proportional to the TC. Stable, oddly shaped rotating patterns (cobras) occur in interstices between stability domains of the different species.

The proposed (2+1)D CGLE model establishes the complex pattern-formation phenomenology in laser cavities and other nonlinear photonic systems. As a consequence, it may be used to monitor real-time stability, and to detect fluctuations causing slight changes of the cavity ( $\epsilon$ ) and pump ( $\Gamma$ ) control parameters in operating lasers, that can be visualized by the change of patterns (e.g., the increase of the number of arms in the star structures). The model may also help in understanding generic features of the pattern formation in other areas, with potential applications to the design of information-processing analog schemes [30].

#### ACKNOWLEDGMENTS

This work was supported, in part, by the **Ministry of Science of Serbia** through Projects No. **OI 171006** and No. **III 45016**. This publication was partially made possible by NPRP Grants No. 5-674-1-114 and No. 6-021-1-005 from the Qatar National Research Fund (a member of Qatar Foundation). D.M. was supported by the **Romanian Ministry of Education and Research** (Project No. **PN-II-ID-PCE-2011-3-0083**).

- 
- [1] G. Nicolis and I. Prigogine, *Self-Organization in Non-Equilibrium Systems* (Wiley, New York, 1977).
- [2] I. S. Aranson and L. Kramer, *Rev. Mod. Phys.* **74**, 99 (2002); N. Rosanov, *Spatial Hysteresis and Optical Patterns* (Springer, Berlin, 2002); *Dissipative Solitons: From Optics to Biology and Medicine*, Lecture Notes in Physics Vol. 751, edited by N. N. Akhmediev and A. Ankiewicz (Springer, Berlin, 2008).
- [3] B. A. Malomed, *Physica D* **29**, 155 (1987); S. Fauve and O. Thual, *Phys. Rev. Lett.* **64**, 282 (1990); W. van Saarloos and P. C. Hohenberg, *ibid.* **64**, 749 (1990); V. Hakim, P. Jakobsen, and Y. Pomeau, *Europhys. Lett.* **11**, 19 (1990); B. A. Malomed and A. A. Nepomnyashchy, *Phys. Rev. A* **42**, 6009 (1990); A. Komarov, H. Leblond, and F. Sanchez, *Phys. Rev. E* **72**, 025604 (2005); J. N. Kutz, *SIAM Rev.* **48**, 629 (2006); W. H. Renninger, A. Chong, and F. W. Wise, *Phys. Rev. A* **77**, 023814 (2008); E. Ding and J. N. Kutz, *J. Opt. Soc. Am. B* **26**, 2290 (2009); M. Tlidi, A. G. Vladimirov, D. Pieroux, and D. Turaev, *Phys. Rev. Lett.* **103**, 103904 (2009); D. Mihalache, *Proc. Rom. Acad. Ser. A* **11**, 142 (2010); J. Jimenez, Y. Noblet, P. V. Paulau, D. Gomila, and T. Ackemann, *J. Opt.* **15**, 044011 (2013); C. Fernandez-Oto, M. G. Clerc, D. Escaff, and M. Tlidi, *Phys. Rev. Lett.* **110**, 174101 (2013).
- [4] P. W. Anderson, *Science* **177**, 393 (1972).
- [5] A. M. Turing, *Philos. Trans. R. Soc. London* **237**, 37 (1952).
- [6] P. Tracqui, *Rep. Prog. Phys.* **72**, 056701 (2009); S. Kondo and T. Miura, *Science* **329**, 1616 (2010).
- [7] M. Eiraku, N. Takata, H. Ishibashi, M. Kawada, E. Sakakura, S. Okuda, K. Sekiguchi, T. Adachi, and Y. Sasai, *Nature* **472**, 51 (2011).
- [8] Y. S. Kivshar and G. P. Agrawal, *Optical Solitons: From Fibers to Photonic Crystals* (Academic Press, San Diego, 2003).
- [9] F. T. Arecchi, S. Boccaletti, and P. L. Ramazza, *Phys. Rep.* **318**, 83 (1999); F. Lederer, G. I. Stegeman, D. N. Christodoulides, G. Assanto, M. Segev, and Y. Silberberg, *ibid.* **463**, 1 (2008).
- [10] D. Mihalache, D. Mazilu, F. Lederer, Y. V. Kartashov, L.-C. Crasovan, L. Torner, and B. A. Malomed, *Phys. Rev. Lett.* **97**, 073904 (2006).
- [11] V. Skarka and N. B. Aleksić, *Phys. Rev. Lett.* **96**, 013903 (2006).
- [12] V. Skarka, N. B. Aleksić, H. Leblond, B. A. Malomed, and D. Mihalache, *Phys. Rev. Lett.* **105**, 213901 (2010).
- [13] E. L. Falcao-Filho, C. B. de Araujo, G. Boudebs, H. Leblond, and V. Skarka, *Phys. Rev. Lett.* **110**, 013901 (2013).
- [14] V. Skarka, N. B. Aleksić, and V. I. Berezhiani, *Phys. Rev. A* **81**, 045803 (2010).
- [15] N. N. Akhmediev and A. Ankiewicz, *Solitons, Nonlinear Pulses and Beams* (Chapman and Hall, London, 1997).

- [16] B. A. Malomed and H. G. Winful, *Phys. Rev. E* **53**, 5365 (1996); P. V. Paulau, *ibid.* **84**, 036213 (2011).
- [17] L.-C. Crasovan, B. A. Malomed, and D. Mihalache, *Phys. Rev. E* **63**, 016605 (2001); V. Skarka, N. B. Aleksić, M. Derbazi, and V. I. Berezhiani, *Phys. Rev. B* **81**, 035202 (2010).
- [18] See Supplemental Material at <http://link.aps.org/supplemental/10.1103/PhysRevA.90.023845> for Movies S1–S6 which display the real dynamics of the self-organized pattern formation of four-, five-, six-, eight-, and ten-pointed stars, as well as of the double-hump structures (with the same color bars as in corresponding figures).
- [19] A. S. Desyatnikov and Yu. S. Kivshar, *Phys. Rev. Lett.* **88**, 053901 (2002); A. S. Desyatnikov, A. A. Sukhorukov, and Y. S. Kivshar, *ibid.* **95**, 203904 (2005); V. M. Lashkin, E. A. Ostrovskaya, A. S. Desyatnikov, and Y. S. Kivshar, *Phys. Rev. A* **80**, 013615 (2009).
- [20] H. Sakaguchi and B. A. Malomed, *J. Phys. B: At. Mol. Opt. Phys.* **37**, 2225 (2004).
- [21] T. Y. Fan, A. Sanchez, and W. E. DeFeo, *Opt. Lett.* **14**, 1057 (1989); W. Koechner and M. Bass, *Solid-State Lasers: A Graduate Text* (Springer, New York, 2003).
- [22] F. Salin, J. Squier, and M. Piche, *Opt. Lett.* **16**, 1674 (1991); X. Yan, Q. Liu, D. Wang, and M. Gong, *Opt. Express* **19**, 6883 (2011); Z. Xiang, D. Wang, S. Pan, Y. Dong, Z. Zhao, T. Li, J. Ge, Ch. Liu, and J. Chen, *ibid.* **19**, 21060 (2011); P. R. Battle, J. G. Wessel, and J. L. Carlsten, *Phys. Rev. A* **48**, 707 (1993); J. E. La Sala, D. A. G. Deacon, and J. M. J. Madey, *Phys. Rev. Lett.* **59**, 2047 (1987); E. E. Fill, *Opt. Commun.* **67**, 441 (1988).
- [23] F. Salin and J. Squier, *Opt. Lett.* **17**, 1352 (1992).
- [24] N. N. Akhmediev, V. V. Afanasjev, and J. M. Soto-Crespo, *Phys. Rev. E* **53**, 1190 (1996); J. Atai and B. A. Malomed, *Phys. Lett. A* **246**, 412 (1998); W. J. Firth and P. V. Paulau, *Eur. Phys. J. D* **59**, 13 (2010).
- [25] D. J. Kaup and B. A. Malomed, *Physica D* **87**, 101 (1995).
- [26] V. Skarka, D. V. Timotijević, and N. B. Aleksić, *J. Opt. A: Pure Appl. Opt.* **10**, 075102 (2008).
- [27] B. N. Aleksić, N. B. Aleksić, V. Skarka, and M. Belić, *Phys. Scr. T* **149**, 014036 (2012).
- [28] T. Bartels-Rausch, V. Bergeron, J. H. E. Cartwright, R. Escribano, J. L. Finney, H. Grothe, P. P. J. Gutiérrez, J. Haapala, W. F. Kuhs, J. B. C. Pettersson, S. D. Price, C. I. Sainz-Díaz, D. J. Stokes, G. Strazzulla, E. S. Thomson, H. Trinks, and N. Uras-Aytemiz, *Rev. Mod. Phys.* **84**, 885 (2012).
- [29] B. A. Malomed, D. Mihalache, F. Wise, and L. Torner, *J. Opt. B: Quantum Semiclassical Opt.* **7**, R53 (2005).
- [30] *Spontaneous Symmetry Breaking, Self-Trapping, and Josephson Oscillations*, edited by B. A. Malomed (Springer-Verlag, Berlin and Heidelberg, 2013).

# Raman–Ramsey electromagnetically induced transparency in the configuration of counterpropagating pump and probe in vacuum Rb cell

Ivan S. Radojičić,\* Milan Radonjić, Marina M. Lekić, Zoran D. Grujić, Dragan Lukić, and Branislav Jelenković

*Institute of Physics, University of Belgrade, Pregrevica 118, 11080 Belgrade, Serbia*

*\*Corresponding author: ivan.radojicic@ipb.ac.rs*

Received November 19, 2014; revised January 22, 2015; accepted January 22, 2015; posted January 22, 2015 (Doc. ID 226841); published February 13, 2015

Counterpropagating, spatially separated hollow pump and coaxial probe laser beams generate narrow Zeeman electromagnetically induced transparency (EIT) resonances in the vacuum Rb cell. The lasers are locked to  $D_2$  line transition  $F_g = 2 \rightarrow F_e = 1$  of  $^{87}\text{Rb}$ . For the probe laser beam intensity between 0.1 and 3.0 mW/cm<sup>2</sup> this Ramsey-type configuration yields dual-structured resonances having a narrow peak on top of a broader pedestal. Linewidths of the narrow peak are nearly independent of the probe laser beam intensity and of the probe diameter (for diameters 0.8 and 2.7 mm), provided that the dark region between the pump and the probe beams is fixed. At the probe laser beam intensities below 0.1 mW/cm<sup>2</sup> Zeeman EIT is a single narrow resonance. With this geometry of laser beams, and at low probe intensity, the presence of the pump enables the probe EIT, i.e., the probe transmission becomes enhanced in a narrow spectral window. Accompanying theoretical model showed good quantitative agreement with the measurements. © 2015 Optical Society of America

*OCIS codes:* (270.1670) Coherent optical effects; (300.3700) Linewidth.

<http://dx.doi.org/10.1364/JOSAB.32.000426>

## 1. INTRODUCTION

Electromagnetically induced transparency (EIT) is a laser(s) transmission peak due to coherences between atomic levels induced by the same laser(s) whose transmission is monitored [1]. EIT as a quantum phenomenon has its classical analog [2]. In a typical interaction scheme, two lasers couple two hyperfine levels (hyperfine coherence) or Zeeman sublevels (Zeeman coherence) with the common excited-state hyperfine level. Hyperfine (Zeeman) level (sublevels) are long lived and degeneracy of the ground-state angular momentum is larger or equal to that of the excited state. Alkali atoms with two long-lived hyperfine levels in the ground state, and optical transitions to excited-state hyperfine level in a suitable wavelength region are most often used in EIT experiments. Quantum EIT, the subject of this investigation, is a manifestation of the coherent superposition of Zeeman sublevels of the ground hyperfine level due to interactions with the laser field. Superposition called dark state [3–5] is decoupled from the interaction and presents foundation of EIT. EIT has gained considerable interest because of nonlinear response and steep dispersion around the atomic resonance at reduced absorption.

A method analog to the Ramsey method of separated oscillatory fields [6] can be utilized for narrowing dark resonances in alkali atoms using thermal atomic beam [7–9] or atoms contained in vacuum glass cells, by spatially separating pump and probe beams [10,11]. Ramsey-like mechanisms yield very narrow EIT resonances in alkali-metal vapor cells with buffer gas (or with antirelaxation wall coating), even with a single laser beam [12,13].

In experiments with vacuum gas cells it is necessary to apply a particular geometry of a hollow pump and a narrow coaxial probe in order to see narrow fringes on the probe EIT [14], or to implement a multizone spectroscopy like in [15]. Instead of spatially separating continuous wave pump and probe, pulses of the pump and probe were used in a Ramsey-like method for narrowing EIT by switching the laser beams on and off. Hyperfine EIT produced in the double  $\Lambda$  scheme with the pump and the weak probe pulse have produced high contrast, very narrow fringes ( $\approx 100$  Hz) in the probe EIT in Cs buffer gas cell [16,17].

In this work we use counterpropagating pump and probe beams to study Ramsey effect on linewidths and amplitudes of the probe Zeeman EIT in Rb vacuum cell. Zeeman coherences are generated in the  $F_g = 2$  hyperfine level of the ground state of  $^{87}\text{Rb}$  by the pump beam, made in the form of a hollow cylinder. The atomic coherence is carried by the atomic thermal motion to a small-diameter probe beam that passes through the center of the hollow pump laser. There is dark region between the pump and probe beam, which we keep constant in the study. This counterpropagating geometry allows EIT with much weaker probe intensity as opposed to the copropagating pump and probe [14] due to reduced multiple scattering of pump light into the direction of the probe and toward the photodetector. Therefore in this work we cover much lower probe laser beam intensities than in [14]. Also, differently than in [14], here we investigate EIT line shapes for  $D_2$  line of  $^{87}\text{Rb}$ . We examine how different probe diameters, for the same dark region, change the shape



of the dual-structured probe EIT resonances having a narrower central peak (due to atomic coherence coming from the pump) and a wider pedestal (due to probe beam influence). The dependence of narrow resonances as a function of the probe laser beam intensity and diameter is studied. Experimental results are compared with the detailed theoretical model based on time-dependent optical Bloch equations (OBEs). We determine the range of the probe intensity when Zeeman EIT has only narrow structure, i.e., the transmission of the probe beam becomes enhanced when the pump is turned on. EIT resonances in vacuum cells, even with the Ramsey method, are wider than EIT in buffer gas cells. However, there is an interest for narrow EIT in vacuum cells at room temperature because atomic collisions, and temperature fluctuations are reduced, which is important for EIT applications.

## 2. EXPERIMENTAL SETUP

The schematic of the experiment, given in Fig. 1, describes the geometry of laser beams we have used to investigate effects of spatially separating the probe and pump beam on the EIT line shapes. A large-diameter hollow pump beam and narrow coaxial probe beam counterpropagate through the Rb cell. The two beams are generated from the same external cavity diode laser (ECDL). Employing counterpropagating probe and pump beams requires precise laser frequency tuning to the optical transition; otherwise the probe and pump will not be able to interact with the same atoms (atomic velocity is not expected to change in the region between the pump and probe). The laser is locked using the Doppler free dichroic atomic laser lock (DDAVLL) technique [18] on  $D_2$  line transition  $F_g = 2 \rightarrow F_e = 1$  of  $^{87}\text{Rb}$ , and is linearly polarized. The vacuum Rb cell, 85 mm long and of 25 mm in diameter, is kept at room temperature. The Rb cell is inside cylindrical solenoid that provides longitudinal magnetic field. The triple layers of  $\mu$ -metal, around the cell, minimize effects of stray magnetic fields. In the experiment we measure the probe transmission as a function of the external magnetic field. Pump intensity is  $11.5 \text{ mW/cm}^2$  and the probe intensity varies from  $0.1$  to  $3.0 \text{ mW/cm}^2$ .

We have measured Zeeman EIT by sweeping the magnetic field for two probe  $1/e^2$  diameters, 2.7 and 0.8 mm. The pump beam inner diameter is changed from 5 to 7 mm when the probe diameter is changed from 0.8 to 2.7 mm, respectively.

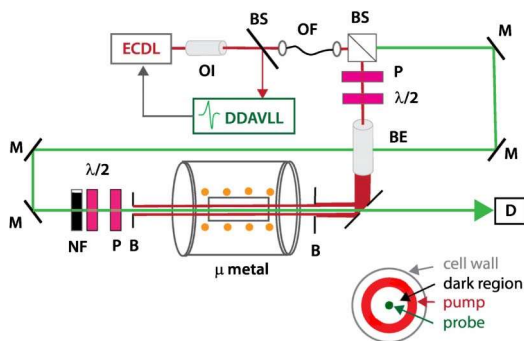


Fig. 1. Experimental setup: ECDL, external cavity diode laser; OI, optical isolator; DDAVLL, Doppler free dichroic atomic laser lock; BS, beam splitter; OF, optical fiber; M, mirrors; P, polarizer; NF, variable neutral density filter; BE, beam expander;  $\lambda/2$ , retardation plate; B, blade iris diaphragm; D, photodetector.

Thus, the distance between pump and the probe, or “dark region,” is the same and equals 2.1 mm.

## 3. THEORY

The model is similar to one described in more detail in [19]. The difference stems from the fact that in this case the pump and probe are counterpropagating. The evolution of Rb atoms interacting with spatially separated pump and probe laser beams is described using time-dependent OBEs for the atomic density matrix

$$\frac{d\hat{\rho}}{dt} = -\frac{i}{\hbar}[\hat{H}_{\text{atom}}(B) + \hat{H}_{\text{int}}(t), \hat{\rho}] + \left(\frac{d\hat{\rho}}{dt}\right)_{\text{SE}} + \left(\frac{d\hat{\rho}}{dt}\right)_{\text{relax}}, \quad (1)$$

where

$$\hat{H}_{\text{atom}}(B) = \sum_j \hbar\omega_j(B)|g_j\rangle\langle g_j| + \sum_k \hbar\omega_k(B)|e_k\rangle\langle e_k| \quad (2)$$

is the Hamiltonian of an atom in the external magnetic field  $\mathbf{B}$ , aligned with the laser beam propagation direction. Zeeman-shifted energies  $\hbar\omega_j(B)$  ( $\hbar\omega_k(B)$ ) correspond to ground (excited) states  $|g_j\rangle$  ( $|e_k\rangle$ ). The interaction of an atom with laser is treated in dipole approximation

$$\hat{H}_{\text{int}}(t) = -\sum_{j,k} \mathbf{E}(t) \cdot \mathbf{d}_{jk}(|g_j\rangle\langle e_k| + |e_k\rangle\langle g_j|), \quad (3)$$

where  $\mathbf{E}(t)$  is the laser electric field (in the atomic reference frame) and  $\mathbf{d}_{jk}$  is the atomic electric dipole moment for the transition between states  $|g_j\rangle$  and  $|e_k\rangle$ . Spontaneous emission is given by

$$\left(\frac{d\hat{\rho}}{dt}\right)_{\text{SE}} = \sum_m 2\hat{\Gamma}_m \hat{\rho} \hat{\Gamma}_m^\dagger - \hat{\Gamma}_m^\dagger \hat{\Gamma}_m \hat{\rho} - \hat{\rho} \hat{\Gamma}_m^\dagger \hat{\Gamma}_m, \quad (4)$$

where  $\hat{\Gamma}_m$  are Lindblad operators related to dipole transitions from the excited- to ground-state manifold. In order to obtain good agreement with experimental line shapes, and in addition to [19], we include relaxation of ground-state populations toward the equilibrium

$$\left(\frac{d\hat{\rho}}{dt}\right)_{\text{relax}} = -\gamma \sum_j \left( \rho_{g_j g_j} - \frac{1 - \pi_e}{8} \right) |g_j\rangle\langle g_j|, \quad (5)$$

where  $\pi_e$  is the total excited-state population. When considering  $D_2$  line transition  $F_g = 2 \rightarrow F_e = 1$ , the excited hyperfine levels  $F_e = 2$  and  $F_e = 3$  are also populated due to the Doppler broadening and therefore have to be taken into account. Equations for  $F_g = 1$  ground-level density matrix elements are disregarded since that level is not laser-coupled. OBEs are numerically integrated for a collection of atoms passing through the laser beams at different trajectories with velocities sampling Maxwell-Boltzmann distribution. The cylindrical symmetric atomic ensemble density matrix is obtained after averaging over velocities and suitable angular integration. This enables the calculation of atomic vapor polarization, the laser electric field after propagation through the Rb cell and, eventually, Zeeman EIT resonances. Additional details can be found in [20,21].

Pump and probe laser beams have linear polarization and the same frequency. Their propagation directions are

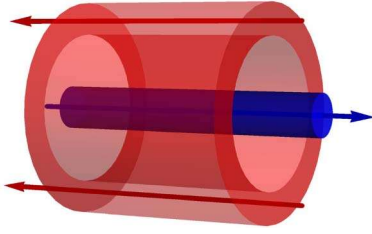


Fig. 2. Radial profiles of counterpropagating hollow pump and coaxial probe laser beams used in the theoretical model.

opposite. As schematically presented in Fig. 2, the probe laser beam passes coaxially through the center of the hollow pump beam. The probe beam profile along radial distance  $r$  at the Rb cell entrance is modeled by a Gaussian,

$$I_{\text{probe}}(r) = 2\bar{I}_{\text{probe}} \exp(-2r^2/r_0^2), \quad (6)$$

where  $r_0$  is  $1/e^2$  the radius of the probe beam and  $\bar{I}_{\text{probe}}$  is the probe beam intensity (total probe power divided by  $r_0^2\pi$ ). The pump beam radial intensity profile is taken to be the same along the cell length and ring-shaped:

$$I_{\text{pump}}(r) = \bar{I}_{\text{pump}} a(\text{erf}(p(r-r_1)) - \text{erf}(p(r-r_2))), \quad (7)$$

where  $\bar{I}_{\text{pump}}$  is the pump beam intensity and  $a$  is the normalization constant. Parameter  $p$  controls the steepness of the profile near the beam inner and outer edge that are determined by the parameters  $r_1$  and  $r_2$ , respectively.

#### 4. RESULTS AND DISCUSSION

We show results of interactions of the probe beam with atoms prepared in the dark state by the spatially separated pump beam. Both the pump and probe have linear and mutually parallel polarizations. Sweep of the magnetic field provides detuning of two circular components from the two photon resonance among Zeeman sublevels for which  $\Delta m_F = 2$ . In the following we present EIT line shapes, amplitudes, and linewidths obtained by measuring the probe transmission at different magnetic fields. In this work we are not concerned with absolute values of the probe transmission. Therefore, we present EIT line shapes normalized such that maximal transmission is set to unity.

Figure 3(a) shows measured and Fig. 3(b) calculated Zeeman EIT resonances for two probe laser beam intensities,  $0.2 \text{ mW/cm}^2$  (upper rows) and  $1.4 \text{ mW/cm}^2$  (lower rows), and two probe laser beam diameters,  $0.8 \text{ mm}$  (left column) and  $2.7 \text{ mm}$  (right column). EIT line shapes for both laser beam intensities have dual structure, a narrow peak with fringes appearing on top of a broader pedestal. A broader pedestal is generated by the probe itself, while narrow peak and fringes result from Ramsey interference. Ramsey fringes are well pronounced for the narrower probe beam because of the shorter interaction time of Rb atoms with the probe light, i.e., smaller probe influence. When the probe laser beam intensity is increased, or its diameter is increased, the Ramsey fringes lose their visibility. Theoretical results in Fig. 3(b) are in quite good agreement with the experiment.

EIT widths and amplitudes of the narrow and wide structures are obtained after resolving the two structures in EIT line shapes. Figure 4 presents widths of the narrow structure

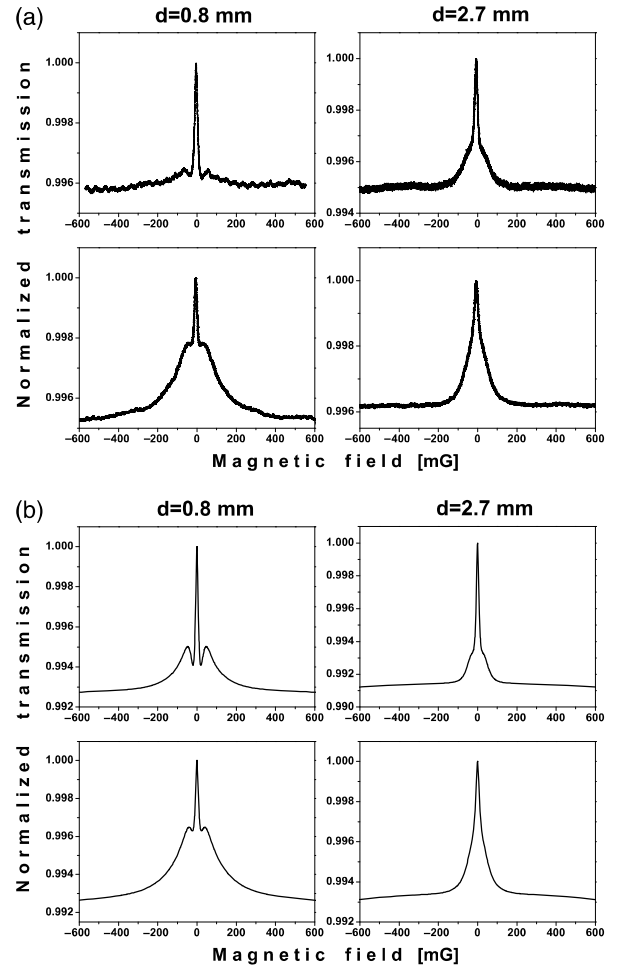


Fig. 3. (a) Experimental and (b) theoretical Zeeman EIT at  $D_2$  line, for two probe laser beam intensities,  $0.2 \text{ mW/cm}^2$  (upper rows) and  $1.4 \text{ mW/cm}^2$  (lower rows), and two probe laser beam diameters,  $0.8 \text{ mm}$  (left column) and  $2.7 \text{ mm}$  (right column).

of EIT resonances, for two probe laser beam diameters. Experimental results are in Fig. 4(a), and theoretical in Fig. 4(b). The linewidth of the narrow structure in our experiment is  $\approx 15 \text{ mG}$  or  $\approx 18 \text{ kHz}$ . This is similar to the narrowest EIT obtained in vacuum alkali gas cells with multizone Ramsey technique [15]. As seen from Fig. 4, the narrow structure EIT linewidth is narrower and also more robust against probe intensity for the narrower probe beam. The behavior of the pedestal width is as expected for a single beam EIT [22]: it is narrower for the wider probe, and it changes much more rapidly with the probe laser beam intensity. Calculated linewidths follow the same trend and the narrower probe beam also gives narrower linewidth.

In the experiment with a single laser beam and coated cell [13], EIT has also dual structure. Similar to our result, narrow structure of EIT in [13] is narrower for the smaller laser beam diameter. Moreover, intensity dependence of the linewidths of the narrower peak is similar as in our setup: EIT linewidth obtained with the narrower beam is less dependent on the laser intensity. Such intensity dependence given in [13] is due to the geometry of the cell and the Ramsey effect of a multiple interaction of atoms with the same laser beam—narrowing the laser increases the dark region, i.e., time that the atom spends in the dark. The similar behavior of the



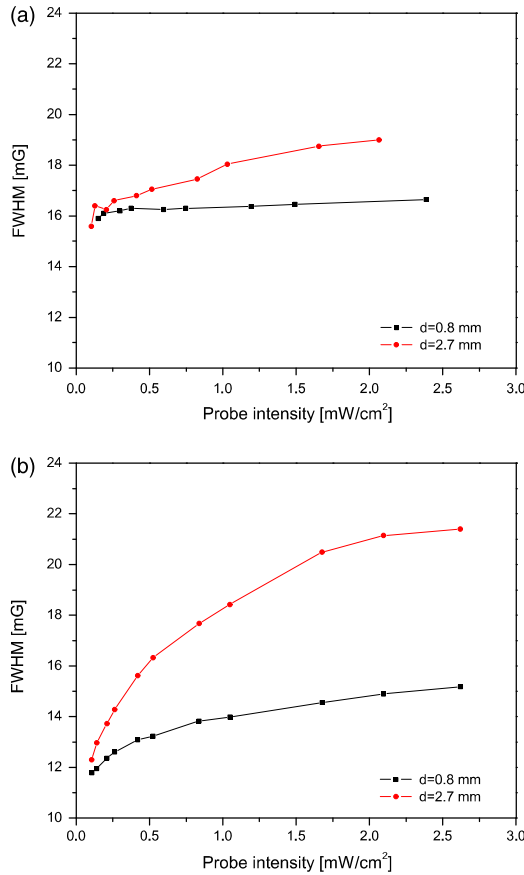


Fig. 4. (a) Experimental and (b) theoretical full width at half-maximum of the narrow structure of EIT as a function of the probe laser beam intensity, for two probe laser beam diameters, 0.8 and 2.7 mm.

narrow peak of the EIT in our work has a different explanation. The probe laser beam, apart from probing the atoms coherently prepared in the pump beam, influences the atomic evolution, which affects the narrow structure linewidth. During atomic passage through the laser beams the atomic state changes due to competitive effects of the laser electric field and the external magnetic field. The laser field continuously prepares the atoms into the dark state. The external magnetic field causes oscillations of the atomic ground-state coherences at the corresponding Larmor frequency and alters the atoms from the dark state. When the external magnetic field is zero the atoms reach the dark state inside the strong pump beam, which consequently leads to a maximum in the probe transmission. At nonzero magnetic field the state of the atoms passing through the probe beam differs from the dark state, so that the probe transmission decreases. However, this decrease in probe transmission due to the influence of the magnetic field is partially compensated by preparation of the atoms into the dark state within the probe beam. Hence, the actual probe transmission at some magnetic field is somewhat larger than the one expected without the probe influence. This causes broadening of the narrow structure in Zeeman EIT resonances that becomes more pronounced as the probe intensity and/or diameter increases.

Figure 5 shows measured and calculated amplitudes of the narrow structure of EIT resonances, for probe laser beam diameters 0.8 mm [Fig. 5(a)] and 2.6 mm [Fig. 5(b)]. As both

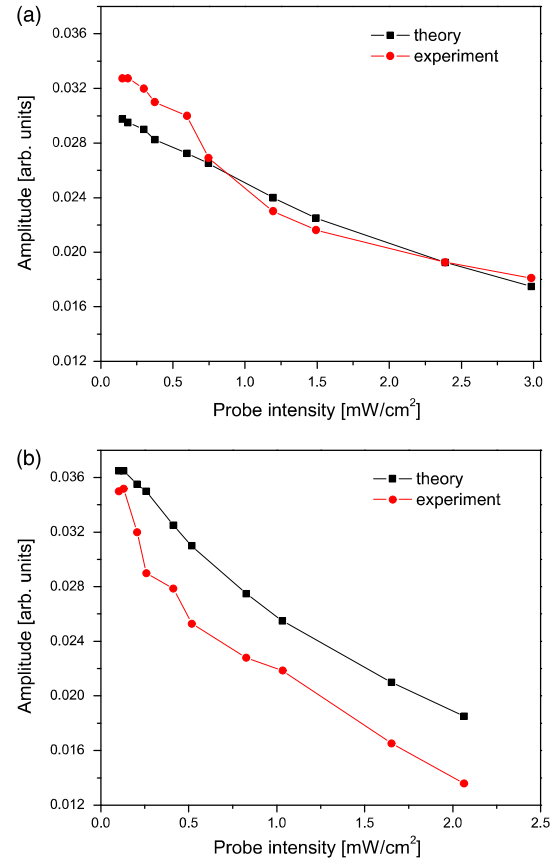


Fig. 5. Experimental and theoretical results for the amplitudes of the narrow structure of EIT resonances for two probe laser beam diameters: (a) 0.8 mm and (b) 2.7 mm.

experiment and theory show, amplitudes of narrow peaks of the probe EIT are nearly independent on probe beam diameter. Their dependence on the probe intensity and diameter is different than the amplitude of the wide structure EIT.

Amplitudes of the narrow peak of the probe EIT (obtained when the pump laser beam is turned on) have different dependence on the probe laser beam intensity than a single beam EIT, tuned to the same Raman resonance and with the same diameter. This is demonstrated in Fig. 6 where we plot amplitudes of both narrow and wide structure as a

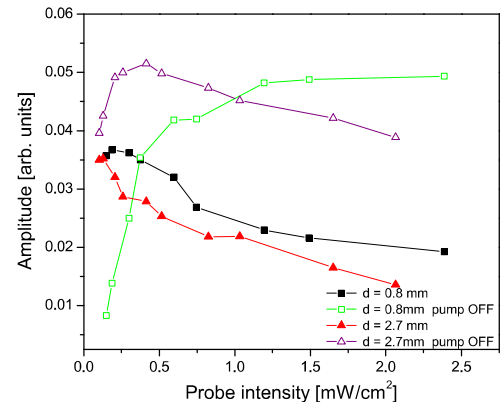


Fig. 6. Amplitudes of the probe EIT with and without pump laser beam, for two probe laser beam diameters: 0.8 and 2.7 mm. Amplitudes of wide (narrow) structures are shown for the pump laser beam turned off (on).

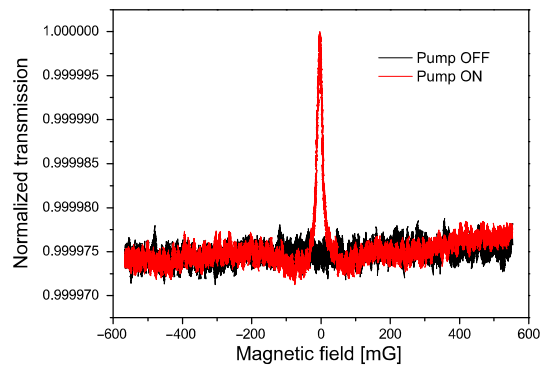


Fig. 7. Probe beam Zeeman EIT at  $D_2$  line, with and without the pump beam. Intensities of the probe and pump beams are  $0.1 \text{ mW/cm}^2$  and  $11.5 \text{ mW/cm}^2$ , respectively.

function of probe intensity, for two probe diameters. The maximum of the narrow structure of the probe EIT in the Raman–Ramsey configuration is at very low laser intensities, below values that we can detect in the experiment.

At very low probe laser beam intensities, below  $0.1 \text{ mW/cm}^2$ , the probe EIT has only narrow structure. The transmission of the weak probe can be controlled in a narrow spectral range around zero magnetic field by switching the pump beam on/off. For small magnetic fields and when the pump laser beam is present, the atoms coming into the probe beam are already coherently prepared into the dark state. This leads to the increase of the probe transmission, as presented in Fig. 7, where we show probe EIT for  $0.8 \text{ mm}$  probe beam diameter and for probe beam intensity of  $0.1 \text{ mW/cm}^2$ , without or with pump beam of intensity  $11.5 \text{ mW/cm}^2$ . Enhancement of the probe transmission is better for larger pump beam intensities.

## 5. CONCLUSION

We presented effects of the counterpropagating spatially separated pump and probe laser beam configuration on the probe Zeeman EIT. Both pump and probe beams are tuned to the  $D_2$  line of  $^{87}\text{Rb}$ . For the geometry of the experiment, with the probe coaxial with the surrounding hollow pump and small dark region between the pump and probe, we showed that in the vacuum cell, like in cells with antirelaxation coating, resonances can be narrower when the probe diameter is smaller. For the probe of  $0.8 \text{ mm}$  in diameter we observed and calculated narrower linewidths, almost independent of the probe laser beam intensity. Also, for this small probe diameter, when its intensity is below  $0.1 \text{ mW/cm}^2$ , dual structure of Zeeman EIT turns in to a single narrow EIT. Probe transmission is enhanced in a narrow range of small magnetic fields when the pump laser beam is present, which is akin to optical switch behavior.

## ACKNOWLEDGMENTS

This work was supported by the Ministry of Education and Science of Serbia, under grants III45016 and OI171038, and also by SCOPES JRP IZ73Z0\_127942.

## REFERENCES

1. S. E. Harris, “Electromagnetically induced transparency,” *Phys. Today* **50**(7), 36–42 (1997).

2. C. L. Garrido Alzar, M. A. G. Martinez, and P. Nussenzveig, “Classical analog of electromagnetically induced transparency,” *Am. J. Phys.* **70**, 37–42 (2002).
3. G. Alzetta, A. Gozzini, L. Moi, and G. Orriols, “An experimental method for the observation of r.f. transitions and laser beat resonances in oriented Na vapour,” *Nuovo Cimento B* **36**, 5–20 (1976).
4. E. Arimondo and G. Orriols, “Nonabsorbing atomic coherences by coherent two-photon transitions in a three-level optical pumping,” *Lett. Nuovo Cimento Soc. Ital. Fis.* **17**, 333–338 (1976).
5. F. Renzoni, W. Maichen, L. Windholz, and E. Arimondo, “Coherent population trapping with losses observed on the Hanle effect of the  $D_1$  sodium line,” *Phys. Rev. A* **55**, 3710–3718 (1997).
6. N. F. Ramsey, *Molecular Beams* (Oxford University, 1956).
7. B. Schuh, S. I. Kanorsky, A. Weis, and T. W. Hänsch, “Observation of Ramsey fringes in nonlinear Faraday rotation,” *Opt. Commun.* **100**, 451–455 (1993).
8. J. E. Thomas, P. R. Hemmer, S. Ezekiel, C. C. Leiby, Jr., R. H. Picard, and C. R. Willis, “Observation of Ramsey fringes using a stimulated, resonance Raman transition in a sodium atomic beam,” *Phys. Rev. Lett.* **48**, 867–870 (1982).
9. G. Theobald, V. Giordano, N. Dimarcq, and P. Cerez, “Observation of narrow Ramsey-type resonances in a caesium beam due to Zeeman coherences,” *J. Phys. B* **24**, 2957–2966 (1991).
10. S. Nakayama, G. W. Series, and W. Gawlik, “Larmor precession in polarization spectroscopy with spatially separated beams,” *Opt. Commun.* **34**, 389–392 (1980).
11. A. S. Zibrov and A. B. Matsko, “Optical Ramsey fringes induced by Zeeman coherence,” *Phys. Rev. A* **65**, 013814 (2001).
12. Y. Xiao, I. Novikova, D. F. Phillips, and R. L. Walsworth, “Diffusion-induced Ramsey narrowing,” *Phys. Rev. Lett.* **96**, 043601 (2006).
13. M. Klein, M. Hohensee, D. F. Phillips, and R. L. Walsworth, “Electromagnetically induced transparency in paraffin-coated vapor cells,” *Phys. Rev. A* **83**, 013826 (2011).
14. Z. D. Grujić, M. Mijailović, D. Arsenović, A. Kovačević, M. Nikolić, and B. M. Jelenković, “Dark Raman resonances due to Ramsey interference in vacuum vapor cells,” *Phys. Rev. A* **78**, 063816 (2008).
15. H. Failache, L. Lenci, and A. Lezama, “Raman–Ramsey multizone spectroscopy in a pure rubidium vapor cell,” *Phys. Rev. A* **81**, 023801 (2010).
16. T. Zanon, S. Guerandel, E. de Clercq, D. Holleville, N. Dimarcq, and A. Clairon, “High contrast Ramsey fringes with coherent-population-trapping pulses in a double lambda atomic system,” *Phys. Rev. Lett.* **94**, 193002 (2005).
17. X. Liu, J.-M. Mérola, S. Guérandel, E. de Clercq, and R. Boudot, “Ramsey spectroscopy of high-contrast CPT resonances with push-pull optical pumping in Cs vapor,” *Opt. Express* **21**, 12451 (2013).
18. K. L. Corwin, Z. Lu, C. F. Hand, R. J. Epstein, and C. E. Wieman, “Frequency-stabilized diode laser with the Zeeman shift in an atomic vapor,” *Appl. Opt.* **37**, 3295–3298 (1998).
19. Z. D. Grujić, M. Lekić, M. Radonjić, D. Arsenović, and B. M. Jelenković, “Ramsey effects in coherent resonances at closed transition  $F_g = 2 \rightarrow F_e = 3$  of  $^{87}\text{Rb}$ ,” *J. Phys. B* **45**, 245502 (2012).
20. M. Radonjić, D. Arsenović, Z. Grujić, and B. M. Jelenković, “Coherent population trapping linewidths for open transitions: cases of different transverse laser intensity distribution,” *Phys. Rev. A* **79**, 023805 (2009).
21. A. J. Krmpot, M. Radonjić, S. M. Ćuk, S. N. Nikolić, Z. D. Grujić, and B. M. Jelenković, “Evolution of dark state of an open atomic system in constant intensity laser field,” *Phys. Rev. A* **84**, 043844 (2011).
22. E. Figueroa, F. Vewinger, J. Appel, and A. I. Lvovsky, “Decoherence of electromagnetically induced transparency in atomic vapor,” *Opt. Lett.* **31**, 2625–2627 (2006).



# Influence of femtosecond pulsed laser irradiation on bismuth germanium oxide single crystal properties



Aleksander Kovačević<sup>a</sup>, Jasna L. Ristić-Djurović<sup>a,\*</sup>, Marina Lekić<sup>a</sup>, Branka Hadžić<sup>a</sup>,  
Giuma Saleh Isa Abudagel<sup>b</sup>, Slobodan Petričević<sup>b</sup>, Pedja Mihailović<sup>b</sup>, Branko Matović<sup>c</sup>,  
Dragan Dramlić<sup>a</sup>, Ljiljana M. Brajović<sup>d</sup>, Nebojša Romčević<sup>a</sup>

<sup>a</sup> Institute of Physics, University of Belgrade, Pregrevica 118, 11080 Belgrade, Serbia

<sup>b</sup> School of Electrical Engineering, University of Belgrade, Bulevar kralja Aleksandra 73, 11000 Belgrade, Serbia

<sup>c</sup> Vinča Institute of Nuclear Sciences, University of Belgrade, P.O. Box 522, 11000 Belgrade, Serbia

<sup>d</sup> Faculty of Civil Engineering, University of Belgrade, Bulevar kralja Aleksandra 73, 11000 Belgrade, Serbia

## ARTICLE INFO

### Article history:

Received 5 December 2015

Received in revised form 16 May 2016

Accepted 12 June 2016

Available online 14 June 2016

### Keywords:

- A. Optical materials
- B. Laser annealing
- C. Raman spectroscopy
- D. Optical properties
- D. Color centers

## ABSTRACT

High quality bismuth germanium oxide single crystals were irradiated by a femtosecond pulsed laser beam of increasing power. Analyses performed on irradiated and unirradiated samples showed significant changes in transmittance, transmission spectra, sample color, Raman spectra, X-ray diffraction (XRD) pattern, Verdet constant, magneto-optical property, and absorption coefficient. After irradiation, the transmission spectra values increased whereas anisotropy detected in the transmission spectra of unirradiated samples disappeared. The change of color caused by irradiation was noticeable to the naked eye. The XRD measurements confirmed structural changes induced by laser irradiation, i.e., the laser-beam-incident side of the sample became almost amorphous, whereas the side opposite to the incident can be indexed to the  $\text{Bi}_{12}\text{GeO}_{20}$  compound. Irradiation caused increase of Raman spectra peaks with the exception of crystal peaks of type E, which disappeared. The femtosecond pulsed laser irradiation can be used to improve bismuth germanium oxide single crystal optical properties.

© 2016 Elsevier Ltd. All rights reserved.

## 1. Introduction

Bismuth germanium oxide ( $\text{Bi}_{12}\text{GeO}_{20}$ ), commonly abbreviated as BGO, or more specifically as s-BGO, belongs to the sillenite group of cubic crystals of the  $I23$  space group. The chemical formula of cubic crystals with the sillenite-type structure is  $\text{Bi}_{12}M^{n+}\text{O}_{20\pm d}$  where  $M$  may be an element from the II–V group of the Periodic Table or a combination of such elements [1–3]. Analysis of the experimental data on the component interaction and the phase equilibrium in the  $\text{Bi}_2\text{O}_3$ – $M_x\text{O}_y$  systems revealed the possibility to achieve phases of the sillenite-type structure with oxides of Rb, Mg, Zn, Cd, B, Al, Ga, In, Tl, Si, Ge, Ti, Pb, P, V, As, Nb, Cr, Mo, W, Fe, Co, Ni, Ru, and Ir [4]. In [2], the atomic structure of  $\text{Bi}_{12}M^{n+}\text{O}_{20\pm d}$  was

discussed in detail for  $\text{Bi}_{12}M^{4+}\text{O}_{20}$  ( $M = \text{Si, Ge, Ti, Mn}$ ),  $\text{Bi}_{12}(\text{A}_{1/2}^{3+}\text{B}_{1/2}^{5+})\text{O}_{20}$  ( $A = \text{Fe, B} = \text{P}$ ),  $\text{Bi}_{12}M^{2+}\text{O}_{20}$  ( $M = \text{Zn, Co}$ ),  $\text{Bi}_{12}M^{3+}\text{O}_{20}$  ( $M = \text{Al, Ga, Fe, Tl}$ ),  $\text{Bi}_{38}\text{B}_2\text{O}_{39}$ ,  $\gamma$ - $\text{Bi}_2\text{O}_3$ , and  $\text{Bi}_{12}\text{VO}_{20\pm d}$ . A more recent study of sillenites  $\text{Bi}_{12}\text{SiO}_{20}$ ,  $\text{Bi}_{25}\text{FeO}_{39}$ , and  $\text{Bi}_{25}\text{InO}_{30}$  gave a representative sillenite structure using  $\text{Si}^{4+}$ ,  $\text{Ti}^{4+}$ ,  $\text{Fe}^{3+}$ , and  $\text{In}^{3+}$  as examples for  $M$  cation [5] and referred to [6] for more details about the sillenite structure. In [6], a general structural formula for the stoichiometric sillenites,  $\text{Bi}_{12}(\text{Bi}_{4/5-nx}\text{M}_{5x}^{n+})\text{O}_{19.2+nx}$ , was developed and discussed in detail for sillenites with  $M^{2+}$  ions (Cd, Co, Zn),  $M^{3+}$  ions (Ga, Fe, Cr, Tl, In, Al),  $M^{4+}$  ions (Si, Ti, Ge, Mn,  $\text{Bi}_{1/2}\text{P}_{1/2}$ ), and  $M^{5+}$  ions (V, As, P).

For BGO, BSO, and BTO crystals the structural formula becomes  $\text{Bi}_{12}M\text{O}_{20}$ , where  $M$  is Ge, Si, and Ti, respectively. The cubic cell unit of  $\text{Bi}_{12}\text{GeO}_{20}$  is composed of two formula units, namely 24 Bi, 40 O and 2 Ge. The Ge atoms occupy the center and the vertices of a cube and are tetrahedrally coordinated by oxygen atoms. The Bi atoms, due to their massiveness, constitute the core of the cell, they are heptacoordinated as  $\text{BiO}_5E$ , where  $E = 6s^2$  is the non-shared electron pair in Bi, and the common edges form dimers. The five oxygen atoms compose an incomplete octahedral arrangement and the remaining two oxygen atoms are electrostatically coordinated on a side of  $E$  [1,3]. Due to its photoconductivity,

\* Corresponding author.

E-mail addresses: [aleksander.kovacevic@ipb.ac.rs](mailto:aleksander.kovacevic@ipb.ac.rs) (A. Kovačević), [jasna@stanfordalumni.org](mailto:jasna@stanfordalumni.org) (J.L. Ristić-Djurović), [marina.lekic@ipb.ac.rs](mailto:marina.lekic@ipb.ac.rs) (M. Lekić), [branka.hadzic@ipb.ac.rs](mailto:branka.hadzic@ipb.ac.rs) (B. Hadžić), [giuma05@yahoo.com](mailto:giuma05@yahoo.com) (G.S.I. Abudagel), [slobodan@etf.bg.ac.rs](mailto:slobodan@etf.bg.ac.rs) (S. Petričević), [pedja@etf.bg.ac.rs](mailto:pedja@etf.bg.ac.rs) (P. Mihailović), [mato@vinca.rs](mailto:mato@vinca.rs) (B. Matović), [dragan.dramlic@ipb.ac.rs](mailto:dragan.dramlic@ipb.ac.rs) (D. Dramlić), [aleksander.kovacevic@ipb.ac.rs](mailto:aleksander.kovacevic@ipb.ac.rs) (L.M. Brajović), [aleksander.kovacevic@ipb.ac.rs](mailto:aleksander.kovacevic@ipb.ac.rs) (N. Romčević).

photochromism, photorefractivity, piezoelectricity, as well as to electro-optic and magneto-optic effects it supports [7,8],  $\text{Bi}_{12}\text{GeO}_{20}$  is suitable for a broad range of applications and devices such as optical limiting, holography, spatial light modulation, optical phase conjugation, optical memories, fiber optic sensors, Pockels cells [8–12]. The properties of non-doped as well as doped  $\text{Bi}_{12}\text{GeO}_{20}$  were investigated and reported in a number of studies, for example in [13–21]. Characteristics of  $\text{Bi}_{12}\text{GeO}_{20}$  single crystals after exposure to thermal treatment [16–19,22], to beams of electrons [23], uranium ions [24], fluorine ions [15],  $\gamma$ -ray [19] or light [9,18,22,25–28] were investigated. Nonlinear properties of  $\text{Bi}_{12}\text{GeO}_{20}$  crystals were measured with pulsed laser beams in the nanosecond range in [9], whereas in [26–28] BGO crystals were irradiated by picosecond laser pulses. Transmission, absorption [16,19], and Raman spectra [19] were found to be significantly influenced by doping and annealing. Thermally stimulated currents as a function of both the temperature at which the crystals are photoexcited and the density of energy used to photoexcite them were reported in [18]. Influences of laser irradiation, thermal treatment [22], and electron beam [23] on luminescence of  $\text{Bi}_{12}\text{GeO}_{20}$  are reported. Photo-induced absorption in  $\text{Bi}_{12}\text{TiO}_{20}$  was thoroughly studied in [29], whereas significant influence of doping and annealing on transmission and absorption of BGO were addressed in [16] and [19]. However, to the best of our knowledge, photo-induced increase in BGO transmission has not been reported so far. Therefore, following the determination of magneto-optical quality and refractive index of BGO single crystals presented in [20], we studied the influence of the femtosecond laser irradiation on  $\text{Bi}_{12}\text{GeO}_{20}$  single crystals. The irradiation caused permanent changes visible to the naked eye, as can be seen in Fig. 1. In order to quantitatively define visually observed changes, we measured the transmittance, transmission spectra, color, Raman spectra, X-ray diffraction patterns, Verdet constant, absorption coefficient, and magneto-optical quality of  $\text{Bi}_{12}\text{GeO}_{20}$  single crystals.

## 2. Experimental

### 2.1. Preparation of crystal samples

Single crystals of  $\text{Bi}_{12}\text{GeO}_{20}$  with diameters of 12–13 mm and length of 70–80 mm were grown by the Czochralski technique. As explained in detail in [20], the critical crystal diameter and critical rotation rate were calculated to be 12 mm and 20 rpm, respectively, whereas the pulling rate was determined experimentally to be 2.8–3 mm/h. The crystal puller MSR 2 combined with the Eurotherm temperature controller was used to grow the crystals. The crystal diameter size was controlled by monitoring the crucible weight, and its deviation from the chosen value was kept below 0.1 mm. The system as a whole provided protection from excessive

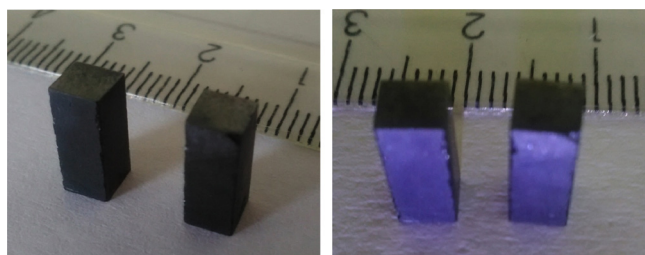


**Fig. 1.** Photographs of unirradiated and laser irradiated samples. The photographs are taken without (left) and with (right) a flash. In each photo the irradiated sample is placed to the right. The femtosecond laser irradiation was incident to the upper base of the prism. The visible laser induced changes span to approximately one quarter into the sample depth.

radiative heat losses and granted melting temperature fluctuations typically smaller than  $0.2^\circ\text{C}$ . The crystals were grown in the air, without crucible rotation during the growth, using the  $\text{Bi}_{12}\text{GeO}_{20}$  seed oriented in the  $\langle 111 \rangle$  direction, and a mixture of  $\text{Bi}_2\text{O}_3$  and  $\text{GeO}_2$  in the stoichiometric ratio 6:1 as a charge. After its growth, the crystal boule was cooled to room temperature at the rate of approximately  $50^\circ\text{C/h}$ . The crystals were not annealed after the growth. Crystal samples of size  $4\text{ mm} \times 4\text{ mm} \times 10\text{ mm}$  were cut from the boule and mechanically as well as chemically polished. The crystal samples were chemically etched using the solutions  $\text{HF} + \text{HNO}_3$  in the ratio 2:1,  $\text{HCl} + \text{H}_2\text{O}$  in the ratio 1:2, and  $\text{HCl} + \text{H}_2\text{O}$  in the ratio 1:5, whereas chemical polishing was performed with the solution  $\text{HCl} + \text{HNO}_3 + \text{H}_2\text{O}$  in the ratio 1:1:5. Observance of the polished crystal surfaces under polarized light confirmed the absence of the core. The purity of  $\text{Bi}_2\text{O}_3$  and  $\text{GeO}_2$  was 99.5 wt.% and 99.98 wt.%, respectively. The technique used to prepare the samples insured maximal sample quality within the limits corresponding to their purity [20].

### 2.2. Crystal irradiation and characterization

Crystal samples were exposed to a femtosecond laser irradiation of increasing power. The femtosecond pulsed laser beam was produced with the Coherent Mira 900 F femtosecond laser using as an input a 532 nm continuous wave pump beam obtained with the Coherent Verdi V-10 pump laser, Fig. 2. The irradiating beam wavelength of 800 nm was determined with the spectrometer Ocean Optics HR2000CG UV-NIR. Crystal samples were irradiated along their longest axis,  $z$ , i.e., along the crystal growth direction. The beam radius provided partial irradiation of the exposed crystal facet. The beam power on a sample was adjusted by a graded filter and was increased from 50 mW to 950 mW, which corresponds to the fluence range of  $75\text{--}1425\text{ nJ/cm}^2$ . The samples were irradiated by each beam power for 3 s, which was measured by a stopwatch with 0.2 s accuracy. The repetition rate of 90 fs long laser pulses was 76 MHz. The total irradiation time and energy were intentionally kept low to avoid significant contribution of an accumulative process caused by repopulation of the traps [28]. The Ophir powermeter with thermal and photometric heads was used to perform beam power measurements.

Sample transmittance in the wavelength range between 200 and 1100 nm with the resolution of 1 nm was determined in the spectrometric device Beckman Coulter DU 720 General Purpose UV/VIS spectrometer. The obtained transmission spectra were used to calculate sample color, as well.

The X-ray diffraction patterns were measured with the Rigaku Ultima IV Multipurpose X-ray diffraction system. The system was operated at 40 kV and 40 mA to produce nickel-filtered  $\text{CuK}\alpha_1$  X-ray with  $\lambda = 0.1540\text{ nm}$ . The XRD data were collected in the  $2\theta$

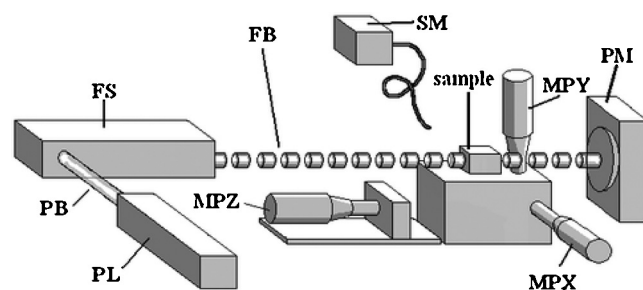


**Fig. 2.** Experimental setup for sample irradiation and power transmission measurements. PL – pump laser, PB – pump beam, FS – femtosecond laser, FB – femtosecond beam, MPX, MPY, MPZ – micro-positioners in  $x$ ,  $y$ , and  $z$  direction respectively, SM – spectrometer, PM – powermeter.



range between 20 and 70° at the scanning rate of 5°/min. The phase analysis was performed using the PDXL2 software, version 2.0.3.0 [30], with reference to the patterns of the International Centre for Diffraction Database (ICDD), version 2012 [31].

Using the backscattering configuration and the 532 nm line of Verdi G optically pumped semiconductor laser as an excitation source, the micro-Raman spectra of crystal samples were obtained with the Jobin Yvon T64000 spectrometer, which has nitrogen cooled charge-coupled-device detector. The spectra were recorded at room temperature in the spectral range between 100 and 1100  $\text{cm}^{-1}$  with 1  $\text{cm}^{-1}$  resolution.

Optical activity and Faraday rotation were measured at the wavelength of 632.8 nm by an orthogonal polarization detection polarimetric method described in detail in [20]. Output signal voltages  $U_1$  and  $U_2$ , obtained respectively from vertically and horizontally polarized component of the laser beam transmitted by the  $\text{Bi}_{12}\text{GeO}_{20}$  crystal sample, after transimpedance stages are

$$U_1 = \frac{k_1 \Gamma_0}{2} (1 + \sin(2\theta)), \quad U_2 = \frac{k_2 \Gamma_0}{2} (1 - \sin(2\theta)),$$

where  $\Gamma_0$  is the beam irradiation,  $k_1$  and  $k_2$  are constants that include optical losses and optoelectronic conversion efficiency. The linear polarization rotation angle  $\theta$  was determined using the difference over sum method that is independent of light source fluctuations. Use of the birefringent crystal instead of polarizing prism led to parallelism of separate optical paths that allowed employment of quadrant photodiode and further enabled matching of optoelectronic conversion gains as much as possible. Setting  $k_1 = k_2$ , the angle  $\theta$  can be calculated as

$$\theta = \frac{1}{2} \sin^{-1} \left( \frac{U_1 - U_2}{U_1 + U_2} \right).$$

In the absence of magnetic field component parallel to the laser beam, the angle  $\theta = \theta_0$  represents the optical activity. When  $\text{Bi}_{12}\text{GeO}_{20}$  crystal sample is placed in a magnetic field generated by an alternating current through the Helmholtz coils, the angle  $\theta$  becomes the sum of the optical activity and Faraday rotation, and can be used to calculate the Verdet constant [32]. The Hall probe was used to measure magnetic induction and to establish its linear relation to the coil current, namely

$$B[\text{T}] = 0.001282 \times I[\text{A}]$$

The Verdet constant is calculated from

$$V = \frac{\theta_{0AC}}{B_0 l} = \frac{1}{2B_0 l} \sin^{-1} \left( \frac{U_1 - U_2}{U_1 + U_2} \right)_{0AC},$$

where  $\theta_{0AC}$  is the amplitude of the AC signal and  $B_0$  is the amplitude of magnetic induction. The coils were powered by a 50 Hz sine wave constant amplitude current that creates magnetic induction of the same frequency. Consequently, FFT was used to separate spectral components of  $U_1$  and  $U_2$ . The Faraday rotation was determined from the magnitude of 50 Hz component.

Bulk absorption measurement was normalized using the reference beam created by the  $\text{CaCO}_3$  birefringent crystal that was used for beam separation. Absorption coefficients were obtained by measuring the difference in beam intensities at the quadrant photodiode with and without  $\text{Bi}_{12}\text{GeO}_{20}$  crystal in the beam path. Background light influence was eliminated by measuring the photodiode output without the laser beam and subtracting it from the two previous measurements.

### 3. Results and discussion

The change of sample transmittance with the increase of irradiating laser power for the two considered crystal samples is

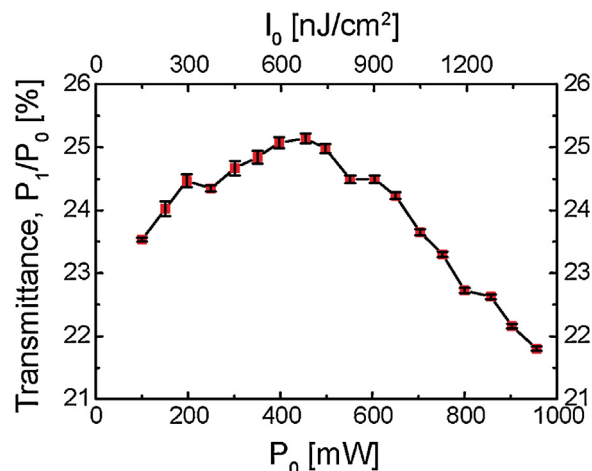


**Fig. 3.** Change of crystal transmittance during increase of irradiating laser power. Each data point corresponds to a 3 s long sample irradiation by the femtosecond laser beam with the incident power  $P_0$ , given in the bottom axis, and the corresponding incident fluence,  $I_0$ , depicted in the top axis. The transmittance is given as  $P_1/P_0$ , where  $P_1$  is the transmitted power. The irradiating beam wavelength was 800 nm.

shown in Fig. 3. The error bars were calculated from the uncertainties of measured values of the incident and transmitted power,  $\Delta P_0$  and  $\Delta P_1$ . The transmittance generally undergoes initial growth followed by a decrease. The maximal transmittance of 25.1% occurs at the irradiating laser power of 455 mW. It seems that curve exhibits local irregularities which occur at 197.4–249.7 mW, 552–605 mW and 800–857 mW. Similarly to our findings about transmittance dependence on the irradiating laser power, initial growth followed by a decrease in transmittance is found to be an outcome of annealing, as well [16]. Skorikov et al. in [16] reported that annealing of  $\text{Bi}_{12}\text{SiO}_{20}$ ,  $\text{Bi}_{12}\text{GeO}_{20}$ , and  $\text{Bi}_{12}\text{TiO}_{20}$  crystals in vacuum or inert atmosphere at 500–750 °C for 2–12 h typically raises the transmittance near the intrinsic edge and observed the most pronounced effect for  $\text{Bi}_{12}\text{SiO}_{20}$  annealed at 650 °C for 2 h. Increase in temperature and/or annealing time was found to be associated with a decrease in transmittance to its initial or an even lower level, particularly in  $\text{Bi}_{12}\text{GeO}_{20}$  and  $\text{Bi}_{12}\text{SiO}_{20}$ .

Transmission spectra of samples were determined along both directions of the longest sample axis and are shown in Fig. 4. In addition to the treated samples, i.e., the samples irradiated by the femtosecond laser beam of increasing power, the unirradiated samples were examined, as well. The unirradiated crystal exhibits

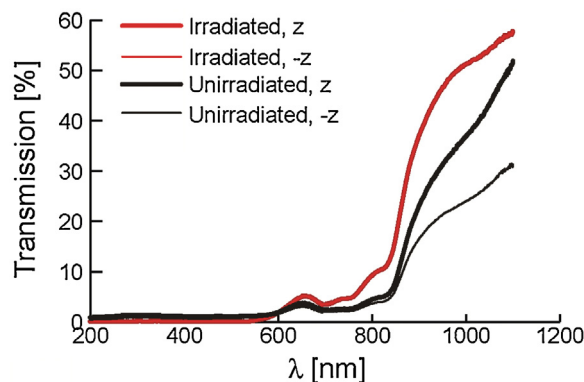


**Fig. 4.** Transmission spectra of irradiated and unirradiated samples. The transmission spectra of all samples were measured in the direction of crystal growth as well as in the direction opposite to it. The unirradiated sample exhibits significant anisotropy, which disappears after irradiation. Irradiation also causes transmission increase.

noticeable anisotropy. The transmissions of the crystal have small irregularities, which are probably caused by impurities, at 655 nm and 800 nm and a steep growth after 850 nm. For the unirradiated crystal the transmission corresponding to the  $z$  direction is larger than the one in the  $-z$  direction. For wavelengths larger than 1000 nm the transmission is larger than 37 % and 24 % in the  $z$  and  $-z$  direction, respectively. After irradiation the anisotropy disappeared, and the transmission of the crystal increased becoming larger than 51 % for wavelengths above 1000 nm. Measurements repeated after prolonged period of time confirmed full reproducibility of the obtained results and verified that the detected light-induced changes are permanent.

Our results are in agreement with the conclusion given in [16] that doping as well as annealing has significant effect on transmission and absorption spectra. They found that annealing at 650 °C for 12 h and at 740 °C for 2 h each cause decrease of absorption spectra throughout the considered range of 300–900 nm, when compared to the absorption spectrum of non-annealed  $\text{Bi}_{12}\text{GeO}_{20}$  crystal. However, after absorption decrease in the low-wavelength range, annealing at 650 °C and 700 °C for 2 h resulted in local absorption minimum at approximately 450 nm and local maximum around 530 nm, followed by the absorption values somewhat larger than those of non-annealed case for wavelengths larger than 530 nm. The absorption spectra of untreated, annealed in  $\text{N}_2$  for 8 h at 450 °C and 550 °C,  $\gamma$ -ray irradiated, and Mo doped  $\text{Bi}_{12}\text{GeO}_{20}$  were studied in [19]. They found that the absorption was higher for annealed and yet higher for doped crystals. The absorption peaks for all studied cases were located at 390 nm followed by local maxima around 400 nm, steep linear decreases between 400 and 500 nm, and approximately constant absorbance values above 550 nm. Absorbance values above 550 nm listed in the increasing order correspond to the untreated, annealed in  $\text{N}_2$  for 8 h at 450 °C, annealed in  $\text{N}_2$  for 8 h at 550 °C,  $\gamma$ -ray irradiated, and Mo doped  $\text{Bi}_{12}\text{GeO}_{20}$ . Consequently, it can be concluded that annealing can be used to alter absorption of  $\text{Bi}_{12}\text{GeO}_{20}$  crystals; however, nature and intensity of the change depend on the temperature and duration of annealing [16,19]. An asymmetric transmission through a photorefractive crystal, shown in Fig. 4, could be attributed to the nonlinear interaction between a beam and its own reflection from the back face of the crystal, as suggested in [33]. Impurities along the beam path, such as defects or color centers, surface irregularities caused by cutting and polishing, as well as mechanical imperfections and structural changes confirmed by XRD measurements given in Fig. 6, may contribute to the asymmetry detected in transmission spectra.

Changes in sample color caused by irradiation were quantified by calculating CIE chromaticity coordinates. The obtained results given in Fig. 5 revealed that the change of crystal color was significant.

The X-ray diffraction (XRD) patterns of prismatic unirradiated and irradiated single crystal samples, as well as of powdered samples taken from unirradiated and irradiated  $\text{Bi}_{12}\text{GeO}_{20}$  crystals are given in Fig. 6. The XRD patterns of the two prism-shaped samples shown in graphs (a) and (b) in Fig. 6 were recorded along the  $z$  as well as along the  $-z$  direction, i.e., using both bases of the prism as the incident facet. The relative shift between the XRD spectra that correspond to the  $z$  and  $-z$  direction indicates that there is an offset between the prism axis and the crystal axis, regardless of the parallelism between the prism's bases, i.e., between the facets used as incident for XRD measurements. In addition, the  $z$  XRD spectrum of laser irradiated prism sample reveals that the side of the crystal sample that was not incident with regard to the laser beam, can be indexed to the  $\text{Bi}_{12}\text{GeO}_{20}$  compound. The XRD spectrum of irradiated prism sample that corresponds to the  $-z$  direction implies that the laser-beam-incident side of the sample is almost amorphous, indicating

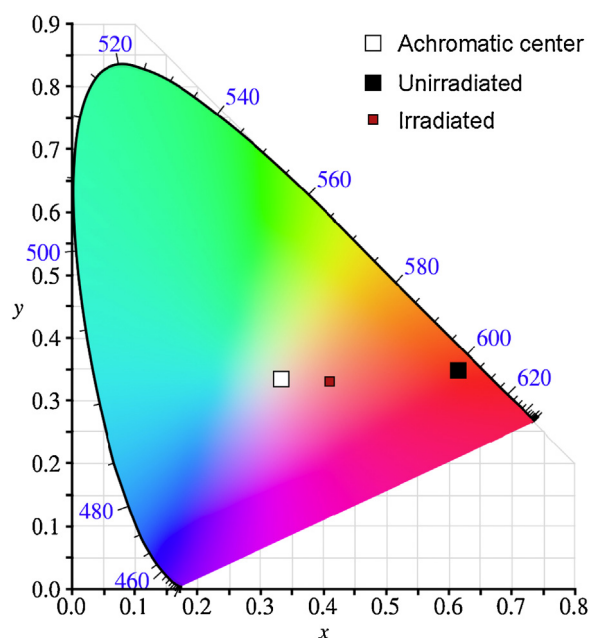


Fig. 5. Sample colors in CIE chromaticity diagram. The change in the crystal color was visible to the naked eye.

fragmentation of a monocrystal into disoriented fractals. This is in good agreement with the defect structure of  $\text{Bi}_{12}\text{GeO}_{20}$  crystal [1], which is sensitive to any extreme conditions.

All the peaks in the powdered unirradiated  $\text{Bi}_{12}\text{GeO}_{20}$  XRD pattern given in Fig. 6(c) correspond to the denoted  $\text{Bi}_{12}\text{GeO}_{20}$  phases, which is in good agreement with the JCPDS Cards No. 34-0096. More details about this spectrum are given in [20].

The comparison between X-ray diffraction patterns of the powdered slices of irradiated prism, collected from the laser-beam-incident side,  $-z$ , and from the side opposite to it,  $z$ , shows significant general decrease in peak intensity as well as disappearance of some peaks in the  $-z$  spectrum, with the exception of peaks (222), (622), and (613) that are somewhat stronger, see Fig. 6(d). This may be explained by an amorphization caused by laser irradiation. The lattice parameter values calculated for unirradiated and irradiated materials confirmed this assumption. Namely, the lattice parameter of the laser-beam-incident side of powdered irradiated sample,  $a_0 = 10.1411$ , is smaller than the one of the powdered unirradiated sample,  $a_0 = 10.1456$ , whereas the lattice parameter of the  $z$ -side of powdered irradiated sample,  $a_0 = 10.1454$ , is very close to that of the powdered unirradiated sample.

The Raman spectra of  $\text{Bi}_{12}\text{GeO}_{20}$  single crystals at room temperature in the spectral range from 150 to 800  $\text{cm}^{-1}$  are shown in Fig. 7. The results obtained for unirradiated crystals are in agreement with those given in [2,20]. Irradiation of the crystal caused all the peaks of symmetry type E, i.e., the peaks at 234, 454, and 619.6  $\text{cm}^{-1}$ , to disappear and intensity increase of all other peaks. The change in the same Raman spectrum peaks of  $\text{Bi}_{12}\text{GeO}_{20}$  was reported in [19]; however, the most, medium, and least intense peaks discussed there correspond to the annealed, doped, and untreated samples, respectively.

The dominant role in formation of peaks at 234, 454 and 619.6  $\text{cm}^{-1}$  is played by oxygen. Generally, it has been shown that all the peaks in the low-frequency region, i.e., below 650  $\text{cm}^{-1}$ , are caused by excitations of the bismuth-oxygen sub-lattice, whereas the main contributors to the high-frequency region, i.e., above 650  $\text{cm}^{-1}$ , are oscillations of  $[\text{GeO}_4]$  tetrahedron [2]. In sillenites all E



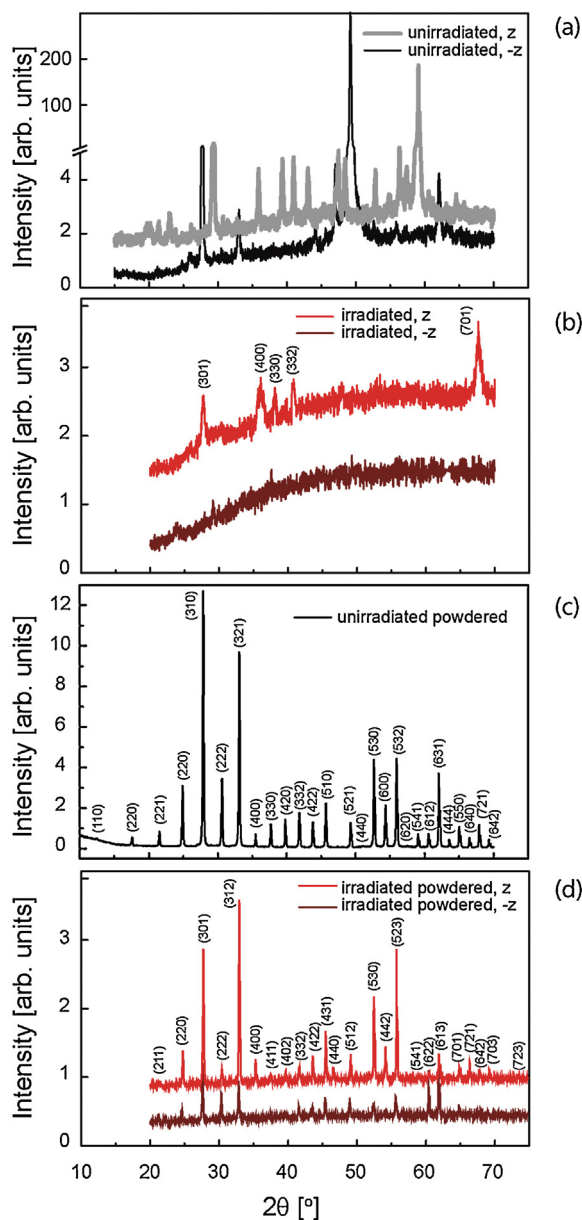


**Fig. 6.** X-ray diffraction spectra of  $\text{Bi}_{12}\text{GeO}_{20}$ . The XRD patterns correspond to the (a) unirradiated prism, (b) irradiated prism, (c) powdered unirradiated prism slice, and (d) powdered irradiated prism slices of  $\text{Bi}_{12}\text{GeO}_{20}$ . The  $-z$  and  $z$  spectra in (d) correspond to the powdered slices taken from the laser-beam-incident side of the irradiated sample and the side opposite to it, respectively. The relative shift between spectra recorded in the  $z$  and  $-z$  direction in (a) and (b) indicates offset between the prism and crystal axes. The laser-beam-incident side of the irradiated sample became almost amorphous, as can be seen from the  $-z$  spectrum in (b) as well as from a significant decrease in  $-z$  spectrum peaks in (d). From the spectra corresponding to the  $z$  direction in (b) and (d) it can be concluded that this side of irradiated crystal prism can be indexed to the  $\text{Bi}_{12}\text{GeO}_{20}$  compound.

modes consist of oxygen vibrations, which elongate the cluster by stretching, rocking, and bending of Bi—O bonds [34–36]. Our results indicate that, under the influence of femtosecond laser irradiation, bonds of this kind are broken, some others are newly formed, and some oxygen have evaporated from the surface, causing the E type peaks at 234, 454, and  $619.6\text{ cm}^{-1}$  to disappear. Similarly, high pressure is reported in [37] and references therein to cause breakage of some of the bonds and formations of new ones. Note that these conclusions are confirmed by the XRD measurements given in Fig. 6.

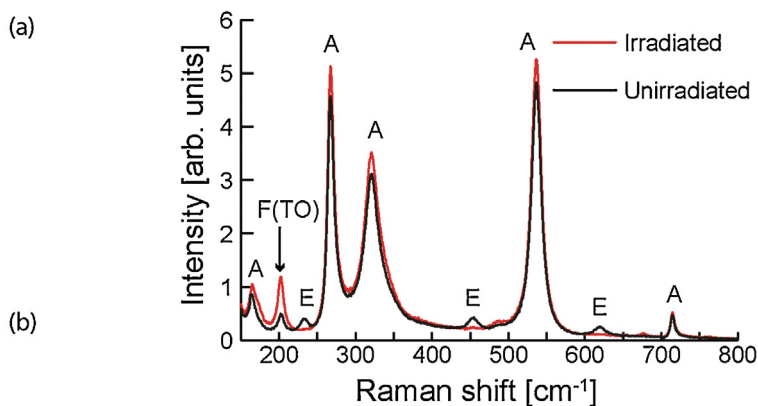


**Fig. 7.** Raman spectra. The E type peaks at 234, 454, and  $619.6\text{ cm}^{-1}$  disappeared after irradiation, whereas all other peaks, i.e., A and F type peaks, underwent a small enhancement.

**Table 1**  
Optical properties at 632.8 nm.

Property	Unirradiated sample	Irradiated sample
Verdet constant ( $\text{rad T}^{-1}\text{ m}^{-1}$ )	47.34	62.64
Absorption coefficient ( $\text{cm}^{-1}$ )	3.3	2.7
Magneto-optical quality ( $\text{rad T}^{-1}$ )	0.143	0.23

Optical properties of unirradiated and irradiated  $\text{Bi}_{12}\text{GeO}_{20}$  crystal samples are compared in Table 1. The unirradiated sample has 24.38% lower Verdet constant compared to the irradiated sample. The absorption coefficient of unirradiated sample is 22.22% higher than the one of the irradiated crystal. The increased Verdet constant and lower absorption of irradiated sample led to its better magneto-optical quality, which is by 37.8% higher than the magneto-optical quality of the sample that has not been irradiated.

Previous work [38] suggests that  $\text{Bi}_{12}\text{GeO}_{20}$  crystal exhibits continuous decrease in Verdet constant with increasing wavelength, which begins with  $140\text{ rad}/(\text{T m})$  at 480 nm and drops down to  $50\text{ rad}/(\text{T m})$  at 700 nm. A typical value for the Verdet constant is around  $60\text{ rad}/(\text{T m})$  at 632.8 nm. Another study [39] suggests an increase in the Verdet constant for undoped and Cr doped BSO and BTO:Cu crystals when exposed to white light for 20 min. The Verdet constant dependence on the wavelength remains monotonically decreasing with illumination causing a few percent increase of the Verdet constant at lower visible wavelengths.

All measurements were performed several months after irradiation, i.e., long after full post-irradiation relaxation of crystal samples; therefore, all the detected changes are stable and permanent.

#### 4. Conclusions

The 800 nm, femtosecond pulsed laser irradiation of increasing power caused significant permanent changes in optical properties of  $\text{Bi}_{12}\text{GeO}_{20}$  single crystals. The transmittance dependence on the applied irradiation power undergoes initial growth, reaches maximum, and then decreases. The maximal transmittance of 25.1% occurred at 455 mW. In the transmission spectra of unirradiated sample anisotropy was detected. After irradiation, the transmission increased, whereas the anisotropy disappeared. To the best of our knowledge, photo-induced increase in BGO transmission has not been reported before. The XRD measurements performed on the prismatic crystal samples as well as on the

powdered slices taken from the crystal facets confirmed mechanical imperfections as well as femtosecond laser induced structural changes. The laser-beam-incident side of the sample became almost amorphous, indicating fragmentation of a monocrystal into disoriented fractals, whereas the side of the crystal sample that was not incident with regard to the laser beam, can be indexed to the  $\text{Bi}_{12}\text{GeO}_{20}$  compound. The Raman spectra peaks became somewhat stronger, except for the E type peaks at 234, 454, and  $619.6\text{ cm}^{-1}$ , which disappeared. Irradiation also caused significant change of the crystal color. The irradiation improved magneto-optical quality by 37.8%, and resulted in 24.4% increase of the Verdet constant as well as 22.2% decrease of the absorption coefficient. Optical properties of  $\text{Bi}_{12}\text{GeO}_{20}$  single crystals can be improved by irradiation with the femtosecond pulsed laser beam. For the best results, the wavelength, duration, and power of irradiating laser beam, need to be optimized.

## Acknowledgements

This work is financially supported by the Serbian Ministry of Education, Science, and Technological Development through the projects III45003 and III45016. We thank Z. Velikić for his assistance with transmission spectra measurements and A. Valčić for his help with sample preparation.

## References

- [1] S.C. Abrahams, P.B. Jamieson, J.L. Bernstein, Crystal structure of piezoelectric bismuth germanium oxide  $\text{Bi}_{12}\text{GeO}_{20}$ , *J. Chem. Phys.* 47 (1967) 4034–4041.
- [2] V.I. Burkov, V.S. Gorelik, A.V. Egorysheva, Y.F. Kargin, Laser Raman spectroscopy of crystals with the structure of sillenite, *J. Russ. Las. Res.* 22 (2001) 243–267.
- [3] S.F. Radaev, V.I. Simonov, Y.F. Kargin, New data on structure and crystal chemistry of sillenites  $\text{Bi}_{12}\text{M}_x\text{O}_{20\pm\delta}$ , *Eur. J. Solid State Inorg. Chem.* 29 (1992) 383–392.
- [4] Kargin YuF, Syntheses, Composition, and Properties of Oxide Compounds of Bismuth with the Structure of Sillenite, Institute of general and inorganic chemistry, Moscow, 1998 (PhD thesis).
- [5] C.A. Scurti, N. Auvray, M.W. Lufaso, S. Takeda, H. Kohno, D.J. Arenas, Electron diffraction study of the sillenites  $\text{Bi}_{12}\text{SiO}_{20}$ ,  $\text{Bi}_{25}\text{FeO}_{39}$  and  $\text{Bi}_{25}\text{InO}_{39}$ : evidence of short-range ordering of oxygen-vacancies in the trivalent sillenites, *AIP Adv.* 4 (2014) 087125, doi:http://dx.doi.org/10.1063/1.489334.
- [6] M. Valant, D. Suvorov, A stoichiometric model for sillenites, *Chem. Mater.* 14 (2002) 3471–3476.
- [7] M. Simon, F. Mersch, C. Kuper, Refractive indices of photorefractive bismuth titanate, barium-calcium titanate, bismuth germanium oxide, and lead germanate, *Phys. Status Solidi A* 159 (1997) 559–562.
- [8] V.M. Skorikov, Kargin YuF, A.V. Egorysheva, V.V. Volkov, M. Gospodinov, Growth of sillenite-structure single crystals, *Inorg. Mater.* 41 (2005) S24–S46.
- [9] R.A. Ganeev, A.I. Rysanyansky, B. Palpant, S. Debrus, Third-order nonlinearities of  $\text{Bi}_{12}\text{GeO}_{20}$  crystal measured by nanosecond radiation, *J. Appl. Phys.* 97 (2005) 104303, doi:http://dx.doi.org/10.1063/1.1891280.
- [10] Introduction to Photorefractive Nonlinear Optics, in: P. Yeh (Ed.), 1st ed., Wiley-Interscience, New York, 1993.
- [11] M.J. Weber, Inorganic scintillators: today and tomorrow, *J. Lumin.* 100 (2002) 35–45.
- [12] M. Itoh, T. Katagiri, H. Mitani, M. Fujita, Y. Usuki, Comparative study of excitonic structures and luminescence properties of  $\text{Bi}_4\text{Ge}_3\text{O}_{12}$  and  $\text{Bi}_{12}\text{GeO}_{20}$ , *Phys. Status Solidi B* 245 (2008) 2733–2736.
- [13] N.C. Deliolanis, I.M. Kourmoulis, G. Asimellis, A.G. Apostolidis, E.D. Vanidhis, N. A. Vainos, Direct measurement of the dispersion of the electrogyration coefficient of photorefractive  $\text{Bi}_{12}\text{GeO}_{20}$  crystals, *J. Appl. Phys.* 97 (2005) 023531.
- [14] C.G.P. Moraes, F.A.A. Jesus, Z.S. Macedo, Electrical and dielectric characterization of  $\text{Bi}_{12}\text{GeO}_{20}$  prepared by modified Pechini method, *Adv. Cond. Matter Phys.* 2014 (2014) 968349, doi:http://dx.doi.org/10.1155/2014/968349.
- [15] O. Peña-Rodríguez, J. Olivares, I. Bányász, Optical properties of crystalline and ion-beam amorphized  $\text{Bi}_{12}\text{GeO}_{20}$ : Relevance for waveguide applications, *Opt. Mater.* 47 (2015) 328–332.
- [16] V.M. Skorikov, I.S. Zakharov, V.V. Volkov, E.A. Spirin, Transmission and absorption spectra of  $\text{Bi}_{12}\text{GeO}_{20}$ ,  $\text{Bi}_{25}\text{SiO}_{20}$ , and  $\text{Bi}_{25}\text{TiO}_{20}$  single crystals, *Inorg. Mater.* 38 (2002) 172–178.
- [17] Z.S. Macedo, C.S.S. Oliveira, A.C. Hernandez, Dielectric relaxation mechanism of single crystal and polycrystal bismuth germanate, *J. Appl. Phys.* 102 (2007) 034105.
- [18] H. Marquet, J.-C. Merle, J.-G. Gies, Charge transfer mechanisms between some shallow-trap centres involved in the photochromism of  $\text{Bi}_{12}\text{GeO}_{20}$ , *Opt. Mater.* 14 (2000) 277–285.
- [19] P.S. Yu, L.B. Su, H.L. Tang, X. Guo, H.Y. Zhao, Q.H. Yang, J. Xu, Study on photoluminescence of thermally treated  $\text{Bi}_{12}\text{GeO}_{20}$  and  $\text{Mo:Bi}_{12}\text{GeO}_{20}$  crystals, *Sci. China Technol. Sci.* 54 (2011) 1287–1291.
- [20] ŽŽ Lazarević, P. Mihailović, S. Kostić, M.J. Romčević, M. Mitrić, S. Petričević, J. Radunović, M. Petrović-Damjanović, M. Gilić, N.Ž. Romčević, Determination of magneto-optical quality and refractive index of bismuth germanium oxide single crystals grown by Czochralski technique, *Opt. Mater.* 34 (2012) 1849–1859.
- [21] S. Kumaragurubaram, S. Moorthy Babu, C. Subramanian, P. Ramasamy, Growth and characterization of  $\text{Bi}_{12}\text{SiO}_{20}$  and  $\text{Bi}_{12}\text{GeO}_{20}$  crystals, *Indian J. Eng. Mater. Sci.* 7 (2000) 331–335.
- [22] A. Cremades, J. Piqueras, A. Remón, J.A. García, M.T. Santos, E. Diéguez, Luminescence study of thermal treated and laser irradiated  $\text{Bi}_{12}\text{GeO}_{20}$  and  $\text{Bi}_{12}\text{SiO}_{20}$  crystals, *J. Appl. Phys.* 83 (1998) 7948–7952.
- [23] A. Cremades, M.T. Santos, A. Remón, J.A. García, E. Diéguez, J. Piqueras, Cathodoluminescence and photoluminescence in the core region of  $\text{Bi}_{12}\text{GeO}_{20}$  and  $\text{Bi}_{12}\text{SiO}_{20}$  crystals, *J. Appl. Phys.* 79 (1996) 7186–7190.
- [24] I. Stefaniuk, P. Potera, I. Rogalska, D. Wróbel, EPR investigations of defects in  $\text{Bi}_{12}\text{GeO}_{20}:\text{Cr}$  single crystal irradiated by high energy uranium ions, *Curr. Topics Biophys.* 33 (2010) 231–235.
- [25] N. Benjelloun, M. Tapiero, J.P. Zielinger, F. Marsaud, J.C. Launay, Characterization of deep levels in  $\text{Bi}_{12}\text{GeO}_{20}$  by photoinduced current transient spectroscopy, *J. Appl. Phys.* 64 (1988) 4013–4023.
- [26] R.A. Ganeev, A.I. Rysanyansky, R.I. Tugushev, M.K. Kodirov, F.R. Akhmedjanov, T. Usmanov, Nonlinear optical characteristics of BSO and BGO photorefractive crystals in visible and infrared ranges, *Opt. Quant. Electron.* 36 (2004) 807–818.
- [27] M. Sylla, D. Rouède, R. Chevalier, X. Nguyen Phu, G. Rivoire, Picosecond nonlinear absorption and phase conjugation in BSO and BGO crystals, *Opt. Commun.* 90 (1992) 391–398.
- [28] B. Taheri, S.A. Holmstrom, R.C. Powell, J.J.F. Song, F. Antonio Munoz, I. Földvári, A. Péter, Nonlinear absorption of laser light in  $\text{Bi}_{12}\text{GeO}_{20}$  single crystals, *Opt. Mater.* 3 (1994) 251–255.
- [29] A. Matusevich, A. Tolstik, M. Kisteneva, S. Shandarov, V. Matusevich, A. Kiessling, R. Kowarschik, Investigation of photo-induced absorption in a  $\text{Bi}_{12}\text{TiO}_{20}$  crystal, *Appl. Phys. B* 92 (2008) 219–224.
- [30] PDXL Version 2.0.3.0 Integrated X-ray Powder Diffraction Software. Rigaku Corporation, Tokyo, Japan, 2011, pp. 196–8666.
- [31] Powder Diffraction File, PDF-2 Database, announcement of new database release 2012, International Centre for Diffraction Data (ICDD).
- [32] P. Mihailovic, S. Petricevic, S. Stankovic, J. Radunovic, Temperature dependence of the  $\text{Bi}_{12}\text{GeO}_{20}$  optical activity, *Opt. Mater.* 30 (2008) 1079–1082.
- [33] K.R. MacDonald, J. Feinberg, Z.Z. Ming, P. Günter, Asymmetric transmission through a photorefractive crystal of barium titanate, *Opt. Commun.* 50 (1984) 146–150.
- [34] B. Mihailova, D. Toncheva, M. Gospodinov, L. Konstatinov, Raman spectroscopic study of Mn-doped  $\text{Bi}_4\text{Ge}_3\text{O}_{12}$ , *Solid State Commun.* 112 (1999) 11–15.
- [35] B. Mihailova, L. Konstatinov, D. Petrova, M. Gospodinov, Effect of doping on Raman spectra of  $\text{Bi}_{12}\text{SiO}_{20}$ , *Solid State Commun.* 102 (1997) 441–444.
- [36] B. Mihailova, M. Gospodinov, L. Konstatinov, Raman spectroscopy study of sillenites I. Comparison between  $\text{Bi}_{12}(\text{Si}, \text{Mn})\text{O}_{20}$  single crystals, *J. Phys. Chem. Solids* 60 (1999) 1821–1827.
- [37] L. Wiehl, A. Friedrich, E. Haussühl, W. Morgenroth, A. Grzechnik, K. Friese, B. Winkler, K. Refson, V. Milman, Structural compression and vibrational properties of  $\text{Bi}_{12}\text{SiO}_{20}$  sillenite from experiment and theory, *J. Phys. Condens. Matter* 22 (2010) 505401 16pp.
- [38] A. Feldman, W.S. Brower Jr., D. Horowitz, Optical activity and faraday rotation in bismuth oxide compounds, *Appl. Phys. Lett.* 16 (1970) 201–202.
- [39] V. Tassev, M. Gospodinov, M. Veleva, Faraday effect of BSO and BTO crystals doped with Cr, Mn and Cu, *Cryst. Res. Technol.* 35 (2000) 213–219.

# Improvement of magneto-optical quality of high purity $\text{Bi}_{12}\text{GeO}_{20}$ single crystal induced by femtosecond pulsed laser irradiation

G. S. I. ABUDAGEL<sup>a</sup>, S. PETRIČEVIĆ<sup>a</sup>, P. MIHAILOVIĆ<sup>a</sup>, A. KOVAČEVIĆ<sup>b</sup>, J. L. RISTIĆ-DJUROVIĆ<sup>b</sup>, M. LEKIĆ<sup>b</sup>, M. ROMČEVIĆ<sup>b</sup>, S. ČIRKOVIĆ<sup>b</sup>, J. TRAJIĆ<sup>b,\*</sup>, N. ROMČEVIĆ<sup>b</sup>

<sup>a</sup>*School of Electrical Engineering, University of Belgrade, Bulevar kralja Aleksandra 73, 11000 Belgrade, Serbia*

<sup>b</sup>*Institute of Physics, University of Belgrade, Pregrevica 118, 11080 Belgrade, Serbia*

Femtosecond pulsed laser irradiation can improve optical properties of  $\text{Bi}_{12}\text{GeO}_{20}$  single crystals. We investigate if the effect occurs if the crystals are grown from high purity components. The samples are irradiated by a femtosecond pulsed laser beam of increasing power. The maximal transmittance of 44% occurs at the irradiating laser power of 451 mW. After irradiation, intensity of Raman spectra peaks increase, except for the peak at  $203\text{ cm}^{-1}$ , whose intensity decreases. The irradiation also changes the sample colour. Although the Verdet constant does not change, the absorption coefficient decreases significantly, which leads to magneto-optical quality improvement of approximately 70%.

(Received March 3, 2017; accepted August 9, 2017)

**Keywords:** Bismuth germanium oxide, Laser annealing, Raman spectroscopy, Crystal colour, Magneto-optical quality

## 1. Introduction

Bismuth germanium oxide ( $\text{Bi}_{12}\text{GeO}_{20}$ ) from the sillenite group of cubic crystals is commonly abbreviated as BGO or s-BGO. Due to its fitting optical characteristics, such as photoconductivity, photochromism, photorefractivity, piezoelectricity, as well as to electro-optic and magneto-optic effects it supports [1, 2], it has been used in a wide range of optical applications and devices [2–6]. Its cubic cell unit is composed of two formula units, namely of 24 Bi, 40 O and 2 Ge. The Ge atoms positioned in the centre and the vertices of a cube are tetrahedrally coordinated by the oxygen atoms, whereas the Bi atoms are heptacoordinated [7–9]. There are numerous studies that considered properties of doped and un-doped BGO, see for example [10–18], as well as those investigating property changes induced by a wide variety of exposure types such as thermal treatments, particle beams or light treatments [3, 12–16, 19–25].

BGO is a good example of a Faraday rotator crystal possibly applicable in sensor systems. In order to evaluate usability of a crystal for sensing purposes not only its Faraday rotation capability, but its ability to be integrated into a sensing optical system must be considered. In general, in fiber-optic sensing systems optical beams used to sense the measured quantity are guided through the fibers, giving rise to the absorption coefficient as the most important optical property. Crystals with high absorption coefficient are in general less useful for sensor systems because they absorb much of the light and cause low signal-to-noise ratio at the receiving photo diode. If the magnetic field is to be detected, the intensity of light caused by magnetic field modulation is proportional to the Verdet constant, whereas the intensity of light reaching the

photodiode as well as the photocurrent is inversely proportional to the crystal absorption. The noise in a fiber optic sensing system is predominantly determined by the noise in the processing electronics and can be expressed as the noise present in the photocurrent. Therefore, the signal-to-noise ratio of the magnetic field sensor is proportional to the Verdet constant and inversely proportional to the absorption coefficient of a crystal. Consequently, due to its proportionality to the signal-to-noise ratio, the magneto-optical quality of a crystal defined as a ratio of the Faraday rotation, which is proportional to the Verdet constant, and the absorption coefficient can be used as a measure of a crystal's applicability in a magnetic field sensing system.

When  $\text{Bi}_{12}\text{GeO}_{20}$  crystals were exposed to pulsed laser beam irradiation, there are examples of laser beam operating in the nanosecond [3], picosecond [23–25], or femtosecond range [26]. In [26] it was determined that femtosecond pulsed laser irradiation of increasing power causes significant changes in the transmittance, transmission spectra, sample colour, Raman spectra, X-ray diffraction pattern, Verdet constant, magneto-optical property, and absorption coefficient of lower quality black  $\text{Bi}_{12}\text{GeO}_{20}$  single crystals. Here we analyze if the same increasing power pattern of femtosecond pulsed laser irradiation has similar effect on the high quality yellow  $\text{Bi}_{12}\text{GeO}_{20}$  single crystals, i.e., on the crystals that were grown from the components whose purity is higher than that of the black crystals, and whose magneto-optical quality is the maximal obtainable by the applied crystal growth technique.

## 2. Experimental procedure

### 2.1. Preparation of crystal samples

Single crystals of  $\text{Bi}_{12}\text{GeO}_{20}$  were grown in the air by the Czochralski technique using the MSR 2 crystal puller, Eurotherm temperature controller and the calculated critical crystal diameter, critical rotation rate and pulling rate, as explained in detail in [17, 26]. The system provided small fluctuations in crystal diameter size as well as in melting temperature. The  $\text{Bi}_{12}\text{GeO}_{20}$  seed was oriented in the  $\langle 111 \rangle$  direction and the charge was a mixture of  $\text{Bi}_2\text{O}_3$  and  $\text{GeO}_2$  in the stoichiometric ratio 6:1. The light yellow crystal samples were obtained using the  $\text{Bi}_2\text{O}_3$  and  $\text{GeO}_2$  purity of 99.999 wt.% and 99.9999 wt.%, respectively. Crystal samples of size  $4 \text{ mm} \times 4 \text{ mm} \times 10 \text{ mm}$  were cut from the boule and mechanically as well as chemically polished. The technique used to prepare the samples insured maximal sample quality within the limits corresponding to their purity [17].

### 2.2. Crystal irradiation and characterization

The equipment used to produce the femtosecond pulsed laser beam and establish its wavelength was the Coherent Mira 900F femtosecond laser, Coherent Verdi V-10 pump laser that provided a 532 nm continuous wave pump beam, and Ocean Optics HR2000CG UV-NIR spectrometer. Crystal samples were irradiated along the crystal growth direction ( $z$ ), i.e. along the samples' longest axis. The irradiating laser beam radius provided partial irradiation of the exposed crystal facet. The beam wavelength was 800 nm, whereas its power was increased from 50 mW to 950 mW and was adjusted by a graded filter. The pulses were 90 fs long and had repetition rate of 76 MHz. The samples were irradiated by each beam power for 3 s. The beam power was measured with the Ophir power meter with the thermal and photometric heads. In order to enable comparison of the irradiation effects on the single crystal samples of different purity, i.e., on yellow and black  $\text{Bi}_{12}\text{GeO}_{20}$  samples, the irradiation conditions were intentionally chosen to be identical to those applied to the lower purity black crystals in [26].

The sample colour was calculated from the transmission spectra measured by the Beckman Coulter DU 720 General Purpose UV/VIS spectrometer.

The micro-Raman spectra were recorded at room temperature in the spectral range between 100 and  $1100 \text{ cm}^{-1}$  with  $1 \text{ cm}^{-1}$  resolution using the backscattering configuration and the 532 nm line of Verdi G optically pumped semiconductor laser as an excitation source, and the Jobin Yvon T64000 spectrometer, which has nitrogen cooled charge-coupled-device detector.

The Faraday rotation and optical activity were measured by  $\Delta/\Sigma$  method at the wavelength of  $\lambda = 632.8 \text{ nm}$ . After the BGO crystal the orthogonal polarizations of the light beam were separated by the  $\text{CaCO}_3$  crystal into two parallel beams 3 mm apart. The quadrant photodiode connected into transimpedance stages was used for

optoelectronic conversion. This method is described in more details in [26].

## 3. Results and discussion

The irradiation pattern applied here to the higher purity yellow crystals is identical to the one utilized in [26] to irradiate black crystals grown from the components of lesser purity. Consequently, the obtained results can be compared and the differences can be attributed solely to different sample purity. With the increase of irradiating laser power, the transmittance of irradiated sample undergoes initial growth followed by a decrease, as can be seen in Fig. 1. Comparison with the dependence corresponding to the black crystal given in [26] reveals that the transmittance curves for the black as well as for the yellow crystal has the same shape and that the slopes of the two curves appear to be approximately equal. The curve corresponding to the yellow crystal is shifted to the larger values by approximately 18.8% compared to the curve corresponding to the black crystal. For the yellow crystal, the maximal transmittance of 44.0% occurs at the irradiating laser power of 451 mW, whereas the lower purity black crystal was reported in [26] to have the smaller maximal transmittance value of 25.1% corresponding to 455 mW. It seems that both curves exhibit local irregularities which occur at 197.4–249.7 mW, 552–605 mW and 800–857 mW for the black crystal and at 593–641 mW for the yellow crystal. It is possible that the irregularity in the yellow sample curve for large values of incident power  $P_0$  is not visible because it is outside the considered range of irradiating laser power, or due to insufficient measurement accuracy achieved for yellow crystal data points above 700 mW.

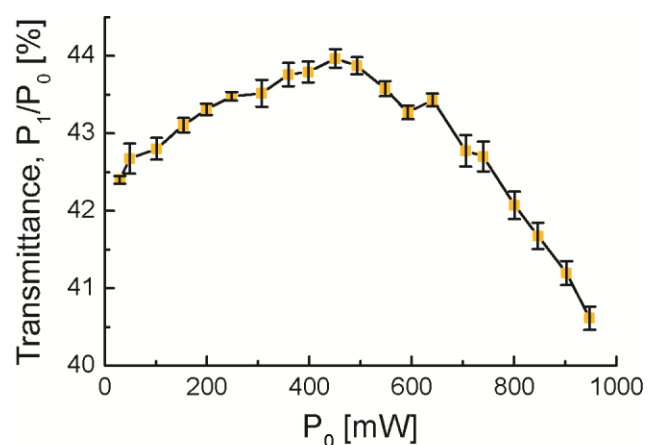


Fig. 1. Change of crystal transmittance with increase of irradiating laser power. For each value of the incident power  $P_0$ , a sample is irradiated by the femtosecond laser beam for 3 s. The transmittance is given as  $P_1/P_0$ , where  $P_1$  is the transmitted power. The error bars were calculated from the uncertainties of measured values of the incident and transmitted power,  $\Delta P_0$  and  $\Delta P_1$ .



The sample colours before and after irradiation were calculated using the CIE chromaticity coordinates and are given in Fig. 2. Comparison with the results corresponding to the black crystal given in [26] revealed that the change of black crystal colour was more pronounced than that of the yellow crystal presented here.

The Raman spectra of unirradiated and irradiated samples are recorded at room temperature in the spectral range from 150 to 800 cm<sup>-1</sup> and are shown in Fig. 3. The results obtained for unirradiated crystals are in agreement with those given in [8, 17]. After irradiation the intensity of the *F(TO)* peak at 203 cm<sup>-1</sup> decreased, whereas all other peaks became more pronounced. Despite the difference in purity between the yellow samples studied here and the black crystals considered in [26] the Raman spectra of unirradiated crystals do not differ significantly. As reported in [26], irradiation of the black crystal caused all the peaks of symmetry type *E*, i.e., the peaks at 234, 454, and 619.6 cm<sup>-1</sup>, to disappear and intensity increase of all other peaks. The change in the same Raman spectrum peaks of Bi<sub>12</sub>GeO<sub>20</sub> was reported in [16]; however, the most, medium, and least intense peaks correspond to the annealed, doped, and untreated samples, respectively.

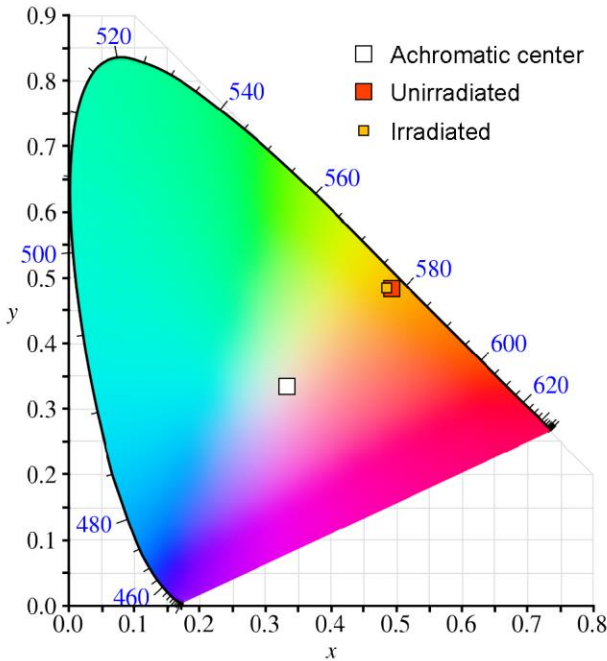


Fig. 2. Colours of irradiated and unirradiated samples in CIE chromaticity diagram.

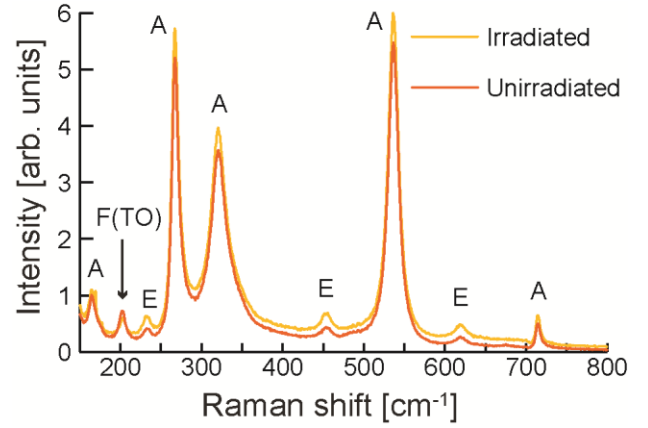


Fig. 3. Raman spectra. Irradiation caused a small upward shift of the crystal spectrum except for the *F(TO)* type peak at 203 cm<sup>-1</sup>.

The Verdet constant is calculated from

$$V = \frac{\theta_{0AC}}{B_0 l} = \frac{1}{2B_0 l} \sin^{-1} \left( \frac{U_1 - U_2}{U_1 + U_2} \right)_{0AC} \quad (1)$$

where  $\theta_{0AC}$  is the amplitude of the AC signal,  $B_0$  is the amplitude of the magnetic induction, whereas  $U_1$  and  $U_2$ , are the output signal voltages obtained after transimpedance stages from the vertically and horizontally polarized components, respectively. The FFT was used to separate spectral components of  $U_1$  and  $U_2$ . The Faraday rotation was determined from the magnitude of the 50 Hz component.

The absorption coefficients were obtained by measuring the difference in beam intensities at the quadrant photodiode [26] with and without BGO crystal in the beam path. The reflection on the BGO crystal was calculated using the normal incidence and BGO refraction index of  $n_{BGO} = 2.55$ .

The absorption coefficient,  $\alpha$ , was calculated from the beam intensities with and without the crystal present in the beam path,  $I(x)$  and  $I(0)$ , and the known crystal length  $l = 9.8$  mm as

$$I(l) = I_0 e^{-\alpha l} \Rightarrow \alpha = -\frac{1}{l} \ln \frac{I(l)}{I_0} \quad (2)$$

The magneto-optical quality is calculated by dividing the Verdet constant by the absorption coefficient. The obtained results are given in Table 1.

Table 1. Magneto-optical properties of irradiated and unirradiated high purity crystal samples.

Property	Unirradiated sample	Irradiated sample
Verdet constant (rad T <sup>-1</sup> m <sup>-1</sup> )	72	72
Absorption coefficient (cm <sup>-1</sup> )	0.58	0.34
Magneto-optical quality (rad T <sup>-1</sup> )	1.24	2.1

The data given in Table 1 show the effects of femtosecond laser irradiation on the magneto-optical properties of the high purity BGO crystal. The irradiation caused 41.4% decrease in the absorption coefficient and did not influence the Faraday constant. Consequently, the increase in crystal transparency resulted in a significant 70% increase in the magneto-optical quality. As explained earlier, increase in crystal transparency is an important gain from the point of view of a sensor system since the system-level signal-to-noise ratio is directly proportional to the magneto-optical quality of a crystal. Therefore, it is expected that the signal-to-noise ratio of a sensor system would be improved by the same amount as the improvement in the magneto-optical quality induced by the irradiation. Consequently, it can be concluded that the femtosecond pulsed laser irradiation affects the crystal in a positive manner.

#### 4. Conclusions

Femtosecond pulsed laser irradiation of increasing power caused significant changes in optical properties of Bi<sub>12</sub>GeO<sub>20</sub> single crystals grown from the components of high purity, as was the case in [26] when the component purity was not so high. The transmittance dependence on the applied irradiation power had the same shape regardless of the purity of the components the crystals were grown from. The curve corresponding to the higher purity crystal, i.e., the yellow crystal, is shifted to the larger values by approximately 18.8%. For the black and yellow crystal, the maximal transmittance of 25.1% and 44.0% occurred at 455 mW and 451 mW, respectively. The Raman spectra peaks became somewhat stronger, except for the *E* type peaks at 234, 454, and 619.6 cm<sup>-1</sup> in the lower purity black crystal, which disappeared and the yellow crystal peak at 203 cm<sup>-1</sup> whose intensity decreased. Irradiation also caused slight colour change of the yellow crystal and significant change of the black crystal colour. The Verdet constant did not change; however, the absorption coefficient significantly decreased leading to equally significant increase of the magneto-optical quality of the sample. Consequently, it can be concluded that optical properties of high quality Bi<sub>12</sub>GeO<sub>20</sub> single crystals can be improved by irradiation with the femtosecond pulsed laser beam.

#### Acknowledgements

This work is financially supported by the Serbian Ministry of Education, Science, and Technological Development through the project III45003. We thank Z. Velikić and D. Dramlić for their assistance with transmission spectra measurements and A. Valčić for his help with sample preparation.

#### References

- [1] M. Simon, F. Mersch, C. Kuper, *Phys. Status Solidi A*. **159**(2), 559 (1997).
- [2] V. M. Skorikov, Yu. F. Kargin, A. V. Egorysheva, V. V. Volkov, M. Gospodinov, *Inorg. Mater.* **41**(1), S24 (2005).
- [3] R. A. Ganeev, A. I. Rysanyansky, B. Palpant, S. Debrus, *J. Appl. Phys.* **97**, 104303 (2005).
- [4] P. Yeh, *Introduction to Photorefractive nonlinear optics*, first ed., Wiley-Interscience, New York, 1993.
- [5] M. J. Weber, *J. Lumin.* **100**, 35 (2002).
- [6] M. Itoh, T. Katagiri, H. Mitani, M. Fujita, Y. Usuki, *Phys. Status. Solidi B*, **245**(12), 2733 (2008).
- [7] S. C. Abrahams, P. B. Jamieson, J. L. Bernstein, *J. Chem. Phys.* **47**(10), 4034 (1967).
- [8] V. I. Burkov, V. S. Gorelik, A. V. Egorysheva, Y. F. Kargin *J. Russ. Las. Res.* **22**, 243 (2001).
- [9] S. F. Radaev, V. I. Simonov, Y. F. Kargin, *Eur. J. Solid. State Inorg. Chem.* **29**(2), 383 (1992).
- [10] N. C. Deliolanis, I. M. Kourmoulis, G. Asimellis, A. G. Apostolidis, E. D. Vanidhis, N. A. Vainos, *J. Appl. Phys.* **97**(2), 023531 (2005).
- [11] C. G. P. Moraes, F. A. A. Jesus, Z. S. Macedo, *Adv. Cond. Matter. Phys.* **2014**, 968349 (2014), <http://dx.doi.org/10.1155/2014/968349>.
- [12] O. Peña-Rodríguez, J. Olivares, I. Bányász, *Opt. Mater.* **47**, 328 (2015).
- [13] V. M. Skorikov, I. S. Zakharov, V. V. Volkov, E. A. Spirin, *Inorg. Mater.* **38**(2), 172 (2002).
- [14] Z. S. Macedo, C. S. S. Oliveira, A. C. Hemandes, *J. Appl. Phys.* **102**(3), 034105 (2007).
- [15] H. Marquet, J-C. Merle, J-G. Gies, *Opt. Mater.* **14**, 277 (2000).
- [16] P. S. Yu, L. B. Su, H. L. Tang, X. Guo, H. Y. Zhao, Q. H. Yang, J. Xu, *Sci. China Tech. Sci.* **54**(5), 1287 (2011).
- [17] Z. Ž. Lazarević, P. Mihailović, S. Kostić, M. J. Romčević, M. Mitrić, S. Petričević, J. Radunović, M. Petrović-Damjanović, M. Gilić, N. Ž. Romčević, *Opt. Mater.* **34**, 1849 (2012).
- [18] S. Kumaragurubaram, S. Moorthy Babu, C. Subramanian, P. Ramasamy, *Indian J. Eng. Mater. Sci.* **7**(5-6), 331 (2000).
- [19] A. Cremades, J. Piqueras, A. Remón, J.A. García, M. T. Santos, E. Diéguez, *J. Appl. Phys.* **83**(12), 7948 (1998).
- [20] A. Cremades, M. T. Santos, A. Remón, J. A. García, E. Diéguez, *J. Piqueras, J. Appl. Phys.* **79**(9), 7186 (1996).



- [21] I. Stefaniuk, P. Potera, I. Rogalska, D. Wróbel, *Current Topics in Biophysics* **33**, 231 (2010).
- [22] N. Benjelloun, M. Tapiero, J. P. Zielinger, F. Marsaud, J. C. Launay, *J. Appl. Phys.* **64**(8), 4013 (1988).
- [23] R. A. Ganeev, A. I. Ryasnyansky, R. I. Tugushev, M. K. Kodirov, F. R. Akhmedjanov, T. Usmanov, *Opt. Quant. Electron.* **36**(9), 807 (2004).
- [24] M. Sylla, D. Rouède, R. Chevalier, X. Nguyen Phu, G. Rivoire, *Opt. Commun.* **90**, 391 (1992).
- [25] B. Taheri, S. A. Holmstrom, R. C. Powell, J. J. Song, A. M. F. I. Földvári, A. Péter, *Opt. Mater.* **3**, 251 (1994).
- [26] A. Kovačević, J. L. Ristić-Djurović, M. Lekić, B. Hadžić, G. S. I. Abudagel, S. Petričević, P. Mihailović, B. Matović, D. Dramlić, L. M. Brajović, N. Romčević, *Mater. Res. Bull.* **83**, 284 (2016).

---

\*Corresponding author: jelena@ipb.ac.rs

# Solitons generated by self-organization in bismuth germanium oxide single crystals during the interaction with laser beam

Vladimir Skarka<sup>1,2,3</sup>  · Marina M. Lekić<sup>1</sup> · Aleksander G. Kovačević<sup>1</sup> · Boban Zarkov<sup>4</sup> · Nebojša Ž. Romčević<sup>1</sup>

Received: 8 November 2017 / Accepted: 19 December 2017 / Published online: 3 January 2018  
© Springer Science+Business Media, LLC, part of Springer Nature 2018

**Abstract** We present here the experimental, theoretical, and numerical investigations of Kerr solitons generated by self-organization in black and yellow high quality bismuth germanium oxide ( $\text{Bi}_{12}\text{GeO}_{20}$ ) single crystals. A picosecond laser beam of increasing power induces competing cubic and quintic nonlinearities. The numerical evolution of two-dimensional complex cubic-quintic nonlinear Schrödinger equation with measured values of nonlinearities shows the compensation of diffraction by competing cubic and quintic nonlinearities of opposite sign, i.e., the self-generation and stable propagation of solitons. Experiments as well as numerical simulations show higher nonlinearity in the black  $\text{Bi}_{12}\text{GeO}_{20}$  than in the more transparent yellow one.

**Keywords** Solitons · Bismuth germanium oxide single crystals · Cubic-quintic Schrödinger equation · Experimental measurements

---

This article is part of the Topical Collection on Focus on Optics and Bio-photonics, Photonica 2017.

---

Guest Edited by Jelena Radovanovic, Aleksandar Krmpot, Marina Lekic, Trevor Benson, Mauro Pereira, Marian Marciniak.

---

✉ Vladimir Skarka  
vladimir.skarka@univ-angers.fr

<sup>1</sup> Institute of Physics, University of Belgrade, Belgrade 11000, Serbia

<sup>2</sup> Texas A&M University at Qatar, P.O. Box 23874, Doha, Qatar

<sup>3</sup> Laboratoire de Photonique d'Angers, EA 4464, University of Angers, 49045 Angers Cedex 01, France

<sup>4</sup> Directorate of Measures and Precious Metals, Mike Alasa 14, Belgrade 11000, Serbia

## 1 Introduction

Dissipative structures far from the thermodynamic equilibrium, need external energy and/or matter supply in order to be self-organized (Nicolis and Prigogine 1977). The self-trapping of robust localized structures, i.e., solitons is based on the balance of antagonistic effects, with e.g. nonlinearity-induced self-contraction arresting diffraction and/or dispersion (Kivshar and Agrawal 2003; Crasovan et al. 2000; Mihalache et al. 2006). The complex nonlinear Schrödinger equation (NLS) adequately models the solitons generation and propagation in plenty of systems including nonlinear optics, nanophotonics, and nanoplasmonics (Aranson and Kramer 2002). The focusing cubic nonlinearity (e.g. Kerr nonlinearity) compensates either diffraction or dispersion generating stable spatial or temporal solitons in conservative  $(1 + 1)$ -dimensional systems (one standing for the transverse coordinate  $x$  or  $t$ , while the remaining one for the propagation coordinate  $z$ ). However, the same focusing cubic nonlinearity dominates the diffraction and/or dispersion leading to the catastrophic collapse in  $(2 + 1)$ - and  $(3 + 1)$ -dimensional systems (two and three standing for the transverse coordinates). The collapse can be prevented in media having, for instance, negative quintic nonlinearity in addition to the positive cubic one, as it was established using synergy of variational method and numerical simulations (Skarka and Aleksić 2006; Skarka et al. 2010, 2014, 2017). Such Kerr solitons are hard to obtain experimentally especially in solid state systems.

The experimental generation of two-dimensional (2D) spatial optical solitons in a cubic-quintic medium has been recently directly demonstrated only in liquid carbon disulfide ( $\text{CS}_2$ ) (Falcao-Filho et al. 2013). The excitation beam at 920 nm was obtained from an optical parametric amplifier pumped by a Ti:sapphire laser (100 fs, 1 kHz).

We present here the theoretical, experimental, and numerical investigations of Kerr solitons generated by self-organization in black and yellow high quality bismuth germanium oxide ( $\text{Bi}_{12}\text{GeO}_{20}$ ) single crystals. A laser beam of increasing power induces competing cubic and quintic nonlinearities. The numerical evolution of  $(2 + 1)$ D complex cubic-quintic nonlinear Schrödinger equation (CQNLS) with measured values of nonlinearities shows the compensation of diffraction by competing cubic and quintic nonlinearities of opposite sign, i.e., the self-generation and propagation of stable solitons.

## 2 Theoretical model

Self-organization, propagation, and stability of solitons can be adequately modelled by the  $(2 + 1)$ D CQNLS that governs the evolution of normalized slowly-varying complex envelope  $E$  of electric waves in nanophotonic or nanoplasmonic media (Skarka et al. 1997, 1999):

$$i \frac{\partial E}{\partial z} + \gamma \left( \frac{\partial^2 E}{\partial x^2} + \frac{\partial^2 E}{\partial y^2} \right) + \kappa E + \sigma |E|^2 E - \nu |E|^4 E = 0 \quad (1)$$

where  $\gamma$ ,  $\sigma$ , and  $\nu$  are respectively the parameters characterizing the diffraction, cubic Kerr nonlinearity, and quintic nonlinearity. Barring rare exceptions, the  $(2 + 1)$ D CQNLS, due to its complexity, do not admit exact solutions. Nevertheless, an analytical approximation for solitons has been developed using the variational method adapted to dissipative systems (Skarka et al. 1997, 1999; Skarka and Aleksić 2006). The variational method makes use of

the following Gaussian trial function representing the electric field of an axisymmetric Gaussian laser beam:

$$E = A \exp[-r^2/R^2 + iCr^2 + i\Psi] \quad (2)$$

where amplitude  $A$ , radius  $R$ , wave-front curvature  $C$ , and phase  $\Psi$  have to be optimized.

Skipping straightforward details, the following system of evolution equations is produced by the variational method:

$$dA/dz = -\gamma 4CA, \quad (3)$$

$$dR/dz = \gamma 4CR, \quad (4)$$

$$dC/dz = -4\gamma C^2 + \gamma/R^4 - (\sigma A^2 - (8/9)vA^4)/(4R^2), \quad (5)$$

$$d\Psi/dz = -2\gamma/R^2 + 3\sigma A^2/4 - 5vA^4/9 + \kappa, \quad (6)$$

with Eq. (6) decoupled from (3) to (5). Fixed points of these equations correspond to steady-state solutions with a zero wave-front curvature. Setting  $dA/dz = dR/dz = 0$  leads to the expression for radius

$$R = 2\sqrt{\gamma}(\sigma A^2 - 8vA^4/9)^{-1/2} \quad (7)$$

and the limitation of amplitude

$$0 < A < \sqrt{\frac{9\sigma}{8v}}. \quad (8)$$

### 3 Experimental results

We present here not only theoretical but also experimental investigations of Kerr solitons generated by self-organization in black and yellow high quality bismuth germanium oxide ( $\text{Bi}_{12}\text{GeO}_{20}$ ) single crystals. Although yellow and black crystals have the same chemical formula, their properties may be quite different (Lazarević et al. 2012; Kovačević et al. 2016; Abudagel et al. 2017). At 1064 nm a Neodymium Yag (17 ps, 10 Hz). laser of increasing power induces competing cubic and quintic nonlinearities into samples. Taking into account that intensity  $I \sim |E|^2$  the corresponding output beam intensity can be deduced from Eq. (1)

$$I_{out} = \kappa I + \sigma I^2 - vI^3 \quad (9)$$

(Skarka et al. 2017).

Increasing incoming beam intensity  $I_{in}$  the outgoing beam intensity  $I_{out}$  for yellow and black crystals are charted respectively in Figs. 1 and 2. Fitting these experimental curves by cubic polynomial we obtain the values of parameters in Eqs. (1) and (9). The fit for yellow semi transparent crystal yields

$$I_{out} = 1.003 + 0.6492I + 0.4636I^2 - 0.0242I^3. \quad (10)$$

Due to the opacity of the black crystal the values of nonlinear parameters are increased

$$I_{out} = 1.6201 + 1.4731I + 0.7186I^2 - 0.0709I^3. \quad (11)$$

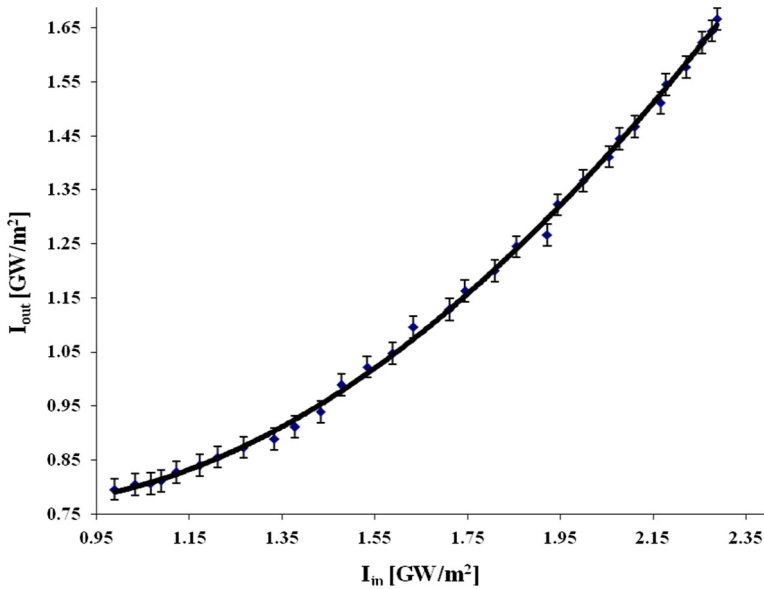


**Fig. 1** Increasing of output beam intensity out of yellow crystal as a function of the increase of input laser intensity

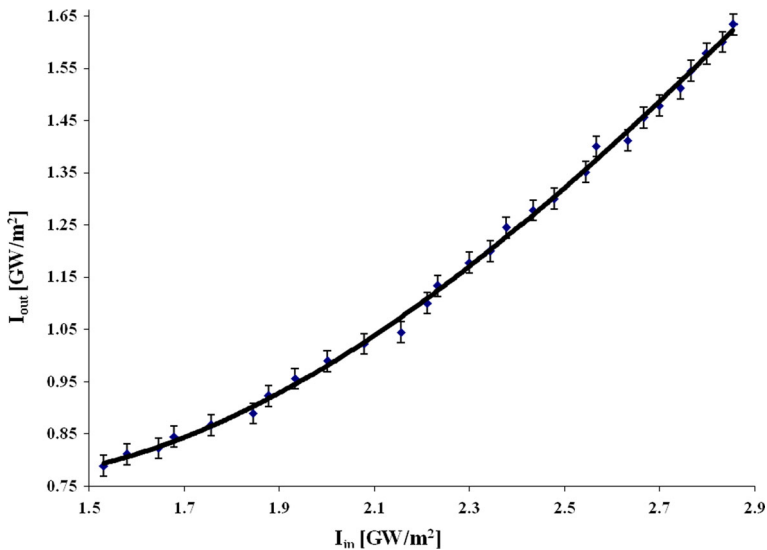


**Fig. 2** Increasing of output beam intensity out of black crystal as a function of the increase of input laser intensity

Notice that the positive sign of quadratic intensity in both equations means the self-focusing of the laser beam induced due to the Kerr effect. In contrast, the negative sign of cubic intensity corresponds to the self-defocusing effect of negative quintic nonlinearity in CQNLS in agreement with our theoretical modeling.

Therefore, experimental results demonstrate that the propagation of laser beam across both yellow and black samples induces positive cubic and negative quintic nonlinearity. In turn, the light beam is modified due to this crossing as can be seen on the output intensity in Figs. 1 and 2. Such a behavior is the example of the control and structuring of light by light due to its crossing of nonlinear medium. The corresponding light-matter interaction leads to the self-organized structuring of laser beam. Following the pioneering work of Prigogine and his team, the self-organization far from thermodynamic equilibrium causes the appearance of dissipative structures (Nicolis and Prigogine 1977). In the case of the structuring of light by light, such a dissipative structure is a soliton. Solitons are completely localized in space and in time. They propagate long distance without altering.

In an experiment long distance propagation cannot be achieved in some solid sample, in particular if it is a crystal. Long crystals are simply not available. However we can resort to a numerical propagation that, under same conditions, may mimic real experiment.

The nonlinear effects are enhanced in black crystal due to its opacity with respect to yellow one, as can be concluded comparing curves in Figs. 1 and 2, as well as the results of their fits [see Eqs. (10) and (11)].

#### 4 Confirmation of experimental results by numerical simulations of the Schrödinger model

In order to identify a pattern as a soliton, this structure has to be self-maintained during a long distance propagation. Obviously, such a drastically restrictive condition cannot be satisfied in an experiment. Both crystals we used for experiment are only 1 cm long. However, even such short samples allow the determination of linear and nonlinear parameters that enter in CQNLS [see Eqs. (1) and (9)–(11)]. Therefore, it is enough to perform numerical simulation of Eq. (1) with experimentally obtained parameters in order to investigate long distance propagation. If during such a evolution the beam profile presents the same form without the alteration, it can be concluded that it is a soliton. In Figs. 3, 4, 5 and 6 are charted results of the numerical propagation in black sample with the parameters from Eq. (11). Following the condition in Eq. (8) imposed by the variational method, the input amplitude is chosen to be three ( $A = 3$ ) in dimensionless units. The input laser beam is initially always Gaussian and it is given by the trial function Eq. (2). In

**Fig. 3** The Gaussian output beam for  $z = 0$

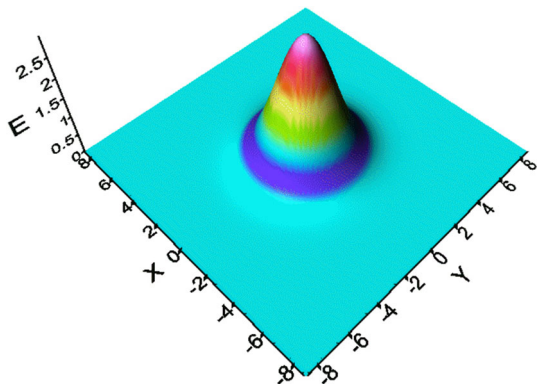




**Fig. 4** The output beam becomes a soliton after  $z = 40$

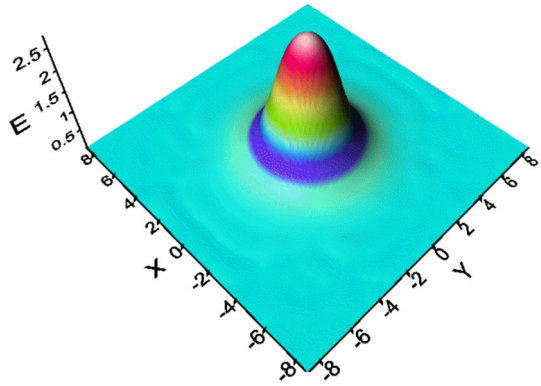


**Fig. 5** The beam is still soliton after  $z = 10,000$  steps

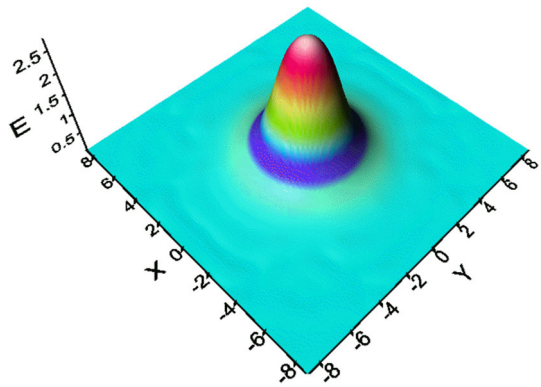
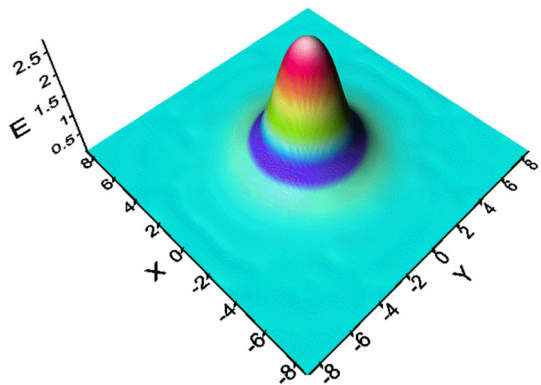


**Fig. 6** Even after  $z = 20,000$  steps the soliton remains stable



the beginning of propagation, e.i. for propagation step  $z = 0$  this Gaussian beam profile is given in Fig. 3.

The initial Gaussian laser beam is modified evolving through the nonlinear medium that itself alters. This is precisely the effect of self-organization (Skarka and Aleksić 2006; Skarka et al. 2010). Already after  $z = 40$  propagation steps, such a laser beam becomes soliton.

The laser beam is still soliton after 10,000 propagation steps, as in Fig. 5.

No changes even after 20,000 propagation steps (see Fig. 6).

Such an extraordinary stability of laser beam during numerical propagation without any alteration is the confirmation of its solitonic nature. Taking into account that the numerical propagation is performed with parameters obtained from an experiment, this confirms that in black  $\text{Bi}_{12}\text{GeO}_{20}$  crystal a stable soliton is self-trapped. The numerical propagation of the laser beam in yellow sample gives sensibly the same results, so that on the figures no difference can be notified.

## 5 Conclusions

In order to study theoretically the propagation of the laser beam through yellow and black  $\text{Bi}_{12}\text{GeO}_{20}$  single crystals the Schrödinger model is used. The variational method gives the conditions for stable propagation of spatial solitons. Indeed, a balance between the diffraction and the competing cubic and quintic nonlinearity insures the self-organization of a soliton. Experimental investigations using propagation of Neodymium Yag laser beam through crystals allow charting of input output-power curves. Fitting these experimental curves, parameters in Schrödinger equation are determined showing cubic-quintic nonlinearity. Very long numerical propagations of beams through crystals are performed demonstrating self-trapping of robust spatial solitons. Consequently, in turn in the experiments, the self-generation of solitons is confirmed. Self-organization of solitons in solid samples open many possibilities for applications.

**Acknowledgements** This publication was made possible by the National Priorities Research Program Grant No. 9-020-1-006 from the Qatar National Research Fund (a member of Qatar Foundation). Work at the Institute of Physics Belgrade is supported by the Ministry of Education and Science of the Republic of Serbia, under Projects OI 171,006 and III 45016.

## References

- Abudagel, G.S.I., Petričević, S.J., Mihailović, P.M., Kovačević, A.G., Ristić-Djurović, J., Lekić, M.M., Romčević, M.J., Cirković, S., Trajić, J.M., Romčević, N.Ž.: Improvement of magneto-optical quality of high purity  $\text{Bi}_{12}\text{GeO}_{20}$  single crystal induced by femtosecond pulsed laser irradiation, *Optoelectronics and advanced materials—rapid. Communications* **11**, 477–481 (2017)
- Anrson, I.S., Kramer, L.: The world of the complex Ginzburg-Landau equation. *Rev. Mod. Phys.* **74**, 99–144 (2002)
- Crasovan, L.-C., Malomed, B.A., Mihalache, D.: Stable vortex solitons in the two-dimensional Ginzburg-Landau equation. *Phys. Rev. E* **63**, 0166051–6 (2000)
- Falcao-Filho, E.L., de Araujo, C.B., Boudebs, G., Leblond, H., Skarka, V.: Robust two-dimensional spatial solitons in liquid carbon disulfide. *Phys. Rev. Lett.* **110**, 0139011–5 (2013)
- Kivshar, Y.S., Agrawal, G.P.: *Optical Solitons: From Fibers to Photonic Crystals*. Academic, San Diego (2003)
- Kovačević, A.G., Ristić-Djurović, J., Lekić, M.M., Hadžić, B., Abudagel, G.S.I., Petričević, S.J., Mihailović, P.M., Matović, B.Z., Dramlić, D.M., Brajović, L.M., Romčević, N.Ž.: Influence of femtosecond pulsed laser irradiation on bismuth germanium oxide single crystal properties. *Mater. Res. Bull.* **83**, 284–289 (2016)
- Lazarević, Z.Ž., Mihailović, P., Romčević, M.J., Kostić, S., Mitrić, M., Romčević, N.Ž.: Determination magneto-optical quality and refractive index of bismuth germanium oxide single crystals grown by Czochralski technique. *Opt. Mater.* **34**, 1849–1859 (2012)

- Mihalache, D., Mazilu, D., Lederer, F., Kartashov, Y.V., Crasovan, L.-C., Torner, L., Malomed, B.A.: Stable vortex tori in the three-dimensional cubic-quintic Ginzburg-Landau equation. *Phys. Rev. Lett.* **97**, 0739041–4 (2006)
- Nicolis, G., Prigogine, I.: *Self-organization in Nonequilibrium Systems*. Wiley, New York (1977)
- Skarka, V., Berezhiani, V.I., Miklaszewski, R.: Spatiotemporal soliton propagation in saturating nonlinear optical media. *Phys. Rev. E* **56**, 1080–1087 (1997)
- Skarka, V., Berezhiani, V.I., Miklaszewski, R.: Generation of light spatiotemporal soliton from asymmetric pulses in saturating nonlinear media. *Phys. Rev. E* **59**, 1270–1273 (1999)
- Skarka, V., Aleksić, N.B.: Stability criterion for dissipative soliton solutions of the one-, two-, and three-dimensional complex cubic-quintic Ginzburg-Landau equations. *Phys. Rev. Lett.* **96**, 0139031–4 (2006)
- Skarka, V., Aleksić, N.B., Leblond, H., Malomed, B.A., Mihalache, D.: Varieties of stable vortical solitons in Ginzburg-Landau media with radially inhomogeneous losses. *Phys. Rev. Lett.* **105**, 2139011–4 (2010)
- Skarka, V., Aleksić, N.B., Lekić, M., Aleksić, B.N., Malomed, B.A., Mihalache, D., Leblond, H.: Formation of complex two-dimensional dissipative solitons via spontaneous symmetry breaking. *Phys. Rev. A* **90**(2), 0238451–6 (2014)
- Skarka, V., Aleksić, N.B., Krolikowski, W., Christodoulides, D.N., Rakotoarimalala, S., Aleksić, B.N., Belić, M.: Self-structuring of stable dissipative breathing vortex solitons in a colloidal nanosuspension. *Opt. Express* **25**, 10090–10102 (2017)